MOLECULAR MECHANISM OF PARVOVIRUS INFECTION

BY

Aaron Yun Chen

Submitted to the graduate degree program in Microbiology, Molecular Genetics and Immunology and the Graduate Faculty of the University of Kansas in partial fulfillment of the requirements for the degree of Doctor of Philosophy.

Dissertation Committee:

_____
Jianming Qiu, Ph.D., Chairperson

_____
Joseph Fontes, Ph.D.

_____
Joe Lutkenhaus, Ph.D.

_____
Edward Stephens, Ph.D.

_____
Charlotte Vines, Ph.D.

_____
Thomas Yankee, Pharm.D., Ph.D.

Date defended: June 25th, 2010

The Dissertation Committee for Aaron Yun Chen

certifies that this is the approved version of the following dissertation:

MOLECULAR MECHANISM OF PARVOVIRUS INFECTION

_____

Jianming Qiu, Ph.D., Chairperson

Acknowledgements

First of all, I would like to take this opportunity to thank my mentor Dr. Jianming Qiu for his guidance and support of my research in the past three years. His mentoring style makes it a very pleasant and fruitful experience working in the lab. Above all, he provides me unwavering encouragement and unreserved support in various ways. His truly scientific intuition and broad knowledge has made him a great resource of ideas and passions in science, which have exceptionally inspired and enriched my growth as a student and a scientist-to-be. I cannot bestow Dr. Qiu with too much appreciation for his generosity, which helped me through the most difficult time of my PhD studies. He took me over in his lab and brought a new life to my career. It turned out to be the best thing that happened to me in my scientific path. I am indebted to him more than he knows.

Drs. Joseph Fontes, Joe Lutkenhaus, Edward Stephens, Charlotte Vines and Thomas Yankee deserve my sincere gratitude for serving on my comprehensive exam and thesis committee. It has always been a pleasure to me.

Also, I want to thank my parents and parents-in-law, whose sacrifice, support and encouragement have carried me and my wife through these years.

Words failed me, and Google did not help, to express my deep appreciation to my wife, Elizabeth Yan Zhang, whose love and persistent confidence in me, has kept me warm all along the path. Meeting and marrying her is the most wonderful thing that could ever happen to me. She is an extraordinary lady, looking after the three men of our little family while amazingly pursuing her PhD degree.

Last but not the least, I would like to extend my gratitude to all the people who have helped me with my research and drafting this thesis. Sorry that I cannot list you all in this short page.

Table of Contents

Chapter 1
Introduction

Part I. Cell Death Induced during Parvovirus Infection

Introduction

Parvoviruses have a nonenveloped icosahedral virion with a diameter of approximately 20-25 nm, which encapsidates a linear, single-stranded DNA (ssDNA) genome of an average size of 5,000 bases (105). The family *Parvoviridae* contains two subfamilies: *Parvovirinae* and *Densovirinae*. The latter infects only invertebrates and will not be the subject of this review. The family *Parvovirinae* is composed of five genera: *Amdovirus*, *Bocavirus*, *Dependovirus*, *Erythrovirus* and *Parvovirus* (102). Adeno-associated viruses (AAVs) in the genus *Dependovirus* require helper viruses (e.g., adenoviruses) for productive infection (13). All other members of *Parvovirinae* do not require helper virus and are called autonomous parvoviruses. In this review, the term "parvovirus" refers to viruses in the subfamily *Parvovirinae*.

Disease outcomes of parvovirus infection vary among members of *Parvovirinae*. Human parvovirus B19 (B19V) is the only member that has been confirmed to be pathogenic to humans (227). B19V infection is the cause of an increasing list of diseases, including fifth disease in children, transient aplastic crisis in patients with chronic hemolytic anemia (e.g., sickle cell disease patients); pure red-cell aplasia in persistent infection in immunocompromised patients; and hydrops fetalis in pregnant women (30, 57, 78, 192, 227). Human bocavirus (HBoV), which was identified in 2005, has been linked to lower respiratory tract infections in children (5, 8, 99) and was is associated with severe pneumonia in children coinfected with other respiratory viruses (98, 121). Of animal parvoviruses, Aleutian mink disease virus (AMDV), the only member in genus *Amdovirus,* causes the main symptoms of gastroenteritis, aplastic anemia and lymphopenia (17). In the genus *Bocavirus*, minute virus of canines (MVC) causes respiratory

diseases with breathing difficulty, enteritis with severe diarrhea, spontaneous abortion of fetuses and death of newborn pups (33, 86, 91). A similar enteritis was also seen in bovine parvovirus (BPV)-infected calves (67, 120). In the genus *Parvovirus*, infection of feline parvovirus (FPV) and canine parvovirus (CPV) causes gastrointestinal disease, e.g., enteritis (166-168). Porcine parvovirus was identified as the cause of stillborn and mummified piglets (215).

The cytopathic effects (CPEs) induced during parvovirus infection have been widely documented. The disease outcomes of parvovirus infection are often the result of CPEs, e.g., cell death of B19V-infected erythroid progenitor cells causes anemia and non-immune hydrops fetalis (6, 29). Cell death induced during parvovirus infection appears to be mediated either by apoptosis or by necrosis (non-apoptotic cell death), whereas cell cycle arrest is often observed as one of the early responses of host cells to parvovirus infection.

Apoptosis and necrosis are two types of cell death tightly controlled by distinct programmed signaling cascades. Apoptosis is divided mechanistically into two major pathways, i.e., extrinsic and intrinsic, both involving sequential activation of caspases. The extrinsic pathway is activated by the ligation of “death” ligands, such as Fas ligand and tumor necrosis factor-alpha (TNFα) to “death” receptors, followed by activation of caspase-8/caspase-10 and a cascade of caspase activation, which eventually leads to apoptosis (9). The mitochondrion-mediated (intrinsic) pathway is activated by multidomain Bcl-2 family proteins, notably Bax and Bak (43, 159). This pathway causes mitochondrial outer membrane permeabilization (MOMP), resulting in the release of cytochrome *c*, Smac and Omi into cytosol, where they work with apoptotic protease-activating factor (Apaf-1) to form the apoptosome complex, followed by the activation of capase-9 and eventually apoptosis (111). Caspase-3, -6 and -7 are the downstream executor caspases (40). In addition, crosstalk between the extrinsic and intrinsic pathways has been well established (11, 186), e.g., activated caspase-8/10 cleaves Bid to tBid, which in turn activates Bax/Bak.

Necrosis, the catastrophic cell death, is characterized by organelle swelling, mitochondrial membrane dysfunction, massive oxidative stress and rapid plasma-membrane permeabilization (62). Previously, necrosis was thought to be un-regulated cell death; however, recently, a number of regulated non-apoptotic cell death pathways have been attributed to necrosis (108).

Cell cycle check points are cellular mechanisms that ensure each and every step of the replication cycle takes place accurately and precisely at the right time. Each cell cycle check point is controlled by different cyclins and cyclin dependent kinases (CDKs) (93, 139). An aberrant cellular environment change or exogenous assault results in cell cycle check point arrest, which provides time for the cells to recover and return to their normal status before proceeding to the next step of the cell cycle (26).

Human parvovirus B19

B19V infection has an exclusive tropism for both $CD36^+$ human erythroid progenitors and erythroblasts of the human bone marrow and fetal liver (132, 163, 199, 225). Clinical symptoms, as seen in anemia and non-immune hydrops fetalis, are the direct result of the destruction of erythroid progenitors in bone marrow and fetal tissues by virus infection (6, 29). Tissue samples from hydrops fetalis patients infected with B19V have been found to have characteristics of apoptosis (225). Fetal erythroid progenitors infected by B19V reveal ultrastructural features of apoptotic cell death (132).

In vitro studies of B19V infection induced CPE have long been hampered by the lack of a permissive culture system. The first productive in vitro culture of B19V, reported in 1987, used bone marrow cells directly collected from a sickle cell patient (162). The establishment of a B19V semi-permissive cell line UT7/Epo-S1, a subclone of megakaryoblastic cell line UT7/Epo (135), allowed study of the role of viral non-structural proteins in B19V infection-induced cell death (131). The parent UT7/Epo cells only showed very limited permissiveness to B19V

infection (193). Ex vivo expanded erythroid progenitor cells have made it possible to carefully examine the cell death induced during B19V infection (38, 195, 222).

B19V infection of human bone marrow has been shown to inhibit both burst-forming erythroid unit (BFU-E) and cloning-forming erythroid unit (CFU-E), an arrest of erythropoiesis (163, 199). Previously, the cytotoxicity of B19V infection was believed to be a direct function of NS1 expression (161). The molecular mechanisms leading to apoptosis during B19V infection of primary erythroid progenitor cells was investigated in parallel with inducible stable NS1 expression in UT7/Epo cells (195). Both B19V infection in erythroid progenitor cells and NS1-induced apoptosis were inhibited by caspase-3, -6, and -8 inhibitors. Substantial caspase -3, -6, and -8 activities were induced by NS1 expression in UT7/Epo cells (195). The caspase-mediated apoptosis by NS1 expression in UT7/Epo cells was evidenced by cell morphology, genomic DNA fragmentation (131) and stable expression of Bcl-2, an anti-apoptotic protein, which resulted in near-total protection from cell death in response to NS1 induction (131). Caspase-8, which mediates the extrinsic apoptotic pathway, was activated during B19V- and NS1-induced apoptosis. Consequently, B19V-infected erythroid progenitors and NS1-expressing UT7/Epo cells were sensitized to TNFα-induced apoptosis (195). Moreover, the ceramide level was enhanced by B19V infection and NS1 expression. Therefore, a connection between the apoptotic pathways activated by TNFα and NS1 in B19V-infected human erythroid progenitor cells was proposed.

B19V NS1 has been shown to induce apoptosis in non-permissive cell lines as well (89, 131, 171). In addition, expressing *NS1*-transgene in mice under the erythroid lineage-specific GATA-1 promoter was demonstrated to be embryonic lethal as a result of fatal anemia (44). In non-permissive liver-derived cell types, both B19V inoculation and NS1 expression were shown to activate caspase-3 and -9, but not caspase-8 (171, 172). Treatment of transfected cells with inhibitors of caspase-3 or -9 significantly inhibited apoptosis. Neutralization of TNFα or Fas ligand had no effect on apoptosis induced in liver cells. In monkey epithelial cells COS-7,

expression of NS1 induced an increased level of apoptosis (89). Consistent with the results from liver cells, the increased expression of p53, the pro-apoptotic Bcl-2 members Bax, Bad and activation of caspase-3 and caspase-9, but not the activation of caspase-8 or Fas, were detected in the NS1-transfected cells. Furthermore, a p53 inhibitor abolished activation of caspase-9 and apoptosis was significantly diminished by the caspase-9 inhibitor (89). Thus, NS1 appears to induce intrinsic mitochondrion-mediated apoptosis in non-permissive cells.

The B19V NS1 protein is a multifunctional protein during the virus life cycle (65, 76, 130, 178, 196). Loss-of-function mutations engineered into the nucleoside triphosphate (NTP)-binding domain of NS1 significantly rescued cells from NS1-induced apoptosis without having any effect on NS1-induced activation of IL-6 gene expression, which is mediated by NF-κB (131). Furthermore, using pentoxifylline, an inhibitor of NF-κB activation, the NF-κB-mediated IL-6 activation by NS1 was shown to be uncoupled from the apoptotic pathway. Thus, induction of apoptosis by NS1, at least in UT-7/Epo-S1 cells, is a separate function from trans-activation. The loss-of-function mutation of the NTP-binding site of NS1 also significantly decreased apoptosis in HepG2 cells (171). Therefore, the NTP-binding motif of the B19V NS1 is required for NS1-induced apoptosis in both B19V semi-permissive and non-permissive cell lines.

Overall, B19V NS1 induced apoptosis is characterized by caspase activation and DNA fragmentation. The extrinsic pathway, TNFα-induced activation of this pathway in particular, is thought to be responsible for NS1-induced apoptosis in permissive cells; while in non-permissive cells, the mitochondrion-mediated intrinsic pathway is activated. Nevertheless, the NTP-binding motif of NS1 is the only domain identified to be required for inducing apoptosis in both permissive and non-permissive cells. Based on above evidence, NS1 has long been thought to be the only viral protein of B19V that induces apoptosis during B19V infection. However, the NS1-induced apoptosis could be exaggerated in both non-permissive and semi-permissive cells as the kinetics of NS1 expression does not correlate with that of induction of apoptosis during B19V infection (134).

Using $CD36^+$ erythroid progenitor cells ex vivo expanded from primary $CD34^+$ hematopoietic stem cells (222), we have identified that the B19V small nonstructural protein 11kDa as a novel inducer of apoptosis during B19V infection, which is mediated through caspase-10 activation (Chapter 2) (38). The 11kDa is expressed predominantly in the cytoplasm during B19V infection at a level at least 100 times more than NS1, which is solely expressed in the nucleus during the course of infection in $CD36^+$ erythroid progenitor cells. By further knock-down of 11kDa expression using antisense oligos, we confirmed that the 11kDa plays a key role in killing $CD36^+$ erythroid progenitor cells during B19V infection. Interestingly, 11kDa was reported to interact with growth factor receptor-bound protein 2 (Grb2) via the SH3 domain binding motif in vitro (71). The mechanism underlying B19V 11kDa induced apoptosis, and especially the potential significance of the 11kDa-Grb2 interaction warrants further investigation.

The G2/M cell cycle arrest induced during B19V infection is observed in both primary $CD36^+$ erythroid progenitor cells(195) and the cell line UT7/Epo-S1 (135). In UT7/Epo-S1 cells, B19V infection induced an accumulation of cyclin A, cyclin B1, and phosphorylated cdc2 and was accompanied by an up-regulation in the kinase activity of the cdc2-cyclin B1 complex, which is consistent with G2/M check point arrest (135). In concert, degradation of nuclear lamina and phosphorylation of histone H3 and H1, markers of M-phase, were not seen in B19V-infected cells. Moreover, accumulation of cyclin B1 was persistently localized in the cytoplasm, but not in the nucleus, suggesting that B19V infection contributes to the suppression of the nuclear import of cyclin B1.

G0/G1 arrest was also demonstrated in B19V-infected UT7/Epo-S1 cells with application of the mitotic inhibitor paclitaxel (133). NS1-expressing UT7/Epo-S1 and 293T cells were shown to undergo ell cycle arrest at G0/G1 rather than G2/M check point. NS1 expression significantly increased $p21^{WAF1}$ expression, a cyclin-dependent kinase inhibitor that induces G0/G1 arrest. In addition, G0/G1 arrest mediated by NS1 was proposed to be a prerequisite for the apoptosis of erythroid progenitor cells during B19 virus infection. In monkey epithelial cells COS-7,

expression of NS1 also induced G0/G1 check point arrest, accompanied by an increased level of apoptosis (89). The expression of p53 and its downstream cell cycle kinase inhibitors $p16^{INK4}$ and $p21^{WAF1}$ were up-regulated in the NS1-transfected cells. Given the requirement of S-phase for the replication of parvoviruses, the role of NS1-induced G0/G1 arrest in the B19V life cell cycle needs to be clarified.

G2/M arrest appears to be important for B19V infection, as inhibition of G2/M arrest by caffeine significantly decreased the expression of NS1 (133). However, the mechanism underlying B19V infection-induced G2/M cell cycle arrest, especially which viral components are involved, was uncertain. In our recent work, we found that the cell cycle arrest occurred as one of the earliest events during infection (134) (Chen AY & Qiu J, unpublished data). While UV-inactivated B19V did not express NS1, it induced G2/M arrest at a level similar to that induced by the infectious virus (133), indicating that the viral genome might paly an improtant role in the cells cycel arrest. Expression of B19V viral proteins (NS1, VP1, VP2, 11kDa and 7.5kDa) in UT7/Epo-S1 cells by transfection did not change the cell cycle pattern. However, transfection of a viral sequence containing half of the left hand inverted terminal repeat did partially produce a G2/M arrest (Chen AY & Qiu J, unpublished data). Only recently, a CpG oligodeoxynucleotide 2006, containing a consensus sequence located in the P6-promoter region of B19V genome (5'-GTTTTGT-3'), directly inhibited the growth of burst-forming erythroid (BFU-E) cells, resulting in the accumulation of cells in the S and G2/M phases and increased cell size and frequency of apoptotic cells (83). Therefore, the B19V viral genome seems to play an important role in arresting the cell cycle at G2/M.

Overall, apoptosis is the programmed cell death pathway underlying B19V infection of erythroid progenitors. Viral proteins, NS1 and 11kDa in particular, are responsible for promoting the apoptotic process; however, the 11kDa protein is likely the major apoptotic inducer, considering it is expressed at a level 100 times more than that of NS1 during B19V infection. Other to-be-identified factors, such as the viral genome and the 7.5kDa small nonstructural

protein, may also contribute to ensure the cell death outcome. G2/M cell cycle arrest by the B19V genome occurs early during infection and may contribute to the CPE during the early phase of B19V infection. Though the underlying mechanism is largely unknown, a viral genome-induced, DNA damage response-mediated pathway is likely involved.

Amdovirus

AMDV is the first parvovirus known to utilize caspase activity to facilitate its replication (16, 17). AMDV infection induces caspase activation and result in apoptotic cell death (17). Pretreatment of infected cells with caspase-3 or broad-spectrum caspase inhibitors not only prevented apoptosis but also caused a reduction [by 2 log(10)] in production of progeny infectious viruses compared with untreated controls. Thus, permissive replication of AMDV in vitro in Crandel Feline Kidney (CrFK) cells depends upon activation of caspase-3. Furthermore, active caspase was shown to be required to specifically cleave NS1 protein at two sites, aa227 (INTD↓S) and aa285 (DQTD↓S), and the cleavage products were crucial for the replication of AMDV genome (16). Importantly, the NS1 products could be identified in AMDV-infected cells but were not present in infected cells pretreated with caspase inhibitors. When the two caspase cleavage sites were mutated (D to E) in an infectious clone, replication of the clones containing either of these mutations was reduced by 3-4 log(10)-fold compared with that of the wild-type clone, and the clone with both mutations was replication defective. Mechanistically, immunofluorescence staining demonstrated that the cleavage was required for nuclear localization of NS1.

Our recent work further demonstrated the critical role of caspase activation during productive infection of AMDV. We proved that expression of the viral capsid proteins alone can activate caspases, including caspase-10 which may serve as an initiator (42). In vitro caspase cleavage assays showed that the effector caspase-7 specifically cleaved the capsid protein VP2 after D420. AMDV mutants that are resistant to caspase-mediated capsid cleavage increased

virus production by approximately 3-5 folds in CrFK cells. Thus, caspase-mediated specific cleavage of capsid proteins might have a role in regulating persistent infection of AMDV in animals. Collectively, caspase activation plays multiple roles in infection of AMDV through both promoting replication of the viral genome and limiting capsid production.

The S-phase of the cell cycle was shown to be required for the expression of AMDV NS1 protein (155). Cells that progressed through S-phase showed a characteristic binary pattern of cell cycle disturbance caused by AMDV infection. While a small portion of NS1-expressing cells escaped the G2/M cell cycle arrest and progressed to the G0/G1 phase, the majority were arrested at a post-mitotic phase with DNA content higher than 4N. Intriguingly, active DNA synthesis was detected in cells arrested at the post-mitotic phase, which implies the potential role of post-mitotic phase arrest for AMDV genome replication. Nevertheless, the nature of the post mitotic DNA content in arrested cells, whether of host or viral origin, is not clear. Which viral components are responsible for the cell cycle arrest still remains to be determined.

In conclusion, apoptosis, and in particular, activated caspases, regulates AMDV infection by specific cleavage of both NS1 and capsid proteins. Infected cells with apparent cell cycle arrest still support AMDV replication.

Bocavirus

The importance of bocavirus infection was raised with the emergence of human bocavirus (HBoV). HBoV infection is thought to be associated with pneumonia, and possibly gastroenteritis, mainly in children (5, 8, 99). As the in vitro infection of HBoV is far from efficient (64), it is currently difficult to reproduce HBoV infection in routine laboratory settings. The genetic map of HBoV1 was recently described and confirmed to be very close to that of MVC (36, 64). Therefore, the study of bocavirus-induced CPE is basically carried out with the two other members of bocavirus, namely minute virus of canines (MVC) and bovine parvovirus (BPV) (37, 175).

Significant CPE has been observed during in vitro infection of Walter Reed canine cell/3873D (WRD) cells by MVC (19, 204). We have established an MVC infectious clone that produces infectious virus efficiently (204). We took advantage of the MVC in vitro infection system as a model for the bocavirus genus and explored the molecular mechanism underlying the cell death induced during bocavirus infection (37). As shown in Chapter 3, we found that MVC infection triggered replication-dependent, mitochondrion-mediated apoptosis, which can be blocked by a pan-caspase inhibitor. Moreover, the level of cell death correlated closely with the level of MVC replication. Expression of viral proteins individually or in combination failed to induce cell death in transfected cells.

Along with apoptosis, we also observed a progressive cell cycle arrest of infected WRD cells (37). At around 18 hrs after infection with MVC, NS1-expressing WRD cells showed a single widened cell cycle peak with a plateau at S-phase, which progressed into prolonged G2/M arrest. The DNA content of NS1-expressing WRD cells did increase to slightly higher than 4N at G2/M arrest. We believe this finding was the result of the replicated viral genome, which was quantified to be approximately 1/8 the amount of the human genome during active replication at 48 hrs post-infection. UV-inactivated MVC also induced cell cycle arrest at the G2/M but not S-phase. The cell cycle was gradually resolved without inducing significant level of cell death. Moreover, when transfected with a panel of mutants of the MVC infectious clone, MVC viral protein expression did not induce either apoptosis or cell cycle arrest, while the genome alone induced G2/M arrest, even when half of the left terminal repeat structure was deleted. The S-phase plateau, which has not been seen in other members of *Parvovirinae*, appeared only when active MVC replication took place.

In contrast, CPE induced during BPV infection was shown to be mediated by necrosis rather than apoptosis (1). With the use of embryonic bovine tracheal cells, BPV infection did not cause alterations in nuclear morphology, membrane changes, apoptotic body formation, membrane phosphatidylserine inversions, caspase activation or cellular DNA fragmentation. On

the other hand, at the end of the virus replication cycle, infected cells released viral hemagglutinin and infectious virus particles, as would be expected from cell membrane failure. Moreover, the infected cells released lactate dehydrogenase, a marker of necrosis, which directly correlated with virus production. Furthermore, assessment of mitochondrial dehydrogenase activity was consistent with cell death by necrosis.

Collectively, bocavirus infection induces either apoptosis or necrosis depending on the type of virus. Cell cycle manipulation by bocavirus is unique in that the S-phase plateau in early infection progresses into G2/M arrest at a later stage.

Dependovirus

AAVs have not been associated with any disease in humans (13). In fact, recombinant AAV has been favorably emphasized as a vector for human gene therapy (197, 198). A series of reports emerged recently that investigated the cell death induced by AAV infection as well as the underlying mechanism (68, 179, 211). Identification of the AAV-mediated killing of cells lacking p53 activity has opened up the exploration of the oncolytic potential of AAV (179). The p53-p21-phosphorylated retinoblastoma protein (pRb) pathway protects normal cells from AAV induced apoptosis (77). The lack of this pathway, due to loss or mutation of p53, p21 or pRb, sensitized cells, particularly tumor cells, to AAV infection-induced apoptosis. Moreover, DNA damage effector kinase Chk1 was also suggested to be the mediator of apoptotic cell death induced during AAV infection of p53-deficient cells (95). In addition, it was reported that the nonstructural protein Rep78 of AAV2, independent of p53, induced apoptosis with activation of a caspase cascade (189).

While apoptotic cell death was attributed to the activation of the caspase cascade, emphasis was placed on mechanistically linking the DNA damage response induced during AAV infection to cell cycle regulation and p53-independent cell death. G2/M arrest was observed during AAV infection, but intriguingly not in $ATM^{-/-}$ cells (179). S-phase progression of

infected cells was inhibited by AAV Rep78 via hypophosphorylation of Rb (187). In addition, the AAV2 genome was shown to trigger DNA damage signaling that resembles the response to an aberrant cellular DNA replication fork (96). The formation of DNA damage response foci induced by the AAV genome strictly depended on ATR (ATM and Rad3-related protein), Chk1 and DNA topoisomerase 2-binding protein 1 but not ATM or NBS1 (96). The p5 promoter sequence of AAV2 was identified to be responsible for inducing the host DNA damage response, which leads to the G2/M arrest (73). Furthermore, in p53-deficient cells, UV-inactivated AAV2 triggered mitotic catastrophe associated with a dramatic Chk1-dependent overduplication of centrioles and the consequent formation of multiple spindle poles in mitosis (90). In p53-proficient cells, H2AX was indispensible for the formation and maintenance of DNA repair foci induced by stalled replication and p21-mediated cell cycle arrest (74). Moreover, the activation of H2AX was shown to be the result of ATR overactivation and diffusion but independent of ATM.

AAV preferentially induces apoptotic cell death in p53-deficient cells, which lack the ability to maintain prolonged G2/M arrest via Chk1 mediated mitotic catastrophe. In p53-proficient cells, AAV infection induced a G2/M arrest that was maintained via the ATR-Chk1-H2AX-p53-p21 pathway preventing significant cell death. During co-infection with adenovirus, however, replication of the AAV2 genome induced a DNA damage response through activation of the primary mediator DNA-PKCs (47, 191).

Parvovirus

Cell death induced by members in the genus *Parvovirus* is cell type dependent. In tissue samples of cats and dogs with panleukopenia and enteritis, respectively, apoptosis has been shown to contribute significantly to the widespread tissue damage caused by parvovirus infection (12). Apoptotic cell death induced by H-1 parvovirus (H-1PV) has been reported (153, 181, 184); however, necrosis also has been shown to mediate the H-1PV-induced CPE in apoptosis-resistant cell types (63), and MVM-induced CPE in permissive murine A9 cells (149).

The oncolytic potential of rodent parvoviruses, particularly MVM and H-1PV, has drawn attention for decades. A rich body of studies has emphasized the CPE induced by MVM and H-1PV, which is selectively seen in tumorized cells, but not their normal counterparts. The selective killing of tumorized cells by MVM and H-1PV was shown in vitro in cultured SV40-transformed cells over 20 years ago (41, 137). A series of animal experiments showed the suppressive effect of MVM and H-1PV on different tumors or tumor grafts (102). Stimulation of the parvovirus life cycle, or lytic activation in tumorized cells vs. normal counterparts, was proposed as the mechanism behind the oncolytic function based on the observation that a higher level of viral replication and production was achieved in tumorized cells than in non-transformed cells (49, 50). This hypothesis is sound given that S-phase, which is pivotal for parvovirus replication, is more active in tumorized cells. On the other hand, the NS1 protein expression level and phosphorylation status, which differs in tumorized cells vs. their normal counterparts, may also contribute to the selective killing function (54, 136, 146, 147).

The CPE induced by MVM infection, shown mainly to affect micro and intermediate filaments of the cytoskeleton network, while the nuclear lamina and microtubules remain intact throughout infection (148), is mainly caused by the activity of NS1 (48). The interaction of MVM NS1 and casein kinase II (CKII) was revealed to mediate CKII-dependent cytoskeletal alterations and non-apoptotic cell death in murine A9 fibroblasts (150). NS1 acted as an adaptor molecule, linking the cellular protein kinase CKIIα to tropomyosin and thus modulating the substrate specificity of the kinase. This action results in an altered tropomyosin phosphorylation pattern both in vitro and in living cells. Moreover, NS1 mutants that abolished binding with either CKIIα or tropomyosin lost the capacity of inducing CPE. The fusion peptide, in which the tropomyosin-binding domain of NS1 and CKIIα are physically linked, was able to mimic NS1 in its ability to induce death of transformed MVM-permissive cells. In addition, the Raf-1 signaling control of nuclear transport was suggested to be the target during MVM infection-induced oncolysis (182).

As for H-1PV, necrosis was detected in infected glioma cells which are resistant to cisplatin and TRAIL-induced apoptosis. H-1PV has been found to kill glioma cells via a non-apoptotic cell death mechanism mediated by cathepsins (63). Lysosomal membrane permeabilization and the resulting release of lysosomal enzymes, and in particular cathepsins, into the cytosol is the main pathway to mediate this type of cell death (72, 82). In contrast, in a recent report, H-1PV NS1 was shown to induce apoptotic cell death via induction of reactive oxygen species in 293 cells, which is inconsistent with the observation in H-1PV infection of NB324K, an SV40-transformed human cell line (88). Inhibition of reactive oxygen species by a different reducing compound significantly decreased NS1-induced apoptosis. More importantly, H-1PV kills human hepatocellular carcinoma cell line (QGY-7703) cells by a non-apoptotic process, though a cDNA microarray analysis of H-1 PV-infected cells showed that genes involved in signal transduction, apoptosis, DNA replication, DNA repair, DNA binding and transcription were differentially expressed after H-1PV infection (112).

As seen in other genera, members of the genus *Parvovirus* are also able to induce cell cycle arrest during infection. An increased S/G2/M-phase population was observed during MVM infection (7, 156-158). G2/M arrest was also detected during H-1PV infection (88). MVM-induced cell cycle arrest in S-phase was shown to be p53-dependent but $p21^{cip1}$-independent, whereas the arrest in G2 was dependent on both p53 and its downstream effector $p21^{cip1}$ (158). The MVM NS1 protein alone was able to reproduce cell cycle arrest as seen during MVM infection (7, 158). An early study implied one of the possible mechanisms underlying MVM NS1-induced cell cycle arrest was the direct nicking of the host cell chromatin by NS1, which took place hours before the cell cycle arrest (157). The damaged chromatin DNA might induce a DNA damage response, which in turn stalls the cell cycle for repair. Indeed, a DNA damage response, together with cell cycle arrest and apoptosis, was detected during H-1PV infection (88), as well as during MVM infection (Pintel D, personal communication). However, whether the

viral genome or the nicked host chromatin triggered the DNA damage response remains unanswered.

Taken together, the CPE induced by members in the genus *Parvovirus* could be either necrosis or apoptosis, depending on the virus and cell type. The NS1 protein clearly plays a role in inducing cell death and cell cycle arrest of infected cells via multiple strategies.

Discussion

Parvoviruses induce both cell death and cell cycle arrest during infection. While necrosis was reported during BPV, MVM and H-1PV infection, apoptosis has been demonstrated as the major pathway mediating parvovirus infection-induced cell death. The cell cycle perturbation during parvovirus infection mainly appears as G2/M-phase arrest. However, S-phase plateau was also reported during MVC infection, through an accumulated/prolonged S-phase (37).

From an organismal standpoint, apoptosis induced during virus infection is thought to be a means for the host to defend itself against viral invasion (207). However, apoptosis may also represent a crucial step in the viral life cell cycle and pathogenesis (15, 145) as apoptotic cell death allows for viral release and induces less immune response than cell lysis, which releases cellular components and triggers an inflammation response (84). In some cases, caspase activation is clearly required to regulate DNA replication and virion production through caspase-mediated specific cleavage of AMDV NS1 and VP2 (16, 17). Apoptotic cell death apparently is a direct cause of diseases during parvovirus infection, especially anemia and fetal death induced during B19V infection (6, 29), and possibly gastroenteritis and pneumonia caused by parvovirus (167). The oncolytic effect of AAV relies on the selective induction of apoptosis in p53-deficient or tumorized cells (170). It may not be critical for the virus life cycle in natural infection with adenovirus (191); however, its potential implication is valuable. MVM and H-1PV can induce cell death in a number of tumor cells while having no cytotoxic effect on healthy tissues. The

mechanism underlying specific cell death of tumorized cells by these viruses is still unclear. H-1PV infection can induce either necrosis or apoptosis, depending on the types of tumorized cells (129, 180, 181).

Virus infection-induced cell cycle arrest has been extensively documented both in DNA and RNA viruses (56, 228). The S-phase is generally critical for parvovirus replication, which takes place in the nucleus and utilizes host polymerase (66, 124, 183, 221). H-1PV protein synthesis coincides with the cellular DNA synthesis (210), while MVM replication has been shown to require mitotically active cells (81). B19V showed a maximal rate of transcription preceding the onset of S-phase dependent replication of the viral genome (24). The prevention of S-phase was reported to decrease the gene targeting of AAV2 (213). Though AAV2 infection has not been reported to elicit S-phase arrest (87, 96, 220), the AAV2 Rep78 was shown to inhibit Cdc25A and arrest the transfected cells at S-phase (14). Thus, it is reasonable to speculate that parvoviruses have the common feature of prolonging the S- or G2-phase in favor of their replication. The G2/M-phase arrest is more likely a pseudo-S-phase, with stalled host DNA replication but an active environment to facilitate viral DNA replication (56). The post-mitotic arrest seen during AMDV infection indicates that the active DNA replication environment is maintained at cell cycle check point arrest (155). In concert, active BrdU incorporation was seen in parvovirus-infected cells with apparent G2/M-phase arrest (157, 187).

Cell cycle disturbance and programmed cell death are two relatively separate events; however, increasing evidence suggests their crosstalk. Prolonged cell cycle arrest can induce apoptosis (122, 216) that is mediated through cyclin/cyclin dependent kinase and Bcl2 family proteins (231). A balance between cell cycle checkpoint maintenance and apoptosis is finely regulated during DNA damage to ensure the accuracy of replication and minimize the unwanted loss (46). The terminal repeat structures of parvoviruses can be easily detected as damaged DNA, thus triggering a DNA damage response, which in turn induces cell cycle arrest for “repair”. As replication of parvovirus requires cellular DNA polymerase (53), parvovirus replication favors

cells in S-phase in which active polymerase and other replication factors are present (143). It is logical to hypothesize that parvoviruses use parts of the single-stranded genome, especially the terminal repeats and/or the left hand promoter region, as triggers to induce a DNA damage response to prolong the S- and G2-phase during the early stage of infection, but not induce apoptosis. At this stage, active DNA polymerase and other necessary replication factors are present and used for genome replication. This hypothesis is supported by the fact that inhibition of DNA damage response significantly reduced AAV Rep expression (191), as well as MVC (Luo Y & Qiu J, unpublished) and MVM replication (Pintel D, personal communication). At the late stage of infection, the collaboration of “irreparable damage” and viral pro-apoptotic protein breaks the balance created by checkpoint arrest and leads to apoptosis, which is beneficial for viral egress. In addition, apoptosis is also likely contributed by a cellular mechanism to defend virus infection if the virus infection cannot be cleaned or limited in the cells.

Concluding remarks:

The CPE induced during parvovirus infection is mediated either by apoptosis or necrosis, and is contributed by cell cycle arrest, mostly at G2/M. While cell cycle arrest and caspase activation create an optimum environment for parvovirus replication at the early stage of infection, the ultimate induction of apoptosis is believed to be beneficial for virus egress at the late stage. The mechanism underlying induction of cell cycle arrest is likely due to a DNA damage response induced by the viral genome via the terminal repeats and left hand promoter region. Yet, apoptosis could be the ultimate consequence of the pro-apoptotic activity of viral proteins, prolonged cell cycle arrest and irreparable DNA damage response to ensure the optimum release of virion. Interestingly, parvovirus infection also uses a novel necrotic mechanism to induce cell death when apoptotic cell death cannot be achieved during virus infection, as seen in H-1PV infection, where the cell death mechanism of H-1PV varies depending on the host. Thus, parvovirus infection may provide a unique model to investigate the

virus-host interaction network that fine tunes the balance among DNA damage response, viral DNA replication, cell cycle arrest and cell death.

Part II. Human Parvovirus B19

B19V was discovered by Australian scientist Yvonne Cossart in 1975 (51). It is a non-enveloped, icosahedral virus with a size of about 20-25 nm. B19V has a linear single-stranded DNA (ssDNA) genome of 5.6 kb, with terminal repeats at both ends (Fig.1-1). Approximately equal numbers of positive and negative stranded DNA are packaged in separate virions.

Replication of parvoviruses was only studied in AAV and MVM. A rolling hairpin replication model of the parvovirus genome has been confirmed in AAV and MVM DNA replication (53, 102) (Fig. 1-2). Briefly, the free 3'-OH group of the left terminal repeat serves as a primer, as a result of the hairpin structure, to produce a double-stranded monomer replication form (mRF). Viral NS1 protein then recognizes and specifically cleaves the mRF. The 3'-OH of the nicked site in turn primes the strand displacement DNA synthesis, yielding an intermediate with an open right-hand end. Via a process called "reinitiation", the open end of the intermediate forms a double-hairpin conformation. Consequently, another round of strand displacement DNA synthesis takes place to produce the double replication form (dRF).

Study of B19V replication has been limited by the lack of a highly permissive culture system and an infectious clone until recently (222, 230). The replication mechanism of the B19V genome is not yet understood, though a model of replication, which is similar to the "rolling-hairpin" model, was proposed (Fig. 1-2) (53). The terminal hairpin structures of a single stranded B19V genome were observed under the electron microscope (10) and were confirmed by priming DNA synthesis using *E. coli.* DNA polymerase in vitro (52). Using blood samples from patients with acute B19V infection, three major replication forms of B19V, dRF, mRF and ssDNA genome, were shown (109). Depending on the sequence variation, the mRF sometimes was susceptible to BamHI digestion, producing two smaller fragments at 3.9k and 1.5k bps respectively. The infectious clone was then shown clearly to produce mRF at a size of ~ 5.6 k bps, which was digested by BamHI to two fragments, 4.1 and 1.5k bps respectively, in

transfection of UT7/Epo-S1 cells. We recently showed that in the presence of adenovirus or adenovirus gene products (E2a, E4orf6, and VA RNA genes), the B19V genome can replicate in 293 cells, which are non-permissive to B19V infection, and produce infectious virus (80). Using this replication system, our lab identified the terminal resolution site and the NS1 binding site on the right terminal palindrome of the viral genome, which is composed of a minimal origin of replication spanning 67 nucleotides.

A single pre-mRNA is transcribed from the single promoter at unit 6 during B19V infection. It is extensively processed by alternative splicing and alternative polyadenylation to generate a total of 12 transcripts (114). Blockade of the production of full-length B19V transcripts by the internal polyadenylation site [(pA)p] was previously reported to be a limiting step in B19V permissiveness (113). In the absence of genome replication, internal polyadenylation of B19V RNAs at (pA)p was favored in both permissive and nonpermissive cells. Recently, our lab demonstrated that replication of the B19V genome, however, enhanced read-through of (pA)p and the polyadenylation of B19V transcripts at the distal site [(pA)d] (79). Therefore, replication of the B19V genome facilitates the generation of sufficient full-length transcripts that encode the viral capsid proteins and the essential 11kDa nonstructural protein. Furthermore, polyadenylation of B19V RNAs at (pA)p likely competes with splicing at the second intron (Guan W & Qiu J, unpublished). Thus, replication of the B19V genome is the critical limiting step governing B19V tropism in addition to virus entry.

B19V shows exclusive tropism to erythroid progenitor cells during infection (163, 199). Both the more-primitive erythroid progenitors [burst-forming units-erythroid (BFU-E)] and the more-mature erythroid progenitors [colony-forming units-erythroid (CFU-E)] are susceptible to B19V infection (199). In addition to the primary erythroid progenitor cells, a few cell lines, basically myeloblastoid cell line like UT7/Epo-S1 (135) and KU812Ep6 (127), support B19V replication but at limited efficiency (3,45). Recently, ex vivo expanded $CD36^{+}$ erythroid progenitor cells were reported highly permissive to B19V infection and support active B19V

replication (at least 100-fold increase of the B19V genome) (195, 222). The remarkable tropism of B19V to human erythroid progenitors was previously believed to be due to the receptor, blood-group P antigen (Globoside) (28), and co-receptors, namely KU80 and intergrin α5β1 (127, 138).

Erythropoiesis is the process whereby a fraction of primitive multipotent hematopoietic stem cells ($CD34^+$) commit to the erythroid lineage, forming BFU-Es (early erythroid progenitors), CFU-Es (later erythroid progenitors), normoblasts, erythroblasts, reticulocytes, and ultimately the mature erythrocytes. While the early erythropoiesis is erythropoietin (Epo) independent (till BFU-E), the later stages are all Epo-dependent (from BFU-E→CFU-E, which is highly Epo-responsive) (70).

Erythropoietin (Epo) was shown to be required for susceptibility of human bone marrow cells to B19V infection (206). From this Epo depending, a conclusion was drawn that the target cells of B19V are in erythroid lineage from BFU-Es to erythroblasts, with permissiveness to B19V increasing along differentiation. Thus, the role of Epo for B19V infection was thought mainly to differentiate bone marrow hematopoietic stem cells (HSCs) to the stage of erythroid progenitors. However, it has been shown that Epo is also required for proliferation of UT7/Epo-S1 cells that are B19V semi-permissive cell line cells (135). Hence, the importance of Epo during B19V infection may not be solely for differentiation and maturation of erythroid progenitors. Nevertheless, the precise role of Epo during B19V infection is not clear.

Epo elicits its function via ligation to its receptor EpoR (115). The Epo/EpoR complex formation induces autophosphorylation of Janus kinase 2 (Jak2), which further phosphorylates multiple tyrosine residues on the cytosolic domain of EpoR. The phosphorylation sites serve as docking sites for signaling molecules, e.g., signal transducer and activator of transcription 5A (STAT5A), Phosphoinositide 3-kinase (PI3K), growth factor receptor-bound protein 2 (Grb2), etc. Those signaling molecules further carry out the functions delegated from the Epo/EpoR ligation.

Based on the evidences listed above, we hypothesize that cellular microenvironment is the essential determinant of B19V permissiveness. It is realized only when the cellular environment permits replication of the viral genomes after their entry into cells. Not only is Epo crucial for cell proliferation and differentiation, but also its signaling is directly essential for tuning cellular microenvironment in favor of replication of the B19V genome. In Chapter 4, our studies demonstrate that Epo/EpoR/Jak2 signaling is indeed required for the replication of B19V genome so that confers B19V permissiveness in erythroid progenitor cells. The inhibition of Jak2 phosphorylation by a specific inhibitor or protein level by lentiviral shRNA significantly blocked B19V replication, whereas the cell cycle and viability of the treated cells were not significantly affected.

Fig. 1-1 Transcription map of B19V. The genome of B19V shown in this figure is based on the sequence of isolate J35 (GenBank accession no. AY386330), which is approximately 5.6 kb. The major transcription landmarks include the terminal repeats, P6 promoter, splice donors (D1 and D2) and acceptors (A1-1, A1-2, A2-1, and A2-2) and the (pA)p and (pA)d sites. All 12 major transcripts are listed below the map (designed R1 through R9), with their sizes and encoded proteins shown to the right. RNA transcripts that are polyadenylated at the minor (pA)p site are designated as R1', R2' and R3'.

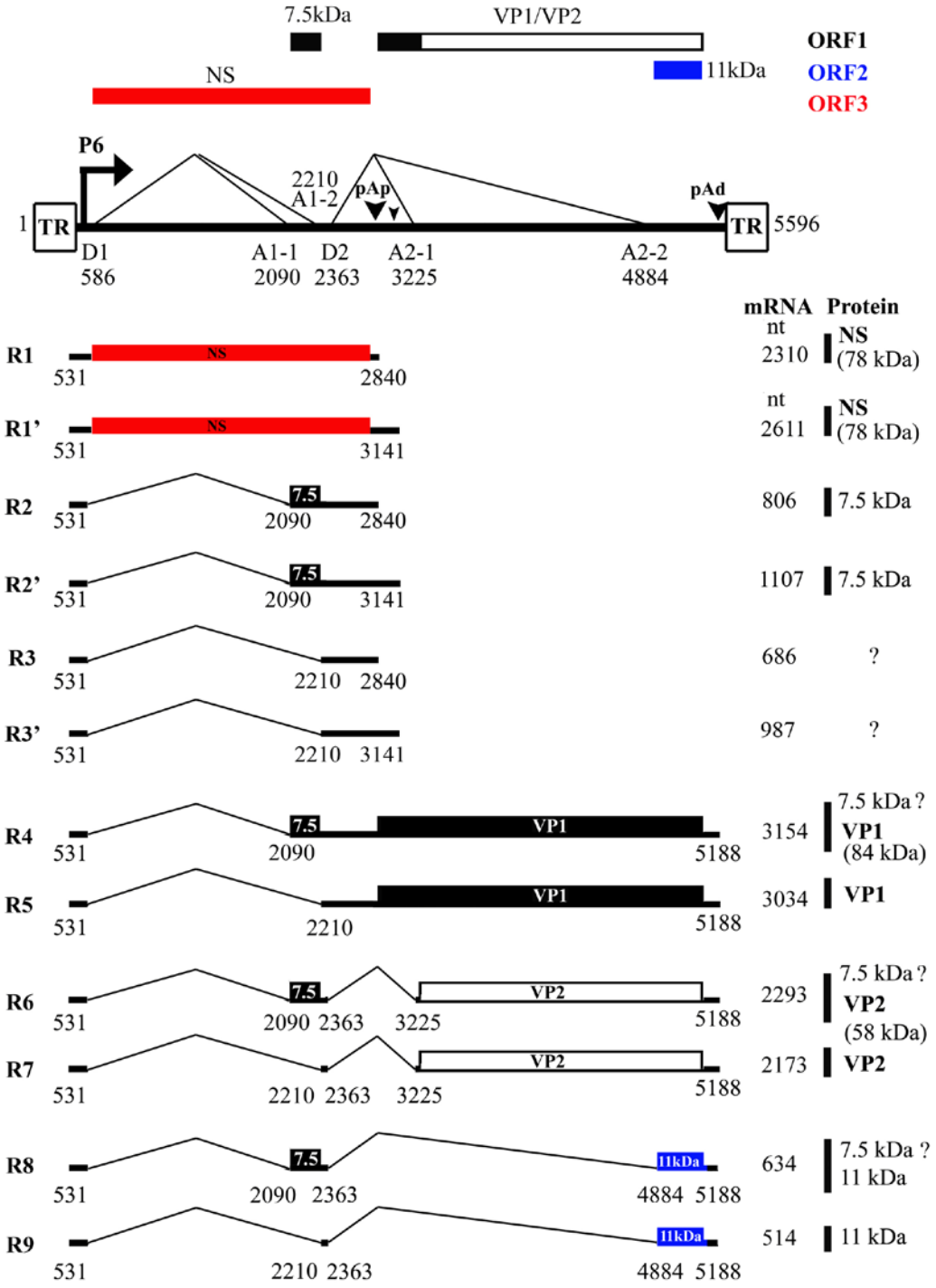
7.5kDa
VP1/VP2
ORF1
NS
11kDa
ORF2
ORF3
P6
2210
A1-2
pAp
pAd
1
TR
TR
5596
D1
586
A1-1
2090
D2
2363
A2-1
3225
A2-2
4884
mRNA
Protein
nt
R1
NS
531
2840
2310
NS
(78 kDa)
R1'
NS
531
3141
2611
NS
(78 kDa)
R2
7.5
531
2090
2840
806
7.5 kDa
R2'
7.5
531
2090
3141
1107
7.5 kDa
R3
531
2210
2840
686
?
R3'
531
2210
3141
987
?
R4
7.5
VP1
531
2090
5188
3154
7.5 kDa ?
VP1
(84 kDa)
R5
VP1
531
2210
5188
3034
VP1
R6
7.5
VP2
531
2090
2363
3225
5188
2293
7.5 kDa ?
VP2
(58 kDa)
R7
VP2
531
2210
2363
3225
5188
2173
VP2
R8
7.5
11kDa
531
2090
2363
4884
5188
634
7.5 kDa ?
11 kDa
R9
11kDa
531
2210
2363
4884
5188
514
11 kDa

Fig. 1-2. Models of parvovirus DNA replication (80). (a) The 3'-OH group of the left hand terminal repeat serves as a primer to initiate the synthesis of viral genome forming a duplex DNA molecule that is covalently closed at one end by the hairpin structure. This procedure yields the mRF. (b) Viral NS1 protein (red filled circle) recognizes the target sequence on terminal repeat and specifically cleaves it. (c) The 3'-OH of the nicked site further primes the DNA synthesis to produce an intermediate with an open end at the right-hand side as shown in (d). (e) The newly synthesized strand is then denatured and reannealed, a.k.a. "reinitiation", to form an intermediate with double-hairpin conformation. (f) Another round of strand displacement synthesis is initiated using the free 3'-OH of the double-hairpin conformation. This step finally yields the dRF. L, L-terminal repeat; R, R-terminal repeat.

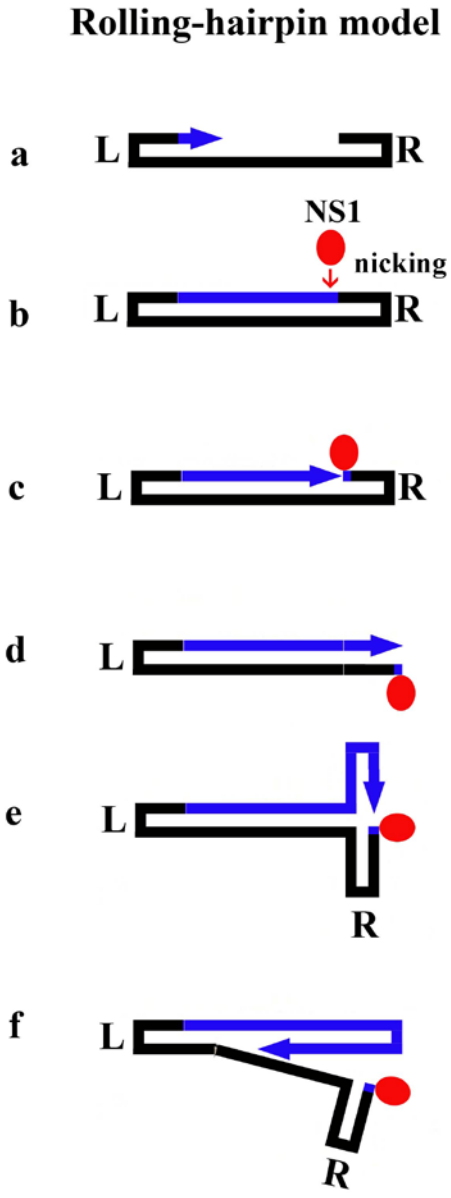
Rolling-hairpin model
a
L
R
NS1
nicking
b
L
R
c
L
R
d
L
e
L
R
f
L
R

Chapter 2

The small 11kDa non-structural protein of human parvovirus B19 plays a key role in inducing apoptosis during B19 virus infection of primary erythroid progenitor cells

Abstract

Human parvovirus B19 (B19V) infection shows a strong erythroid tropism and drastically destroys erythroid progenitor cells, thus leads to most of the disease outcomes associated with B19V infection. In this study, we systematically examined the three B19V nonstructural proteins, 7.5kDa, 11kDa and NS1, for their function in inducing apoptosis in transfection of primary ex vivo expanded erythroid progenitor cells, in comparison with apoptosis induced during B19V infection. Our results show that 11kDa is a more significant inducer of apoptosis than NS1, while 7.5kDa does not induce apoptosis. Furthermore, we determined that caspase-10, an initiator caspase in death receptor signaling, is the most active caspase in apoptotic erythroid progenitors induced by 11kDa and NS1 as well as during B19V infection. More importantly, cytoplasm-localized 11kDa is expressed at least 100 times more than nucleus-localized NS1 at the protein level in primary erythroid progenitor cells infected with B19V; and inhibition of 11kDa expression using anti-sense oligos targeting specifically to the 11kDa-encoding mRNAs reduce apoptosis significantly during B19V infection of erythroid progenitor cells. Taken together, our results demonstrate for the first time that 11kDa plays a key role in executing erythroid progenitor cell death during B19V infection.

Introduction

B19V infection is the cause of "fifth disease", a highly contagious infection of childhood. B19V infection can result in serious and occasionally fatal hematologic diseases in susceptible patients (227). In patients with increased destruction of red cells and a high demand for the production of erythrocytes, acute B19V infection can cause transient aplastic crisis. Pure red-cell aplasia can also be a manifestation of persistent B19V infection in immunocompromised or immunodeficient patients.

B19V belongs to the genus *Erythrovirus* in the family *Parvoviridae* (208). Spanned by two identical terminal hairpin repeats, the 5.6-kb linear single stranded DNA genome of B19V encodes a single nonstructural protein (NS1), and two capsid proteins (VP1 and VP2). Two other smaller non-structural proteins, 7.5kDa and 11kDa, have been detected during B19V infection (118, 200). The 11kDa protein is translated from a small left-ORF that overlaps with the C-terminal of the VP1/VP2 ORF in a different frame. The 7.5kDa protein is translated from a small mid-ORF. NS1 is a multiple functional polypeptide essential to viral replication and regulation of gene expression that is cytotoxic to host cells (27, 131, 161, 178). The 11kDa protein has been shown to have a role in virion production and trafficking in infected cells, while the 7.5kDa protein has not yet been reported to have functions during B19V infection (229).

B19V shows extreme tropism for erythroid progenitor colony forming unit-erythroid cells (CFU-E) and burst-forming unit-erythroid cells (BFU-E) in the bone marrow of patients (162, 163, 199). Disease manifestations of B19V infection, as seen in transient aplastic crisis, pure red cell aplasia and hydrops fetalis, are due to the direct cytotoxicity of the virus (29), a direct outcome of the cell death of erythroid progenitors that are targets of B19V replication. A progressive host cell apoptosis has been identified during B19V infection of primary erythroid progenitor cells and megakaryoblastoid cell lines (131, 195). NS1 expression in megakaryoblastoid cell lines has been associated with B19V-induced apoptosis (131, 195); however, the kinetics of NS1 expression has not correlated with that of induced apoptosis during B19V infection of

megakaryoblastoid cell line UT7/Epo-S1, which are semi-permissive to B19V infection (45, 135). These findings raise the question about the role of NS1 in inducing apoptosis during B19V infection.

In the present study, we show for the first time that 11kDa is a more significant inducer of apoptotic cell death than NS1 in transfection of primary erythroid progenitor cells. Since 11kDa is expressed at least 100 times more than NS1 at the steady-state protein level in erythroid progenitor cells during B19V infection, we conclude that the B19V infection-induced apoptosis of erythroid progenitor cells, is largely mediated by the small non-structural 11kDa protein.

Materials and Methods

Cells and virus infection:

HeLa cells, 293 cells, K562 cells and UT7/Epo-S1 cells were maintained as previously described (79, 176). Human primary $CD36^+$ erythroid progenitor cells ($CD36^+$ EPCs) were expanded ex vivo in the expansion medium as previously described (79, 222). Large numbers of $CD36^+$ EPCs, which were used for either transfection or B19V infection, were obtained on day 8 or day 9.

Twenty microliters of B19V viremic plasma that contained 1×10^{12} copies of B19V genome per ml was incubated with 2×10^6 cells, in a volume of 500 µl medium with slow rotation at 4°C for 2 hrs. Infected cells were then cultured in the expansion medium at a concentration of 2×10^5 cells/ml at 37°C with 5% CO_2.

Caspase inhibitors:

Two general caspase inhibitors, pan-caspase fmk Inhibitor Z-VAD-fmk (Z-VAD) and Oph inhibitor Q-VD-Oph (Q-VD), and nine individual caspase inhibitors (caspase-1, -2, -3&7, -4, -6, -8, -9, -10 & -13 inhibitors) were purchased from R&D Systems (Minneapolis, MN).

Morpholino oligos:

Three Morpholino anti-sense oligos were designed to specifically target sequences in the region of the AUG translation start site of the 11kDa-encoding mRNAs, which are diagramed in Fig. 2-5A. Their sequences written from 5' to 3' and complementary to the 11kDa-encoding mRNA are as follows: MO-1: TCTTCAGGCTTTTCATATCCATGTC; MO-2: CCATGTCTGTGGTGTTGTTTTGCAT and MO-3: TGTAGAGTTCACGAAACTGGTCTGC. The Morpholino oligos were synthesized at Gene Tools, LLC (Philomath, OR), and Endo-Porter was used for delivery following a manufacturer protocol. A random control Morpholino was used as a control.

Plasmid construction:

NS1, 7.5kDa and 11kDa expression plasmids in mammalian cells: GFP was cloned into pNTAP-B (Strategene) by BamH I and EcoR I as pGFP. Then we cloned the NS1 ORF (nt 616-2631), the 7.5kDa mid-ORF (nt 2090-2305) and the 11kDa ORF (nt 4890-5171) into this pGFP plasmid through EcoR I/Xho I sites as pGFP-NS1, pGFP-7.5kDa and pGFP-11kDa, respectively. pRFPHA, pRFP-NS1HA and pRFP-11kDaHA were constructed by replacing GFP with RFPHA (C-terminal HA tagged red fluorescent protein, DsRed, Clontech), RFP-NS1HA and RFP-11kDaHA (NS1 and 11kDa were HA tagged at C-terminal) in the pGFP, respectively.

Bacterial expression plasmids of glutathione S-transferase (GST) fused B19V proteins: The 11kDa ORF and the N-terminus encoding sequence (nts 616-1158) of the NS1 were cloned into pGEX4T3 (GE Health) as pGEX11kDa and pGEXNS1(aa1-181), respectively.

All the nucleotide (nt) numbers refer to the sequence of the B19V J35 isolate (Genbank accession no.: AY386330).

Reverse transcription (RT)–real time PCR:

A multiplex RT-real time PCR system was performed to detect B19V 11kDa-encoding and NS1-encoding mRNAs, with β-actin mRNA serving as an internal control as previously reported (80, 222).

Production of antisera against B19V non-structural proteins:

GST- fused full length 11kDa (GST-11kDa) and NS1 amino acids (aa) 1-181 [GST-NS1(aa1-181)] were expressed and purified as we previously described (204). Polyclonal production was performed following protocols as previously described (204).

Transfection:

The 293 and Hela cells were transfected with 2 μg of DNA per 60-mm dish using Lipofectamine and Plus reagent (Invitrogen) as previously described (177). K562 cells were electroporated with 2 μg of DNA per 2×10^6 cells using reagent V and program T6 with the Amaxa® Nucleofector® (Lonza Inc.). UT7/Epo-S1 cells and $CD36^+$ EPCs were electroporated with 2 μg of DNA per 2×10^6 cells, using a universal transfection reagent with program X-005 as previously described (79). After transfection, $CD36^+$ EPCs were maintained in the expansion medium (79, 222).

SDS-PAGE, Western blotting and immunofluorescence:

SDS-PAGE, Western blotting and immunofluorescence assay were performed as previously described (174).

Flow cytometry analysis:

AnnexinV/Propidium Iodide (PI) staining: Cells were stained alive with Cy5-conjugated AnnexinV (BD Biosciences) and PI (Sigma) together to detect apoptotic cells according to the manufacturer's instructions (BD Biosciences).

TUNEL (Terminal Deoxynucleotidyl Transferase dUTP Nick End Labeling) assay: TUNEL assay was basically performed according to the manufacturer's protocol (MBL International, MA) with the modification that streptavidin-Cy5 (Jackson ImmunoResearch, PA) was used to develop fluorescence.

FLICA (Fluorochrome Inhibitor of Caspase Assay): Live cells (1×10^6) were stained with respective FAM-labeled FLICA peptide according to the manufacturer's manual (Immunochemistry Tech, MN).

All the samples were analyzed on the three-laser flow cytometer (LSR II, BD Biosciences) within an hour of staining at the Flow Cytometry Core on campus. All flow cytometry data were analyzed using FACS DIVA software (BD Biosciences).

Results

11kDa induces apoptosis in both B19V permissive and nonpermissive cells.

To examine the potential role of 11kDa in inducing apoptosis, we transfected pGFP-11kDa and pGFP plasmids, respectively, into both B19V permissive and nonpermissive cells. The GFP positive (GFP+) population was selectively gated and analyzed in comparison with the GFP negative [GFP(-)] population using AnnexinV/PI double staining. There were significantly more AnnexinV positive (AnnexinV+) cells in GFP-11kDa expressing UT7/Epo-S1, $CD36^+$ EPCs, HeLa and K562 cells than these in GFP control expressing cells (Fig. 2-1 A&B, GFP+), but no significant difference was observed between the GFP-11kDa and GFP expressing 293 cells (Fig. 2-2-1 A&B, GFP+ 293).

In UT7/Epo-S1 cells, the population of AnnexinV+ cells induced by GFP-11kDa reached a high rate of 48.0% at 48 hrs posttransfection in GFP+ cells (Fig. 2-2-1A, GFP+ S1). In contrast, GFP(-) cells in the same sample showed only 5.1% AnnexinV+ cells [Fig. 2-2-1A, GFP(-) S1]. Less than 13.1% of GFP+ cells in the pGFP-transfected cells (as control) were stained with AnnexinV (Fig. 2-2-1B, GFP+ S1). GFP-11kDa induced an average of 37.1% more AnnexinV+ cells in GFP+ cells than in GFP(-) cells at 48 hrs posttransfection (Fig. 2-2-1C, GFP-11kDa S1), indicating that the AnnexinV+ population of GFP+ cells in the pGFP-11kDa-transfected cells is predominately induced by the 11kDa, not the GFP.

The GFP-11kDa also induced a high AnnexinV+ population in $CD36^+$ EPCs that are highly permissive to B19V infection *in vitro* and are the primary cells most closely resembling the CFU-E and BFU-E in the bone marrow of patients (222). Similar to UT7/Epo-S1 cells, GFP-11kDa induced an average of 42.6% more AnnexinV+ cells in GFP+ cells than in GFP(-) cells at 24 hrs posttransfection (Fig. 2-2-1C, GFP-11kDa $CD36^+$). In comparison, pGFP control transfection only resulted in approximately 7% AnnexinV+ cells over the background (Fig. 2-2-1C, GFP $CD36^+$). Notably, we observed a significant amount of background cell death in transfected $CD36^+$ EPCs, which presumably was induced by the electroporation and despite the optimized conditions that allowed us to transfect the $CD36^+$ EPCs. At 24 hrs posttransfection, as much as 30% of the background AnnexinV+ population was detected in GFP(-) cells of pGFP-transfected $CD36^+$ EPCs [Fig. 2-2-1B, GFP(-) $CD36^+$]. This amount increased to more than 50% at 48 hrs posttransfection, which made assessing apoptosis induced by transfection of the GFP-11kDa less accurate (data not shown). Therefore, we chose to assay transfected $CD36^+$ EPCs only at 24 hrs posttransfection.

The 11kDa also induced a significant amount of AnnexinV+ cells in B19V nonpermissive cells, HeLa and K562 cells, in addition to these B19V permissive cells. We observed more than 30% of AnnexinV+ cells in GFP+ population of the pGFP-11kDa-transfected cells of both types at 48 hrs posttransfection (Fig. 2-2-1A, GFP+ HeLa&K562). Conversely, pGFP transfection

Fig. 2-1. Transfection of 11kDa induces apoptosis in both B19V permissive and nonpermissive cells. (A&B) UT7/Epo-S1, $CD36^+$ EPCs, HeLa, K562 and 293 cells were transfected with pGFP-11kDa plasmid **(A)** or pGFP as a control **(B)**. $CD36^+$ EPCs were stained at 24 hrs posttransfection; other cells were stained at 48 hrs posttransfection with AnnexinV/PI double staining, followed by flow cytometry analysis. Both GFP negative [GFP(-)] and positive (GFP+) cell populations were gated to plot cells by PI *vs* AnnexinV. Only a representative experiment is shown, and the percentage of each quadrant is indicated. AnnexinV+ population is a combination of the AnnexinV+/PI+ population (number in the upper right quadrant) with the AnnexinV+/PI(-) population (number in the lower right quadrant). **(C)** The experiments as described in A&B were performed at least three times independently. The percentage value of AnnexinV+/PI+ or Annexin V+/PI(-), as shown in individual panel with indicated cell type, was calculated by subtracting the AnnexinV+/PI+ population or the AnnexinV+/PI(-) population of GFP+ cells by that of GFP(-) cells (background apoptosis). **(D)** UT7/Epo-S1 cells were transfected with pGFP-11kDa and stained with DAPI. Confocal images were taken at a magnification of 60 × (objective lens) with an Eclipse C1 Plus confocal microscope (Nikon). Arrows show apoptotic nuclei, which were enclosed in the apoptotic bodies visualized by GFP fluorescence. S1: UT7/Epo-S1; $CD36^+$: $CD36^+$ EPCs; TX: transfection.

Results that are shown as average ± standard deviation in all the figures are generated from at least three independent experiments.

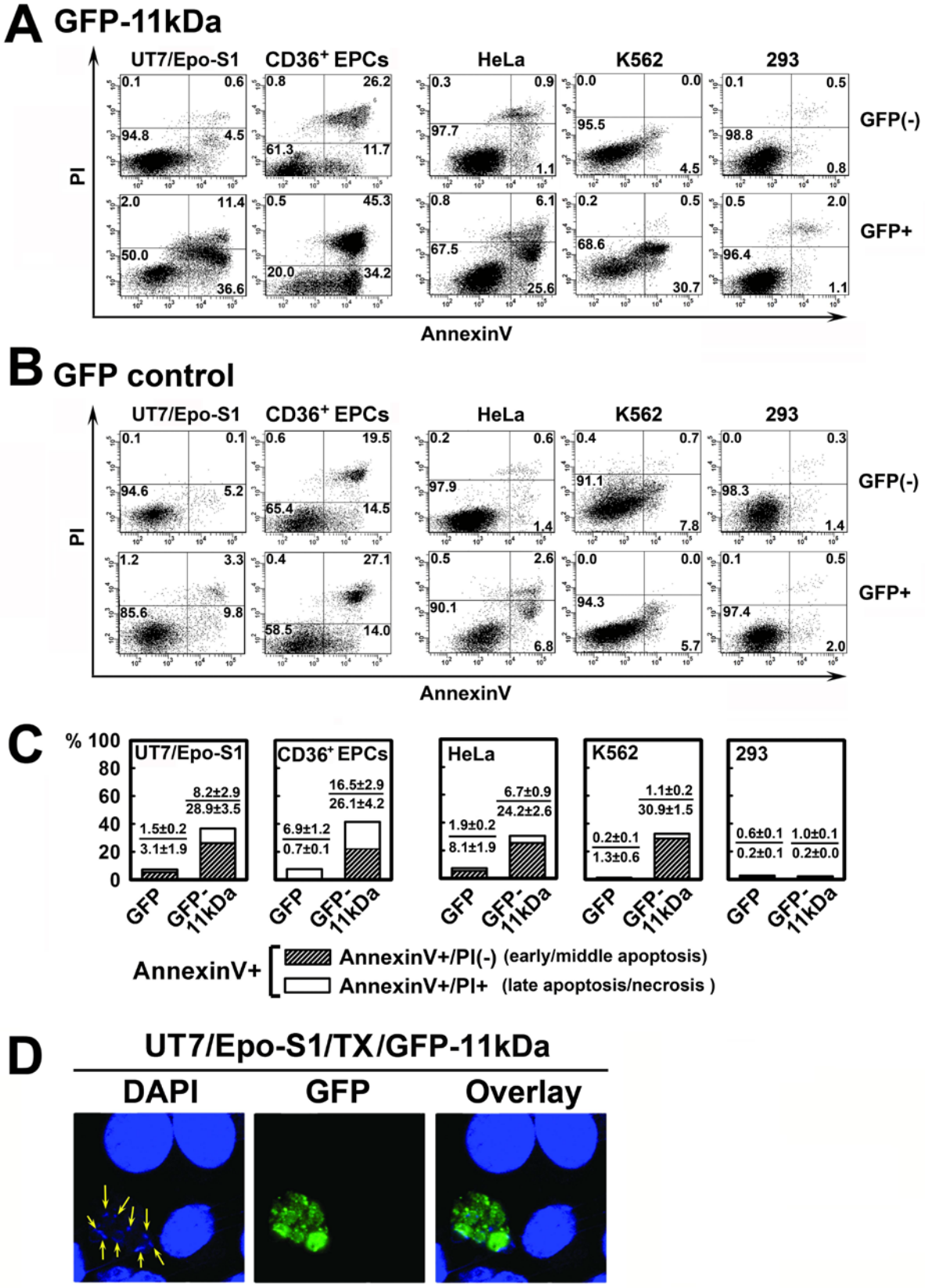
A GFP-11kDa
UT7/Epo-S1
CD36+ EPCs
HeLa
K562
293
GFP(-)
GFP+
PI
AnnexinV
B GFP control
C
% 100
80
60
40
20
0
8.2±2.9
28.9±3.5
1.5±0.2
3.1±1.9
16.5±2.9
26.1±4.2
6.9±1.2
0.7±0.1
6.7±0.9
24.2±2.6
1.9±0.2
8.1±1.9
1.1±0.2
30.9±1.5
0.2±0.1
1.3±0.6
0.6±0.1
0.2±0.1
1.0±0.1
0.2±0.0
GFP
GFP-11kDa
AnnexinV+
AnnexinV+/PI(-) (early/middle apoptosis)
AnnexinV+/PI+ (late apoptosis/necrosis)
D
UT7/Epo-S1/TX/GFP-11kDa
DAPI
GFP
Overlay

alone only induced 10% and 8% of the AnnexinV+ population in GFP+ HeLa and K562 cells, respectively (Fig. 2-2-1B, GFP+ HeLa&K562). However, the GFP-11kDa was not able to induce a significant amount of AnnexinV+ population in 293 cells (Fig. 2-2-1 A&C, 293); E1b-19kDa protein that is expressed in 293 cells perhaps inhibits apoptosis in a way similar to that of Bcl-xL (123, 212). In the pGFP transfection control of all the five cell types, GFP did not significantly induce the AnnexinV+ population in GFP+ cells of transfected cells in comparison with that in GFP(-) cells (Fig. 2-2-1B). When we transfected the $CD36^+$ EPCs, however, we noted a relatively high percentage of AnnexinV+ population in GFP(-) cells of both pGFP-11kDa- and pGFP-transfected cells (Fig. 2-2-1 A&B, $CD36^+$), which indicated background cell death that was caused in part by the electroporation.

The majority of AnnexinV+ cells induced by GFP-11kDa were PI stained negative [AnnexinV+/PI(-)], and thus were in the early or middle stage of apoptosis. Specifically, more than 80% of AnnexinV+ cells were PI stained negative in UT7/Epo-S1, HeLa and K562 cells, and 60% were PI stained negative in $CD36^+$ EPCs [Fig. 2-2-1C, AnnexinV+/PI(-)]. The cell population of AnnexinV+/PI+ is an indicator of either late apoptosis or necrosis (Fig. 2-2-1C, AnnexinV+/PI+). In addition, we directly visualized a representative cell with GFP-11kDa expression with distinct cellular nucleus degradation. We also observed small apoptotic bodies enclosing a degraded nucleus by green fluorescence (Fig. 2-2-1D) (85, 232). Overall, these results suggest that the 11kDa induces cell death with apoptotic features rather than necrosis in both B19V permissive and nonpermissive transfected cells. Further supporting this finding, 11kDa did not induce an AnnexinV+ cell population in 293 cells.

11kDa is a more significant inducer of apoptosis than NS1.

The apoptotic nature of NS1 has not been examined in primary erythroid progenitor cells. We sought to determine which protein, 11kDa or NS1, was more potent in inducing apoptosis in UT7/Epo-S1 cells and $CD36^+$ EPCs. For comparison, we also studied the 7.5kDa,

another small nonstructural protein shown to be expressed during B19V infection but with an unknown function (118).

While the GFP-11kDa and the GFP-NS1 both extensively induced AnnexinV+ cells when transfected to UT7/Epo-S1 cells, the GFP-7.5kDa poorly induced the AnnexinV+ population in GFP+ cells (Fig. 2-2A). In a time-dependent manner, the GFP-11kDa caused the AnnexinV+ population to increase from less than 20% to more than 60%, at 24 to 72 hrs posttransfection (Fig. 2-2A). At all three time points, the extent of the GFP-11kDa-induced AnnexinV+ population was significantly higher than that induced by the GFP-NS1 (Fig. 2-2A). However, at 72 hrs posttransfection only, an increased population of AnnexinV+ cells, approximately 16%, was observed in pGFP-7.5kDa-transfected cells compared with the pGFP-transfected control (8%) (Fig. 2-2A). To better evaluate the potency of the NS1 and the 11kDa in inducing apoptosis, we normalized the level of AnnexinV+ population by the level of protein expression represented by the mean intensity of the green fluorescence of the GFP detected by flow cytometer (Fig. 2-2B) (94, 101, 201). Results normalized by GFP were plotted as relative values to that of the GFP+ population of pGFP-11kDa-transfected cells, which was arbitrarily set to 100% (Fig. 2-2C). Transfecting the GFP-11kDa induced approximately two-fold more AnnexinV+ cells than transfecting the GFP-NS1 did (Fig. 2-2C), indicating that the 11kDa is twice more potent in inducing apoptosis than the NS1 in UT7/Epo-S1 cells. However, the difference between the GFP control and GFP-7.5kDa transfection groups was not statistically significant after normalization, suggesting that the 7.5kDa is not a significant apoptosis inducer in UT7/Epo-S1 cells.

Similar results were obtained by transfecting $CD36^+$ EPCs (Fig. 2-2D). At 24 hrs posttransfection, while pGFP control transfection induced approximately 10% AnnexinV+ cells in the GFP+ population of transfected cells, transfection of pGFP-7.5kDa, pGFP-NS1 and pGFP-11kDa induced a significantly higher level of the AnnexinV+ population, approximately 22%, 36% and 42%, respectively (Fig. 2-2D). After normalized by the GFP expression level (Fig.

Fig. 2-2. Comparison of apoptosis induced by transfection of three B19V nonstructural proteins and by B19V infection. (A, B&C) Comparison of apoptosis induced by 7.5kDa, 11kDa and NS1 in UT7/Epo-S1 cells. UT7/Epo-S1cells were transfected with pGFP control, pGFP-7.5kDa, pGFP-11kDa and pGFP-NS1. Cells were analyzed at the three time points of posttransfection as indicated. **(A)** The absolute percentages of AnnexinV+ populations of GFP+ cells were subtracted by that of GFP(-) cells and are plotted to the time points of posttransfection as shown. **(B)** UT7/Epo-S1 cells were transfected with plasmids expressing GFP or GFP-fused proteins as indicated. The mean fluorescence intensity (MFI) of GFP or GFP-fused proteins was detected by flow cytometer and plotted at three time points posttransfection. **(C)** The absolute values shown in panel A were normalized by the MFI of GFP shown in panel B that serves as a marker of protein expression level. The normalized data were plotted as relative values to GFP-11kDa, arbitrarily set as 100%. **(D, E&F) Comparison of apoptosis induced by 7.5kDa, 11kDa and NS1 in CD36$^+$ EPCs.** The same plasmids, as indicated, were transfected to CD36$^+$ EPCs. **(D)** The absolute values of AnnexinV+ cells were plotted at 24 hrs posttransfection. **(E)** CD36$^+$ EPCs were transfected with plasmids expressing GFP or GFP-fused proteins as indicated. The mean fluorescence intensity (MFI) of GFP or GFP-fused proteins was detected by flow cytometer and plotted at 24 hrs posttransfection. **(F)** Results shown in panel D were normalized by following the same method used in panel C. **(G) Apoptosis induced during B19V infection of CD36$^+$ EPCs.** The extent of apoptosis induced by mock/B19V infection of CD36$^+$ EPCs was detected by TUNEL assay. Cells were also immunostained at the time points as indicated with an anti-B19V capsid antibody (clone 521-5D, Millipore) at 1:100 dilution followed by a FITC-conjugated secondary antibody with the TUNEL assay simultaneously. Stained cells were analyzed by flow cytometer, and both capsid+ and capsid(-) cell populations of B19V infected cells were gated for TUNEL+ population.

The symbols of a single star and double stars indicate $P<0.05$ and $P<0.01$, respectively. S1: UT7/Epo-S1; CD36$^+$: CD36$^+$ EPCs; TX: transfection.

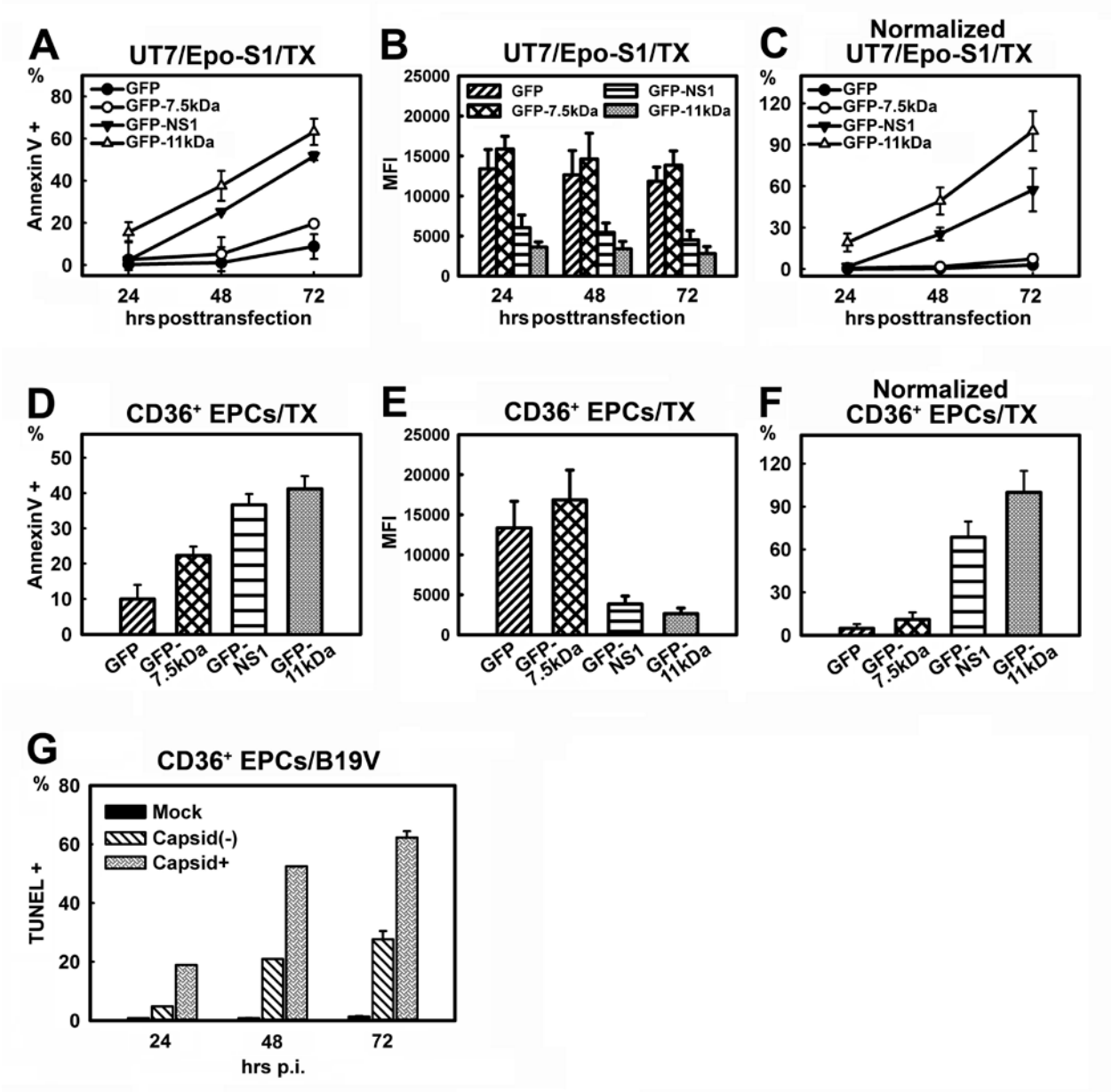
A
UT7/Epo-S1/TX
%
Annexin V +
GFP
GFP-7.5kDa
GFP-NS1
GFP-11kDa
hrs posttransfection
B
UT7/Epo-S1/TX
MFI
GFP
GFP-7.5kDa
GFP-NS1
GFP-11kDa
hrs posttransfection
C
Normalized
UT7/Epo-S1/TX
%
GFP
GFP-7.5kDa
GFP-NS1
GFP-11kDa
hrs posttransfection
D
CD36+ EPCs/TX
%
Annexin V +
GFP
GFP-7.5kDa
GFP-NS1
GFP-11kDa
E
CD36+ EPCs/TX
MFI
F
Normalized
CD36+ EPCs/TX
%
G
CD36+ EPCs/B19V
%
TUNEL +
Mock
Capsid(-)
Capsid+
hrs p.i.

2-2E), the GFP-11kDa induced approximately 1.5 times more AnnexinV+ cells than did the GFP-NS1 (Fig. 2-2F), results similar to those obtained with UT7/Epo-S1 cells (Fig. 2-2C). Again, the difference between the GFP-7.5kDa and GFP alone did not continue to be statistically significant after normalization (Fig. 2-2F). Given the unique nature of ex vivo culture of $CD36^+$ EPCs (even the GFP control induced about 10% AnnexinV+ cells), we determined that the GFP-7.5kDa was not a significant inducer of apoptosis, and thus focused our study on the NS1 and the 11kDa thereafter.

For comparison, we also determined the apoptosis level represented by TUNEL positive (TUNEL+) population during B19V infection of $CD36^+$ EPCs. B19V infected positive (capsid+) population was specifically selected to assess the extent of nicked-DNA-containing cells, compared to those of the capsid negative [capsid(-)] population. As shown in Fig. 2-2G, at 24, 48 and 72 hrs pi, about 20%, 50% and 64% TUNEL+ populations were detected, respectively, in the capsid+ population. Interestingly, we also found a time-dependent increase of TUNEL+ population in the B19V uninfected infected [capsid(-)] cell population, from 2% at 24 hrs p.i. to 19% at 48 hrs p.i., which rose to more than 25% at 72 hrs p.i. The TUNEL+ populations in capsid(-) cells is likely due to the sensitivity of the capsid-recognizing antibody, but not to the release of apoptosis-inducing molecules from infected cells (Fig. S4). However, a significant difference was consistently found between the capsid+ and capsid(-) cell populations. Similar results were obtained when the NS1-expressed cell population was selected for TUNEL assay using the anti-NS1 sera (data not shown). Thus, our results confirmed the apoptotic nature of $CD36^+$ EPCs during B19V infection.

11kDa localizes dominantly in cytoplasm and is expressed at least 100 times more than NS1 during B19V infection of $CD36^+$ EPCs.

Induction of apoptosis is often caused by accumulation of the apoptotic inducer in the cytoplasm, nuclear translocation is often a means to inactivate the apoptotic inducer (20, 169).

Fig. 2-3. Cellular localization and expression of 11kDa and NS1 in transfection.

(A) Specificity of αNS1 and α11kDA polyclonal antibodies. UT7/Epo-S1 cells transfected with pGFP-NS1 or pGFP-11kDa were stained with respective antisera followed by a Texas red-conjugated secondary antibody. Images were taken from an Eclipse SE TE2000-S UV microscope (Nikon) at a 20 × magnification. **(B) Cellular localization of GFP-NS1 and GFP-11kDa in transfected UT7/Epo-S1 cells and CD36$^+$ EPCs.** UT7/Epo-S1 cells and CD36$^+$ EPCs were transfected with pGFP-NS1 or pGFP-11kDa and stained with DAPI at 48 hrs posttransfection. DAPI was used to stain the nuclei. The confocal images (both panel B and C) were taken at 60 × (objective lens) magnification with an Eclipse C1 Plus confocal microscope (Nikon). **(C) Cellular localization of 11kDa and NS1 in B19V-infected CD36$^+$ EPCs.** Infected CD36$^+$ EPCs (at 48 hrs p.i.) were stained with α11kDa and αNS1 antisera followed by a Texas red-conjugated secondary antibody, respectively. DAPI was used to stain the nuclei. **(D) The protein levels of GFP-NS1 and GFP-11kDa in transfected UT7/Epo-S1 cells and CD36$^+$ EPCs *vs* the NS1 and the 11kDa expressed in B19V-infected CD36$^+$ EPCs, respectively.** UT7/Epo-S1 cells and CD36$^+$ EPCs were transfected with either pGFP-11kDa or pGFP-NS1 and stained at 48 hrs posttransfection. CD36$^+$ EPCs were infected with B19V and stained at 48 hrs p.i. Cells were fixed with 1% paraformaldehyde and permeabilized in 0.2% Tween-20. Either α11kDa or αNS1 antisera at a dilution of 1:100 was used to immunostain cells, followed by a Cy5-conjugated secondary antibody. Stained cells were analyzed by flow cytometer. The protein level, represented by the mean fluorescence intensity, was compared between transfected and infected cells. S1: UT7/Epo-S1; CD36$^+$: CD36$^+$ EPCs; TX: transfection.

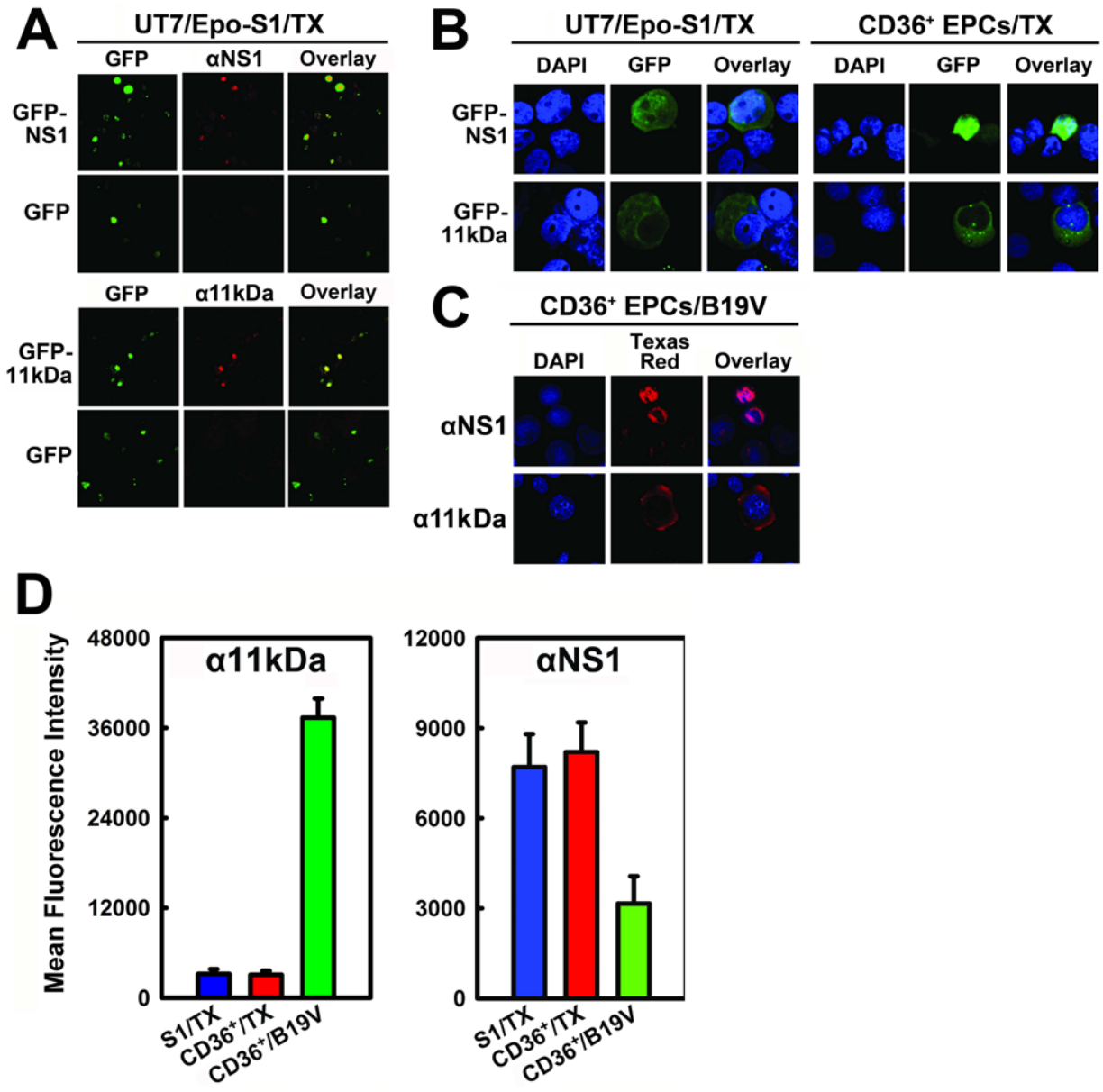
A
UT7/Epo-S1/TX
GFP
αNS1
Overlay
GFP-NS1
GFP
GFP
α11kDa
Overlay
GFP-11kDa
GFP
B
UT7/Epo-S1/TX
CD36+ EPCs/TX
DAPI
GFP
Overlay
GFP-NS1
GFP-11kDa
C
CD36+ EPCs/B19V
DAPI
Texas Red
Overlay
αNS1
α11kDa
D
Mean Fluorescence Intensity
α11kDa
48000
36000
24000
12000
0
S1/TX
CD36+/TX
CD36+/B19V
αNS1
12000
9000
6000
3000
0
S1/TX
CD36+/TX
CD36+/B19V

By using anti-NS1 (αNS1) and anti-11kDa (α11kDa) specific sera (Fig. 2-3A), GFP-11kDa and GFP-NS1 in transfected UT7/Epo-S1 cells and $CD36^+$ EPCs showed similar cellular localization as the 11kDa and the NS1 expressed in B19V-infected $CD36^+$ EPCs (Fig. 2-3 B&C). The blue nuclear DPAI staining did not overlap with either the green GFP-11kDa (Fig. 2-3B) or the 11kDa stained with α11kDa (red) (Fig. 2-3C), indicating that the GFP-11kDa and the 11kDa localize predominantly in cytoplasm. Conversely, nuclear DAPI staining overlapped exactly with NS1 stained with αNS1(red) in B19V-infected $CD36^+$ EPCs (Fig. 2-3C), confirming that NS1 is expressed exclusively in nucleus in B19V infected cells as previously reported (172, 229). In pGFP-NS1-transfected UT7/Epo-S1 cells and $CD36^+$ EPCs, the GFP signal diffused to cytoplasm to some extent, however, the GFP-NS1 localized mainly in the nucleus.

We next compared the expression level of GFP-11kDa and GFP-NS1 with that of 11kDa and NS1, respectively, during B19V infection. The level of the GFP-11kDa in transfected UT7/Epo-S1 cells and $CD36^+$ EPCs at 48 hrs posttransfection, as quantified by flow cytometry analysis using α11kDa antiserum, was approximately 12 times lower than that of the 11kDa expressed in B19V-infected $CD36^+$ EPCs at 48 hrs p.i. (Fig. 2-3D, α11kDa), implying that a stronger proapoptotic effect is induced by 11kDa in B19V-infected $CD36^+$ EPCs than that induced by the GFP-11kDa in transfected cells. In contrast, nearly twice as much GFP-NS1 was expressed in both transfected UT7/Epo-S1 cells and $CD36^+$ EPCs cells at 48 hrs posttransfection than the NS1 expressed in B19V-infected $CD36^+$ EPCs at 48 hrs p.i. (Fig. 2-3D, αNS1), indicating that the GFP-NS1 in transfected cells likely mimics the function of the NS1 during B19V infection.

To determine the relative expression level of 11kDa and NS1 during B19V infection of the native targets, erythroid progenitor cells, we quantified the mRNA levels of the two non-structural proteins using RT-real time PCR. By normalizing to copy numbers of β-actin mRNA (relative copies per β-actin mRNA), the 11kDa-encoding mRNA remained at a consistent level

Fig. 2-4. Quantification of 11kDa and NS1 expression during B19V infection of CD36+ EPCs.

(A) Quantification of B19V 11kDa- and NS1-encoding mRNAs. $CD36^+$ EPCs were infected with B19V. At 24, 48 and 72 hrs p.i., total RNA was isolated, treated with DNase, reverse-transcribed and quantified for absolute copies of mRNA by multiplex real-time PCR for NS1-mRNA/β-actin-mRNA and 11kDa-mRNA/β-actin-mRNA as described in Materials and Methods. The copy numbers of the 11kDa- and NS1-encoding mRNAs were normalized by copy numbers of β-actin mRNA in the same reaction and presented as numbers per copy of β-actin mRNA. **(B) Purity of purified fusion proteins GST-NS1(aa1-181) and GST-11kDa.** Purified GST-NS1(aa1-181) and GST-11kDa proteins were resolved in SDS-10%PAGE gel and stained with Coomassie blue as shown. **(C&D) Quantification of the stead-state protein level of 11kDa *vs* NS1 during B19V infection.** 100 ng of GST-NS1(aa1-181) and 100 ng of GST- 11kDa as seen in panel B and a serial dilution of them as shown were loaded in SDS-8%PAGE and SDS-15%PAGE for Western blot (panel C&D, respectively). At 48 hrs p.i., 1.5×10^5 of $CD36^+$ EPCs with or without (Mock) B19V infection were harvested, directly dissolved in SDS lysis buffer and loaded in lanes 6&7 (SDS-8%PAGE) and lanes 8&9 (SDS-6%PAGE) (panel C), and lanes 3&4 (SDS-15%PAGE) (panel D). Results from lanes as indicated also were quantified with Quantity One software (GE Health) and plotted to the right in panel C&D. Arrow and arrow head in panel C show NS1 specific band and GST-NS1(aa1-181), respectively; and arrow and arrow head in panel D show 11kDa specific band and GST-11kDa, respectively. $CD36^+$: $CD36^+$ EPCs.

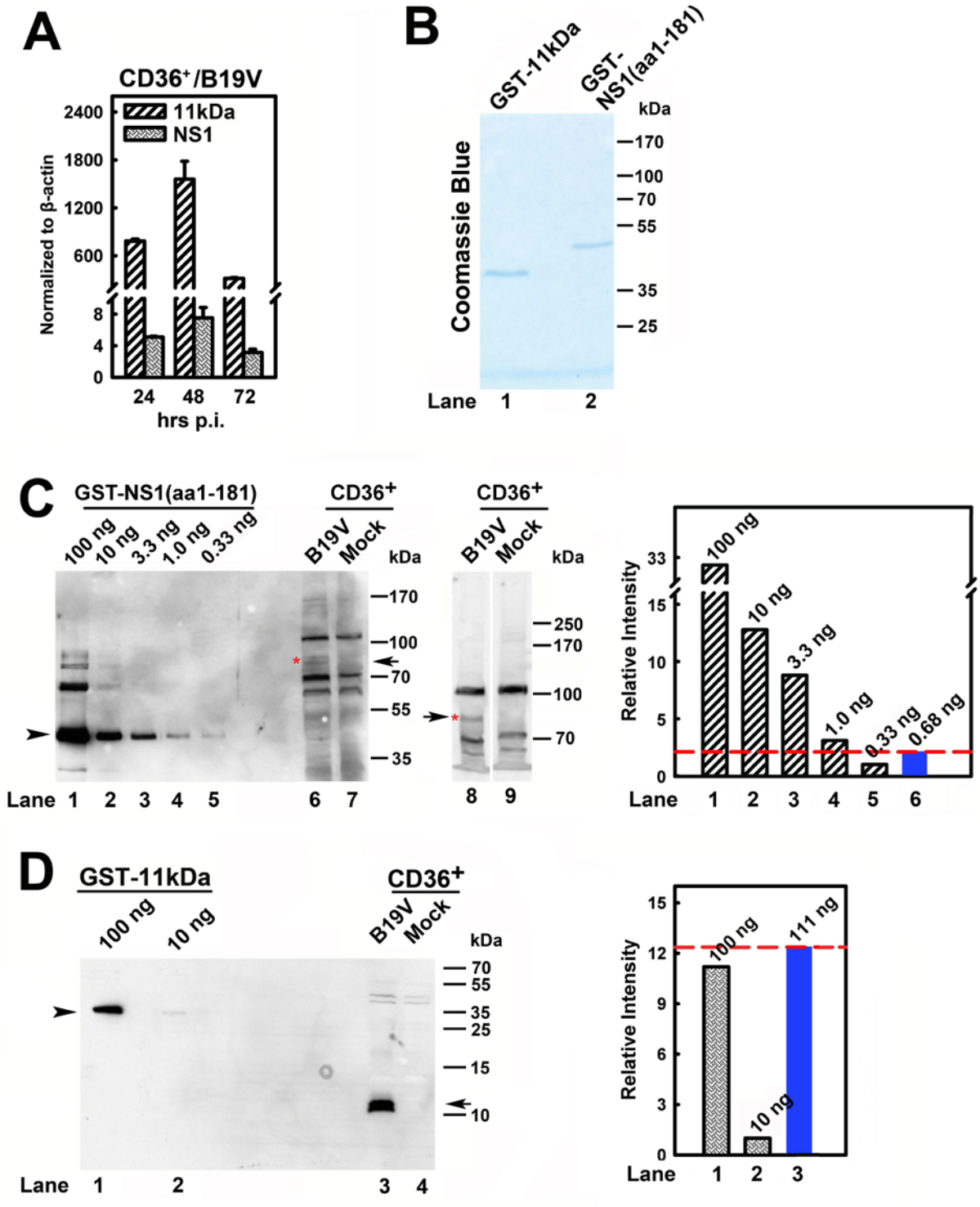
A
CD36+/B19V
11kDa
NS1
Normalized to β-actin
2400
1800
1200
600
8
4
0
24
48
72
hrs p.i.
B
GST-11kDa
GST-NS1(aa1-181)
kDa
Coomassie Blue
170
100
70
55
35
25
Lane 1 2
C
GST-NS1(aa1-181)
100 ng
10 ng
3.3 ng
1.0 ng
0.33 ng
CD36+
B19V
Mock
kDa
170
100
70
55
35
CD36+
B19V
Mock
kDa
250
170
100
70
Lane 1 2 3 4 5 6 7 8 9
Relative Intensity
33
15
10
5
0
100 ng
10 ng
3.3 ng
1.0 ng
0.33 ng
0.68 ng
Lane 1 2 3 4 5 6
D
GST-11kDa
100 ng
10 ng
CD36+
B19V
Mock
kDa
70
55
35
25
15
10
Lane 1 2 3 4
Relative Intensity
15
12
9
6
3
0
100 ng
10 ng
111 ng
Lane 1 2 3

that was approximately 100 to 200 times higher than that of the NS1-encoding mRNA during the course of B19V infection (Fig. 2-4A).

Further, to ascertain the steady-state protein level of 11kDa and NS1 during B19V infection, we attempted to estimate the relative protein level of 11kDa vs. NS1 during B19V infection. GST-NS1(aa1-181) and GST-11kDa were purified (Fig. 2-4B). The purified protein standards (Fig, 4C, lanes 1-5 and Fig. 2-4D, lanes 1&2, respectively) and cell lysates from B19V-infected $CD36^+$ EPCs (at 48 hrs p.i.) and mock cells were blotted with α11kDa and αNS1 antisera, respectively (Fig. 2-4 C&D). We observed significant nonspecific protein bands by the αNS1 antisera; however, the blots clearly showed the specific NS1 band with both 8% and 6% PAGE gels (Fig. 2-4C, compare lane 6 with 7 and lane 8 with 9, respectively). The intensity of this specific NS1 band from B19V-infected $CD36^+$ EPCs (Fig. 2-4C, lane 6) fell between 1.0 ng and 0.33 ng of the GST-NS1(aa1-181) standards (Fig. 2-4C, lanes 4&5). In contrast, the signal of the 11kDa from B19V-infected $CD36^+$ EPCs was stronger than that from 100 ng of the GST-11kDa (Fig. 2-4D, compare lane 3 with 1). This result suggests that during B19V infection of $CD36^+$ EPCs at 48 hrs p.i., at a steady-state protein level, 11kDa expresses at least 100 times more than NS1 (Fig. 2-4 C&D), which presented during the course of B19V infection of $CD36^+$ EPCs (Fig. S2).

Both high expression and cytoplasmic localization of 11kDa and the low expression and nuclear localization of NS1 during B19V infection of $CD36^+$ EPCs suggest the important role of the 11kDa in apoptosis of B19V-infected erythroid progenitors.

Inhibition of 11kDa expression by 11kDa-specific Morpholinos reduces apoptosis significantly during B19V infection of $CD36^+$ EPCs.

To confirm a key role of 11kDa in inducing apoptosis during B19V infection, we next applied specific Morpholino anti-sense oligos to knock down 11kDa expression through inhibition of translation initiation(32, 203). $CD36^+$ EPCs were pre-treated with Morpholino oligos

Fig. 2-5. The inhibitory effects of 11kDa-specific Morpholinos on B19V-infection-induced apoptosis. $CD36^+$ EPCs were pre-treated with a control Morpholino (MO-Ctrl) or 11kDa-specific Morpholinos, MO-1, MO-2 and MO-3, as indicated, at a final concentration of 6 μM, 24 hrs prior to B19V infection. **(A)** A schematic diagram of the 11kDa-encdoing mRNA and targets for specific Morpholino is shown. Regions in the 11kDa-encoding mRNA that Morpholinos target are shown with their respective nucleotide numbers. **(B)** Detection of B19V 11kDa protein. The same samples used for TUNEL assay were used for Western-blot using anti-11kDa antiserum. Detection of β-actin using a polyclonal antibody (ab1801, Abcam) served as a loading control. **(C)** TUNEL assay was performed with co-staining of B19V capsid using an anti-B19V capsid antibody (clone 521-5D, Millipore) for selection of infected cells at 48 hrs p.i. by flow cytometer. The TUNEL+ population is shown as a percentage in capsid positive cells.

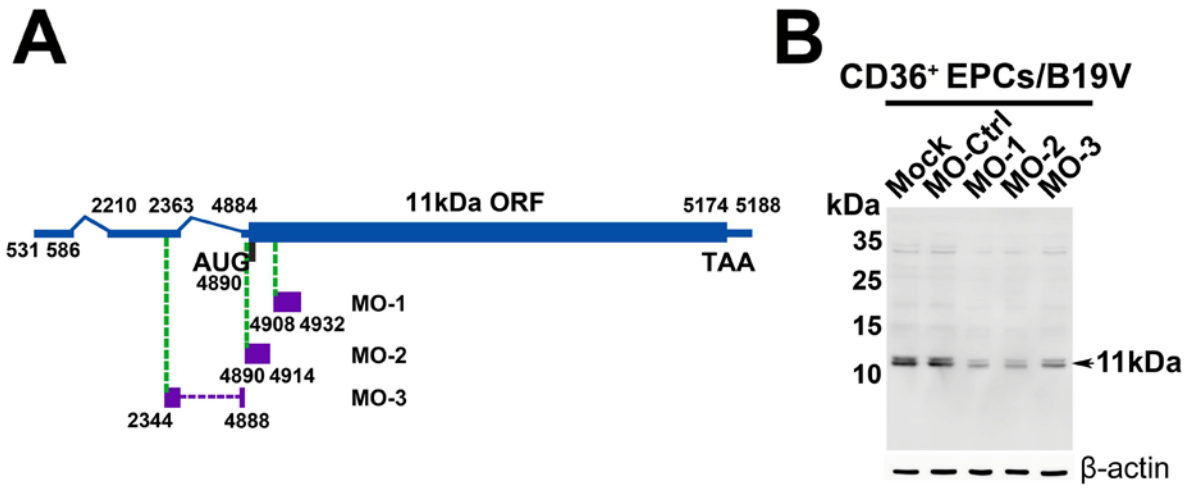
A
2210 2363 4884
11kDa ORF
5174 5188
531 586
AUG
4890
TAA
MO-1
4908 4932
MO-2
4890 4914
MO-3
2344
4888
B
CD36+ EPCs/B19V
Mock
MO-Ctrl
MO-1
MO-2
MO-3
kDa
35
25
15
10
11kDa
β-actin
C
CD36+ EPCs/B19V
Mock
MO-Ctrl
MO-1
MO-2
MO-3
TUNEL
57.4 ±3.5
62.1 ±3.4
41.4 ±2.2
41.2 ±5.5
46.1 ±0.4

24 hrs prior to infection. The expression of 11kDa was reduced by approximately 60% in B19V-infected $CD36^+$ EPCs treated with MO-1, MO-2 and MO-3 at 48 hrs p.i., as indicated by Western-blot (Fig. 2-5B). Consequently, as a result, the level of apoptosis, indicated by TUNEL+ population, was reduced by approximately 20%, in comparison with the cells treated with the control Morpholino (MO-Ctrl) (Fig. 2-5C). The expression levels of NS1 and capsid protein VP1 and VP2 were not affected with treatment of Morpholinos as determined (data not shown), indicating MO-1, MO-2 and MO-3 target specifically to the 11kDa-encoding mRNAs. Thus, we have demonstrated that inhibition of 11kDa expression reduces apoptosis during B19V infection of $CD36^+$ EPCs, supporting a key role of the 11kDa in inducing apoptosis in B19V infection.

Caspase-10 inhibitor is as effectively as pan-caspase inhibitors in reducing B19V-induced apoptosis.

Transfecting UT7/Epo-S1 cells with GFP-11kDa, we observed an 80% inhibition of AnnexinV+ population at 48 hrs posttransfection when Q-VD, a newly developed pan-caspase inhibitor without cross-inhibition of cathepsin (34) was used at 10 μM (Fig. 2-6A). Among individual caspase inhibitors (caspase-1, -2, -3&7, -4, -6, -8, -9, -10 and -13 inhibitors), the caspase-10 inhibitor was particularly effective; treatment with caspase-10 inhibitor at 20 μM reduced the percentage of the AnnexinV+ population by 55%. However, treatments with caspase-1, -2, -3&7, -4, -6 and -8 inhibitors at 20 μM only reduced the AnnexinV+ population by approximately 20% at 20 μM. The inhibition of the GFP-NS1-induced AnnexinV+ population in UT7/Epo-S1 cells generally shared the same profile but had less sensitivity compared with the population induced by 11kDa. At 48 hrs posttransfection, less inhibition was observed in pGFP-NS1-transfected cells with the treatment of the same dose of inhibitors; treatments with Q-VD, Z-VAD and caspase-10 inhibitor reduced the AnnexinV+ population by 55%, 45% and 40%, respectively (Fig. 2-6A). Notably, after transfecting both UT7/Epo-S1 cells and $CD36^+$ EPCs, the percentage of the GFP+ population (out of the total) in pGFP-NS1-transfected cells was

Fig. 2-6. The inhibitory effects of caspase inhibitors on 11kDa/NS1- transfection- and B19V-infection-induced apoptosis. (A&B) Inhibitory effects of caspase inhibitors on apoptosis induced by 11kDa- and NS1-transfection. (A) UT7/Epo-S1 cells were transfected with pGFP-11kDa or pGFP-NS1. **(B)** $CD36^+$EPCs were transfected with pGFP-11kDa and pGFP-NS1, respectively, as shown. Individual caspase inhibitors (at 20 μM), caspase-1, -2, -3&7, -4, -6, -8, -9, -10, and -13 inhibitors, as indicated by 1, 2, 3&7, 4, 6, 8, 9, 10 and 13, and pan-caspase inhibitors, Z-VAD (20 μM) and Q-VD (10 μM) were applied at the time of transfection. DMSO served as a control at 0.5% v/v. Apoptosis was measured by AnnexinV/PI staining at different times posttransfection as indicated. The AnnexinV+/PI+ population is shown as a relative percentage (%) to the DMSO control that is arbitrarily set as 100%. **(C) Inhibitory effects of caspase inhibitors on apoptosis induced by B19V infection.** $CD36^+$ EPCs were infected with B19V. Caspase inhibitors were applied upon infection at the concentrations described above. TUNEL assay was used to measure apoptosis induced in capsid+ cell population at 48 hrs p.i. by flow cytometer. The TUNEL+ population is shown as a relative % to the DMSO control, arbitrarily set as 100%.

All the numbers shown as percentage (%) are averages from at least two individual experiments.

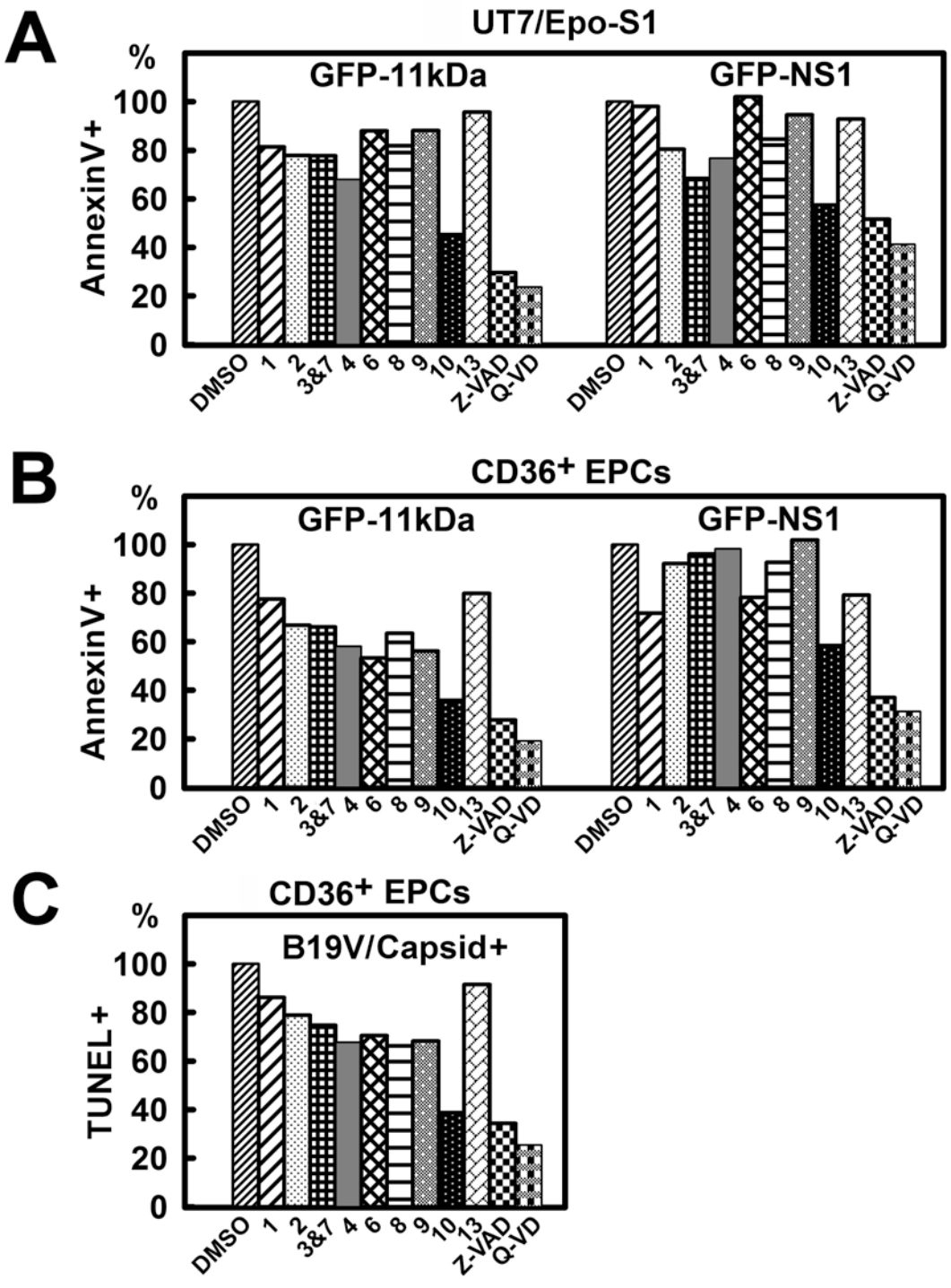
A
UT7/Epo-S1
%
GFP-11kDa
GFP-NS1
AnnexinV+
100
80
60
40
20
0
DMSO 1 2 3&7 4 6 8 9 10 13 Z-VAD Q-VD
DMSO 1 2 3&7 4 6 8 9 10 13 Z-VAD Q-VD
B
CD36+ EPCs
%
GFP-11kDa
GFP-NS1
AnnexinV+
100
80
60
40
20
0
DMSO 1 2 3&7 4 6 8 9 10 13 Z-VAD Q-VD
DMSO 1 2 3&7 4 6 8 9 10 13 Z-VAD Q-VD
C
CD36+ EPCs
%
B19V/Capsid+
TUNEL+
100
80
60
40
20
0
DMSO 1 2 3&7 4 6 8 9 10 13 Z-VAD Q-VD

approximately 1.6 times that of pGFP-11kDa-transfected cells as determined by flow cytometer (data no shown). This perhaps can partially explain why pGFP-NS1-transfected cells were less sensitive to these caspase inhibitors. Nevertheless, caspase-10 inhibitor clearly was the most effective in inhibiting both GFP-11kDa- and GFP-NS1-induced apoptosis in transfected UT7/Epo-S1 cells.

As expected, a similar inhibitory effect of all the caspase inhibitors was observed after transfecting GFP-11kDa and GFP-NS1 in $CD36^+$ EPCs (Fig. 2-6B). Q-VD treatment showed the strongest inhibition in both the GFP-11kDa- and the GFP-NS1-induced AnnexinV+ cells, followed by Z-VAD and caspase-10 inhibitor. Similar to UT7/Epo-S1 cells, the GFP-NS1-induced AnnexinV+ cells were less sensitive to inhibition caused by caspase inhibitors. For example, caspase-10 inhibitor reduced the GFP-11kDa-induced AnnexinV+ population by 62%; however, the NS1-induced AnnexinV+ population was only inhibited by 45%.

In B19V infection of $CD36^+$ EPCs, Q-VD was also the most effective inhibitor in decreasing the TUNEL+ population (Fig. 2-6C). Treatment with QVD at 10 μM inhibited B19V infection-induced TUNEL+ population by an efficiency of 70%. Similar to what was observed in the above transfection experiments, treatment with caspase-10 inhibitor showed a particularly high potency in inhibiting TUNEL+ population induced by B19V infection compared to treatments with other individual caspase inhibitors. At 20 μM, both caspase-10 inhibitor and Z-VAD treatments inhibited B19V infection-induced TUNEL+ population by more than 60%.

Collectively, our results show that caspase-10 inhibitor is the most effective inhibitor besides the two pan-caspase inhibitors in GFP-11kDa and GFP-NS1 transfection-induced apoptosis as well as in B19V infection-induced apoptosis.

Caspase-10 is the most active caspase in 11kDa/NS1 transfection- and B19V infection-induced apoptosis.

The proteolytic cleavage of poly(ADP-ribose)polymerase-1 (PARP1) is one of the hallmarks of apoptosis (100, 110). The cleaved PARP1 band at a size of approximately 85 kDa was specifically detected in pGFP-NS1- and pGFP-11kDa-transfected UT7/Epo-S1 cells (Fig. 2-7A, lanes 5&6) as well as in B19V-infected $CD36^+$ EPCs (Fig. 2-7A, lane 2), but not in GFP only transfected cells and mock cells (Fig. 2-4A, lanes 1, 3&4), supporting the apoptotic nature of cell death induced by transfection of the GFP-11kDa and the GFP-NS1 and by B19V infection. Moreover, the cleaved band of caspase-10 was specifically detected in the pGFP-NS1- and the pGFP-11kDa-transfected UT7/Epo-S1 cells (Fig. 2-7B, lanes 5&6, respectively), as well as in B19V-infected $CD36^+$ EPCs (Fig. 2-7B, lane 2), but not in pGFP-transfected control cells (Fig. 2-7B, lane 4) and mock cells (Fig. 2-7B, lanes 1&3), suggesting that the caspase-10 is activated in 11kDa/NS1 transfection- and B19V infection-induced apoptosis.

Since caspase-3&7, -6 and -8 were reported active in NS1-expressing cell lines and B19V-infected erythroid progenitor cells (131, 195), FLICA was employed to further evaluate the importance of the active caspase-10. Since GFP and FAM share similar excitation and emission wavelength, we transfected cells with RFP-11kDaHA, RFP-NS1HA and RFPHA (as a control). Cellular localization and expression level of these RFP fusion proteins were observed to be similar to that of GFP fusion proteins (data not shown). At 48 hrs posttransfection, RFP-NS1HA and RFP-11kDaHA activated caspase-10 in 24% and 48% of the transfected cells (αHA positive, HA+), respectively; in contrast, only 10% of RFPHA-expressing cells contained active caspase-10 (Fig. 2-7C). Similarly, activation of caspase-10 was detected in more than 53% of B19V infected-$CD36^+$ EPCs (capsid+) at 48 hrs p.i. (Fig. 2-7D). Not surprisingly, all other analyzed caspases (caspase-3&7, -6, -8 and -9) were also activated, however, at a much lower level, compared with capsaspe-10 in the RFP-NS1HA- and the RFP-11kDaHA-expressing cells (Fig. 2-7C) and in $CD36^+$ EPCs infected with B19V (Fig. 2-7D). Our results show that caspase-10 is the most active caspase both in 11kDa- and NS1-expressing UT7/Epo-S1 cells and in B19V-infected $CD36^+$ EPCs, and 11kDa is more efficient in activating caspase-10 than NS1.

Fig. 2-7. PARP1 is cleaved and caspase-10 is the most active caspase in 11kDa/NS1-transfection- and B19V-infection-induced apoptosis. (A&B) Detection of cleaved PARP1 and cleaved caspase-10. $CD36^+$ EPCs were infected with B19V, and capsid+ cells were sorted at 48 hrs p.i. by flow cytometer. UT7/Epo-S1 cells were transfected with pGFP control, pGFP-11kDa and pGFP-NS1. At 48 hrs posttransfection, the GFP+ populations of transfected cells were sorted by flow cytometer. **(A)** Sorted cells were used for detecting the cleaved PARP1 by Western blot using anti-cleaved PARP1 at a dilution of 1:1000 (Cell Signaling). **(B)** Sorted cells were used for detecting of active caspase-10 by Western blot using anti-caspase-10 at a dilution of 1:1000 (Sigma). Uninfected or pGFP transfected cells served as Mock as shown. The blots were reprobed with anti-β-actin (Sigma). **(C) Detection of activated caspase-3&7, -6, -8, -9 and -10 in 11kDa- and NS1- transfected cells.** UT7/Epo-S1 cells were transfected with pRFPHA control, pRFP-11kDaHA and pRFP-NS1HA. FAM- labeled FLICA peptides, FAM-DEVD-FMK, FAM-VEID-FMK, FAM-LETD-FMK, FAM-LEHD-FMK and FAM-AEVD-FMK, were used to detect active caspase-3/7, caspase-6, caspase-8, caspase-9 and caspase-10, respectively. Individual FLICA staining was performed to determine active caspases at 48 hrs posttransfection. Transfected cells were selected by intracellular staining of anti-HA tag at 1:100 dilution (clone HA-7, Sigma), shown as HA+ and HA(-) respectively, and were plotted to FLICA signal detected by flow cytometer. **(D) Detection of activated caspase-3&7, -6, -8, -9 and -10 in B19V-infected $CD36^+$ EPCs**. $CD36^+$ EPCs were infected with B19V. At 48 hrs p.i., cells were used for individual FLICA staining followed by intracellular staining with the antibody against B19V capsid. Both capsid positive and negative cells were plotted to FLICA signal detected by flow cytometer. TX: transfection.

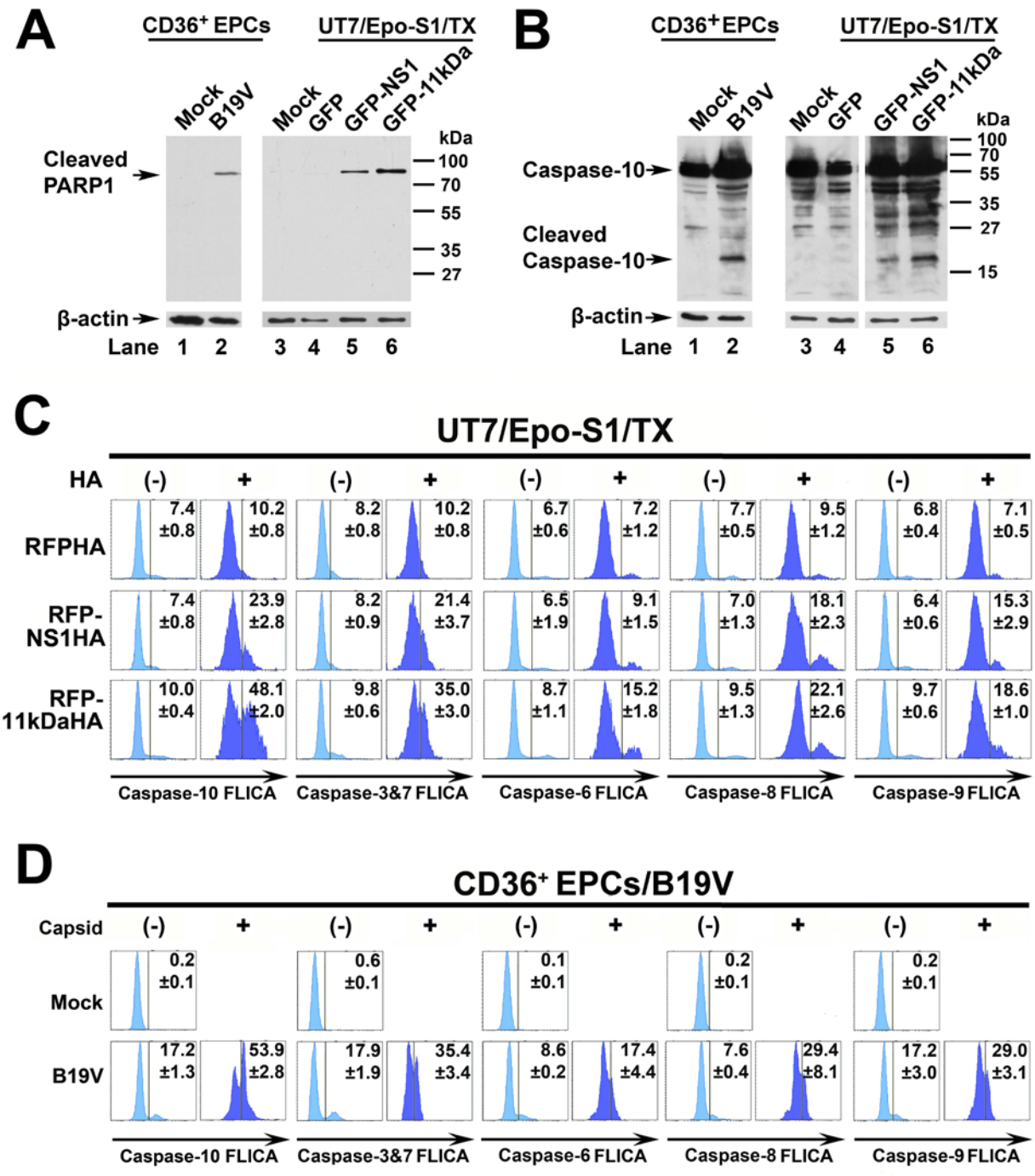
A
CD36+ EPCs
UT7/Epo-S1/TX
Mock
B19V
Mock
GFP
GFP-NS1
GFP-11kDa
kDa
100
70
55
35
27
Cleaved PARP1
β-actin
Lane 1 2 3 4 5 6
B
CD36+EPCs
UT7/Epo-S1/TX
Caspase-10
Cleaved Caspase-10
15
C
UT7/Epo-S1/TX
HA
(-)
+
RFPHA
RFP-NS1HA
RFP-11kDaHA
7.4 ±0.8
10.2 ±0.8
8.2 ±0.8
10.2 ±0.8
6.7 ±0.6
7.2 ±1.2
7.7 ±0.5
9.5 ±1.2
6.8 ±0.4
7.1 ±0.5
7.4 ±0.8
23.9 ±2.8
8.2 ±0.9
21.4 ±3.7
6.5 ±1.9
9.1 ±1.5
7.0 ±1.3
18.1 ±2.3
6.4 ±0.6
15.3 ±2.9
10.0 ±0.4
48.1 ±2.0
9.8 ±0.6
35.0 ±3.0
8.7 ±1.1
15.2 ±1.8
9.5 ±1.3
22.1 ±2.6
9.7 ±0.6
18.6 ±1.0
Caspase-10 FLICA
Caspase-3&7 FLICA
Caspase-6 FLICA
Caspase-8 FLICA
Caspase-9 FLICA
D
CD36+ EPCs/B19V
Capsid
Mock
B19V
0.2 ±0.1
0.6 ±0.1
0.1 ±0.1
0.2 ±0.1
0.2 ±0.1
17.2 ±1.3
53.9 ±2.8
17.9 ±1.9
35.4 ±3.4
8.6 ±0.2
17.4 ±4.4
7.6 ±0.4
29.4 ±8.1
17.2 ±3.0
29.0 ±3.1
Caspase-10 FLICA
Caspase-3&7 FLICA
Caspase-6 FLICA
Caspase-8 FLICA
Caspase-9 FLICA

Discussion

We report here for the first time that B19V 11kDa is a more significant inducer of apoptosis than NS1 during B19V infection of primary erythroid progenitor cells. B19V-11kDa–induced apoptosis is mediated by caspase-10 as an initiator. Strikingly, 11kDa expresses at least 100 times more than NS1 at the protein level during B19V infection of primary erythroid progenitor cells. In contrast with NS1, which localizes exclusively in the nucleus, 11kDa localizes predominately in cytoplasm, where apoptotic inducers usually reside. Although we used GFP-fused 11kDa and NS1 to analyze apoptosis induced in transfected cells, localization of the fused proteins recapitulates their native cellular localization. Moreover, the protein level of 11kDa in transfected cells was approximately 12 times lower than that during B19V infection of erythroid progenitor cells, while the level of the NS1 was comparable between transfection and infection. Therefore, the 11kDa-induced apoptosis by transfection closely reproduces apoptosis induced during B19V infection of primary erythroid progenitor cells. In addition, our results have shown that inhibition of 11kDa expression reduces apoptosis during B19V infection of $CD36^+$ EPCs, and thus we conclude that the B19V 11kDa is the major functional protein in destroying erythroid progenitors during B19V infection.

Apoptosis is defined mechanistically as regulated cell death involving the sequential activation of caspases. Activation of caspase-8, -9 and -10, which are believed to be the initiator caspases at the top of the caspase signaling cascade, leads to the activation of downstream caspases, including caspase-3,-6 and -7, which in turn induce apoptosis (40). As has been previously reported, caspase-3&7, -6 and -8 inhibitors can significantly reduce apoptosis induced by NS1 in established NS1-expressing cell lines (131, 195) as well as by B19V infection of erythroid progenitor cells (195), though at a high concentration of 200 μM. At this high concentration, we did observe more than 90% inhibition of cell death in both the transfection and infection system (data not shown). Instead of using such this “saturated” concentration, however, we applied the inhibitors at a low concentration (20 μM) to probe precisely the potency

of the individual caspase inhibitor. Using FLICA, we detected a significantly higher level of the active caspase-10 than caspase-3&7, -6, -8 and -9 in 11kDa/NS1-transfection- and B19V-infection-induced apoptotic cells, strongly indicating that caspase-10 is the initiator caspase.

Caspase-10, previously considered as the ortholog of caspase-8 (22), has been shown to be able to substitute the function of caspase-8 (104, 217). However, we found caspase-8 could not be substituted for caspase-10 in our study, as caspase-8 inhibitor was not nearly as effective as caspase-10 inhibitor in counteracting apoptosis induced by 11kDa and NS1 transfection in UT7/Epo-S1 and primary erythroid progenitor cells or induced during B19V infection of primary erythroid progenitor cells. In addition, the activation of caspase-10 is significantly higher than caspase-8 in both 11kDa- and NS1-transfected UT7/Epo-S1 cells and B19V-infected primary erythroid progenitor cells. This finding suggests a potential role of caspase-10 in the pro-apoptotic pathway that is not directly regulated by caspase-8.

Notably, B19V permissive cells are erythroid or magakaryoblastoid cells that require Epo to sustain differentiation and proliferation. Epo positively regulates erythropoiesis by preventing apoptosis and stimulating differentiation and proliferation of erythroid progenitors and erythroblasts (107). We observed that the amount of Epo, ranged from 0.1 to 10 units/ml in B19V infection of erythroid progenitor cells, does not influence the degree of apoptosis significantly (Fig. S1). On other hand, the Fas/Fas ligand pathway has been identified to have an apoptotic role in the regulation of erythropoiesis (58, 59). Thus, the balance between the apoptosis by the Fas/Fas ligand and the antiapoptotic role in the presence of Epo is important for the homeostasis of erythroid progenitors. Since Epo strongly presents an antiapoptotic stimulation, apoptosis induced during B19V infection may require a high level of a potent inducer that is the 11kDa. We hypothesize that the high level of the 11kDa expression during B19V infection disturbs the balance between the apoptosis by the Fas/Fas ligand and the antiapoptotic role by Epo and further the homeostasis of erythroid progenitors. Thus, the B19V-

11kDa-induced apoptosis provides us with a unique model to investigate further the mechanism underlying the caspase-10-dependent apoptosis, especially, in primary erythroid progenitor cells

Although an infectious clone of B19V was established, progeny virus produced from transfection of this clone is apparently limited, and transfection of an 11kDa-knockout-clone only results in a few assembled particles exclusively localized in the nucleus (229, 230). Therefore, we are unable to produce 11kDa-knockout virus to examine the role of the 11kDa in causing cell death of erythroid progenitors.

Direct cell death of infected erythroid progenitors results in the disease outcome of B19V infection (29). B19V must express abundant executors to erythroid progenitors during infection, among which the 11kDa is the most significant and abundant executor. Collectively, our data demonstrate that the B19V 11kDa protein is the major protein in executing erythroid progenitor cell death during B19V infection by inducing apoptotic cell death during B19V infection of erythroid progenitor cells that is mediated by activating caspase-10.

Chapter 3

Bocavirus infection induces a mitochondrion-mediated apoptosis and cell cycle arrest at G2/M-phase

Abstract

Bocavirus is a newly classified genus of the family *Parvovirinae*. *Bocavirus* minute virus of canines (MVC) infection produces a strong cytopathic effect in permissive Walter Reed/3873D (WRD) canine cells. We have systematically characterized the MVC infection-produced cytopathic effect in WRD cells, namely, the cell death and cell cycle arrest, and carefully examined how MVC infection induces the cytopathic effect. We found that MVC infection induces an apoptotic cell death characterized by Bax translocalization to the mitochondrial outer membrane, disruption of the mitochondrial outer membrane potential, and caspase activation. Moreover, we observed that the activation of caspases occurred only when the MVC genome was replicating, suggesting that replication of the MVC genome induces apoptosis. MVC infection also induced a gradual cell cycle arrest from the S-phase in early infection to the G2/M-phase at a later stage, which was confirmed by the upregulation of cyclin B1 and phosphorylation of cdc2. Cell cycle arrest at the G2/M-phase was reproduced by transfection of a non-replicative NS1 knock-out mutant of the MVC infectious clone, as well as by inoculation of UV-irradiated MVC. In contrast with other parvoviruses, only expression of the MVC proteins by transfection did not induce apoptosis or cell cycle arrest. Taken together, our results demonstrate that MVC infection induces a mitochondrion-mediated apoptosis that is dependent on the replication of the viral genome, and the MVC genome *per se* is able to arrest the cell cycle at the G2/M-phase. Our results may shed light on the molecular pathogenesis of *Bocavirus* infection in general.

Introduction

The *Bocavirus* genus is newly classified within the subfamily *Parvovirinae* of the family *Parvoviridae* (38). The currently known members of the *Bocavirus* genus include bovine parvovirus type 1 (BPV1) (39), minute virus of canines (MVC) (190), and the recently identified human bocaviruses (HBoV, HBoV2 and HBoV3) (5, 8, 99).

MVC was first recovered from canine fecal samples in 1970 (18). The virus causes respiratory disease with breathing difficulty (33, 91, 173) and enteritis with severe diarrhea (19, 128), which often occurs with co-infection of other viruses (128), spontaneous abortion of fetuses and death of newborn puppies (33, 86). Pathological lesions in fetuses in experimental infections were found in the lymphoid tissue of the lung and small intestine (33). MVC was isolated and grown in the Walter Reed/3873D (WRD) canine cell line (18), which is derived from a subdermoid cyst of an irradiated male dog (18). The full length 5.4-kb genome of MVC was recently mapped with palindromic termini (209). Under the control of a single P6 promoter, through the mechanism of alternative splicing and alternative polyadenylation, MVC expresses two nonstructural proteins (NS1 and NP1) and two capsid proteins (VP1 and VP2). Like the NS1 proteins of other parvoviruses, the NS1 of MVC is indispensible for genome replication. The NP1 protein, which is unique to the *Bocavirus* genus, appears to be critical for optimal viral replication, as the NP1 knock-out mutant of MVC suffers from severe impairment of replication. A severe cytopathic effect during MVC infection of WRD cells has been documented (209).

The HBoV genome has been frequently detected worldwide in respiratory specimens from children under two years old with acute respiratory illnesses (3, 97, 188). HBoV is associated with acute expiratory wheezing and pneumonia (4, 97, 188), and is commonly detected in association with other respiratory viruses (97, 188). Further studies are necessary, however, to identify potential associations of HBoV infection with clinical symptoms or disease of acute gastroenteritis (8, 99). The full length sequence of infectious MVC DNA (Genbank accession no.: FJ214110) that we have reported shows 52.6% identity to HBoV, while the NS1,

NP1 and VP1 proteins are 38.5%, 39.9% and 43.7% identical to those of HBoV, respectively (204).

The cytopathic effect induced during parvovirus infection has been widely documented, e.g., in infections of minute virus of mice (MVM) (25), human parvovirus B19 (B19V) (195), parvovirus H-1 (63, 181) and BPV1 (1). In *Bocavirus*, cell death during BPV1 infection of embryonic bovine tracheal cells has been shown to be achieved through necrosis, independent of apoptosis(1). B19V-induced cell death of primary erythroid progenitor cells has been shown to be mainly mediated by an apoptotic pathway (195), in which the nonstructural protein 11kDa plays a key role (38). In contrast, the MVM-induced cytopathic effect has been revealed to be mediated by NS1 interference with intracellular CKII signaling (54, 149, 150), a non-apoptotic cell death. Oncolytic parvovirus H-1 infections can induce either apoptosis or no-apoptotic cell death, depending on the cell type (63, 129). Therefore, the mechanisms underlying parvovirus infection-induced cell death vary, although NS1 has been widely shown to be involved in both apoptotic and non-apoptotic cell death. The nature of the cytopathic effect during *Bocavirus* MVC infection has not been studied.

Parvovirus replication requires infected cells at the S-phase. Infection of parvovirus has been revealed to accompany a cell cycle perturbation that mostly leads to an arrest in the S/G2-phase or the G2/M-phase during infection (87, 96, 135, 158, 220). MVM NS1 expression induces an accumulation of sensitive cells in the S/G2-phase (7, 156, 158). Whether MVC infection-induced cell death is accompanied by an alternation of cell cycle progression, and whether the viral non-structural protein is involved in these processes have not been addressed.

In this study, we found, in contrast with other members of the family *Parvoviridae*, expression of both the non-structural and structural proteins of MVC by transfection did not induce cell death or cell cycle arrest. However, the cytopathic effect induced during MVC infection is a replication-coupled, mitochondrion-mediated and caspase-dependent apoptosis,

accompanied with a gradual cell cycle arrest from the S-phase to the G2/M-phase, which is facilitated by the MVC genome.

Materials and Methods

Cells and virus:

WRD cells (18) were maintained in Dulbecco's modified Eagle's medium with 10% fetal calf serum in 5% CO_2 at 37°C. The MVC used in this study, the original strain GA3, was isolated at the School of Veterinary Science, Cornell University. MVC was cultured and quantified as previously described, and the virus titer was determined as the number of fluorescence-foci forming units (ffu) per ml (21). The WRD cell line and MVC were obtained as gifts from Dr. Parrish (Cornell University).

MVC was inactivated by UV irradiation as follows: In each well of a 96-well plate, 50 µl of purified MVC (204) containing the cell culture medium was added. The plate was placed in a Hoefer UVC 500 Ultraviolet Crosslinker (Hoefer Inc.) for UV irradiation at a dose of 720 mJ/cm^2 (74, 119).

Infection and transfection:

WRD cells were seeded one day prior to infection or transfection. MVC at indicated multiplicity of infection (MOI= ffu/cell) was added to the culture right after the medium was refreshed.

Transfection was performed using the LipoD293 transfection reagent (SignaGen Laboratories, MD) following the manufacturer's instructions.

Plasmid constructs:

All the nucleotide (nt) numbers of MVC refer to the MVC GA3 isolate (Genbank accession no.: FJ214110).

(i) Constructs for expressing non-structural proteins: The NS1 ORFs (nt 403-2724), NP1 ORF (nt 2537-3094) and VP1 ORF (nt 3081-5192) were inserted separately into BamHI/XhoI-digested pcDNAGFP vector (19) to construct the pGFP-NS1, pGFP-NP1 and pGFP-VP1, respectively. pMVCNSCap was constructed by inserting the MVC sequence of nt 150-5305 into SacII-ApaI-digested pBluescript SK(+) (Strategene).

(ii) Mutants of infectious clone pIMVC: The MVC infectious clone, pIMVC, and its derivative pIMVCNS1(-), pIMVCNP1(-), pIMVCVP1(-) and pIMVCVP2(-) were described previously (60). pIMVCVP1/2(-) was constructed by combing the VP1 and VP2 ATG mutations in pIMVC. pIMVCΔ1/2LTR was constructed by deleting the MVC sequences of nt 1-101 in the left palindromic repeat of the pIMVC through NotI digestion.

(iii) Constructs for glutathione S-transferase (GST)-fusion expression: The MVC NP1 ORF (nt 2537-3094) was cloned into pGEX4T3 (GE Health) as pGEX-MVCNP1.

Antibodies:

GST-fused MVC NP1 protein was expressed from pGEX-MVCNP1-transformed *Escherichia coli* BL21 cells and purified as described previously (60). The anti-NP1 antiserum was produced by immunizing animals with purified GST-MVCNP1 following a protocol described previously (60). The animal protocol used was approved by the KUMC **Institutional Animal Care and Use Committee.**

Anti-Bax, anti-cyclin B1, anti-phospho-cdc2 (pY15) and anti-cyclin A were purchased from BD Biosciences. Anti-β-actin (clone AC-15) was purchased from Sigma. We used dilutions of antibodies for Western blotting and immunofluorescence as suggested in the manufacturers' instructions.

SDS-PAGE, Western blotting and immunofluorescence:

SDS-PAGE, Western blotting and immunofluorescence assay were performed as previously described (27,50,60). Mitochondria were stained by incubating cells with a mitochondrion-staining specific dye, MitoTracker Red CMXRos (Invitrogen), at 500 nM in the cell culture medium for 30 min before fixation in ice-cold acetone. Confocal images were taken at a magnification of 60 × (objective lens) with an Eclipse C1 Plus confocal microscope (Nikon) controlled by Nikon EZ-C1 software.

Southern blotting:

WRD cells were transfected with the MVC constructs as shown in Fig. 3-3C. At 48 h posttransfection, low-molecular-weight DNA (Hirt DNA) was extracted from transfected cells as described previously (27). Southern blotting was performed as described previously (48) using the MVC NSCap probe (60).

Flow cytometry analysis:

AnnexinV/Propidium Iodide (PI) staining: Cells were dissociated by 0.25% trypsin in Versene buffer. The cells were recovered in culture medium at 37°C for 30 min with agitation prior to staining, then washed twice with AnnexinV binding buffer. Of these cells, 1×10^6 were resuspended in 100 µl of AnnexinV binding buffer, followed by the addition of 5 µl Cy5-conjugated AnnexinV (BD Biosciences) and 5 µl Propidium Iodide (PI) (60 µg/ml, Sigma). The mixture was then incubated at room temperature (RT) for 15 min, followed by the addition of 400 µl AnnexinV binding buffer. Flow cytomerty was performed after staining.

FLICA (Fluorochrome-labeled Inhibitor of Caspase) assay and FLICA/Live-Dead Violet co-staining: Cells were dissociated by 0.25% trypsin in Versene and stained with carboxyfluorescein(FAM)-labeled FLICA peptides(Immunochemistry Tech, MN), FAM-VAD-FMK (Poly-FLICA), FAM-DEVD-FMK (Caspase-3&7 FLICA), FAM-VEID-FMK (Caspase-6 FLICA), FAM-LETD-FMK (Caspase-8 FLICA), FAM-LEHD-FMK (Caspase-9 FLICA), FAM-

AEVD-FMK (Caspase-10 FLICA) and the fluorescein isothiocyanate(FITC)-labeled FLICA peptide (Biovision), FITC-ATAD-FMK (Caspase-12 FLICA), as described previously (20).

For FLICA/Live-Dead Violet co-staining, cells were stained with FAM-VAD-FMK (poly-FLICA peptide) followed by Live-Dead Violet staining (Invitrogen) according to the manufacturer's instructions. Specifically, 2 µl of poly-FLICA reagent was added into 300 µl of cell suspension [10^6 cells/ml in phosphate-buffered saline (PBS) containing 2% fetal calf serum (PBS-2%FCS)], which was incubated at 37°C for 1 hr. The cells were washed once by PBS-2%FCS and resuspended in of 500 µl of PBS-2%FCS with 1 µl of Live-Dead Violet dye. The mixture was kept on ice for 30 min. Cells were then washed twice with PBS-2%FCS, and fixed in 1% paraformaldehyde for 30 min before analysis. For co-staining with anti-NS1 of MVC, fixed cells were permeabilized in PBS-2%FCS containing 0.2% Tween-20 (PBST) for 30 min, stained with a 1: 50 dilution of anti-NS1 antiserum, followed by staining with a Cy5-labeled secondary antibody.

DAPI staining: Cells were dissociated by 0.25% trypsin in Versene and fixed in 1% paraformaldehyde at RT for 30 min. The cells were washed, stained with DAPI, 4',6-diamidino-2-phenylindole, at 20 µg/ml in PBST, and then analyzed by flow cytometry. When co-staining was required, cells were first stained with anti-NS1 or anti-NP1 followed by DAPI staining.

Cell proliferation assay (DDAO staining): DDAO, 7-hydroxy-9H-(1,3-dichloro-9,9-dimethylacridin-2-one), a fixable, far-red-fluorescent tracer for very long-term cell labeling, was purchased from Invitrogen and applied following the manufacturer's instructions. Briefly, every 5 million cells were collected and washed twice with pre-warmed PBS. The cells were then resuspended in 1 ml of 10 µM DDAO in PBS and kept at 37°C for 10 min. The mixture was then immediately transferred to 15 ml of pre-warmed cell culture medium to quench the reaction. After cells were washed twice with the warmed medium, they were then resuspended in the medium, and incubated at 37°C. The next day, stained cells were used either for MVC infection or transfection. When required, DDAO-stained cells were fixed and further stained intracellularly

with anti-NS1. DDAO fluorescence decays when cells proliferate; therefore, the lower the fluorescence detected, the better the proliferation of cells (Fig. 3-3-1D&4D).

MOMP (Mitochondrial Outer Membrane Permeabilization) detection [$DiIC_1(5)$/PI or poly-FLICA co-staining]: The level of MOMP was determined by the MitoProbe $DiIC_1(5)$ Assay Kit (Invitrogen). $DiIC_1(5)$ (1',1',3,3,3',3'-hexamethylindodicarbo-cyanine iodide) accumulates primarily in mitochondria with active mitochondrial membrane potentials. $DiIC_1(5)$ staining decreases as the mitochondrial membrane potential is reduced. Cell membrane permeability was probed by propidium iodide (PI, Sigma). Co-staining of $DiIC_1(5)$ with PI was performed following the manufacture's instruction (Invitrogen). Briefly, WRD cells were trypsinized and resuspended at 10^6 cells/ml of the cell culture medium, into which 5 µl of $DiIC_1(5)$ at 10 µM in DMSO (dimethyl sulfoxide) was added, followed by incubation at 37°C for 15 min. PI was added to the mixture to a final concentration of 0.3 µg/ml. The mixture was then incubated for another 15 min at 37°C. For co-staining with poly-FLICA peptide, cells were stained with ploy-FLICA for 30 min at 37°C prior to the addition of $DiIC_1(5)$, then incubated at 37°C for another 30 min. CCCP(carbonyl cyanide 3-chlorophenylhydrazone) was used as a positive control for disrupting mitochondrial outer membrane potential at a final concentration of 50 µM. The stained cells were analyzed on a flow cytometer.

All the samples were analyzed on a three-laser flow cytometer (LSR II, BD Biosciences) within an hour of staining at the Flow Cytometry Core of the University of Kansas Medical Center. All flow cytometry data were analyzed using FACS DIVA software (BD Biosciences).

Results

MVC infection induces cell death and cell cycle arrest in WRD cells.

To analyze cell death and cell cycle arrest induced during MVC infection, we infected WRD cells with MVC and stained them with anti-NS1, Live-Dead Violet and FAM-VAD-FMK (poly-FLICA peptide) at the indicated times p.i. We selected the MVC-infected cells, which were

anti-NS1 positive, and plotted as Live-Dead Violet fluorescence *vs.* FLICA fluorescence intensity in Fig. 3-3-1A. MVC infection induced a cell death in a time-dependent manner during infection as shown by the Live-Dead Violet staining. From 18 to 96 hrs p.i., the live cell population (Live-Dead^{-}) decreased from 91.7% to 45.2% (Fig. 3-3-1A, Control). In addition, dead cells (Live-Dead^{+}) in the control group were almost all stained with FAM-VAD-FMK (poly-FLICA^{+}), indicating that caspases were activated in all the dead cells (Fig. 3-3-1A, Control). Active caspase is a hallmark of apoptotic cell death (61). This result indicates that MVC infection induces an apoptotic cell death. Moreover, with the addition of a specific pan-caspase inhibitor, Q-VD-OPH (Q-VD), cell death in MVC-infected cells was inhibited even at 96 hrs p.i. (Fig. 3-3-1A, Q-VD). Q-VD is a newly developed pan-caspase inhibitor without significant cross reactivity with cathepsin (35). Thus, the rescue of cell death by Q-VD further confirmed the apoptotic nature of MVC infection-induced cell death.

MVC infection not only induced apoptosis, but also a severe cell cycle arrest of infected WRD cells. We gated MVC NS1-expressing cells and plotted them in the histogram of DAPI staining (Fig. 3-3-1B). Cell cycle analysis of MVC-infected cells by DAPI staining showed a clear transition from an S-phase accumulation to a G2/M arrest during MVC infection (Fig. 3-3-1B). As early as 18 hrs p.i., we observed a widened peak with apex in the S-phase (Fig. 3-3-1B, 18 hrs p.i.). Only 6 hrs later, the S-phase accumulation became weaker and was replaced by G2/M arrest at 24 hrs p.i. (Fig. 3-3-1B, 24 hrs p.i.). After that, the cell cycle of NS1-expressing cells was mostly seized in the G2/M-phase (Fig. 3-3-1B, 48, 72 and 96 hrs p.i., respectively). The Q-VD treatment, while completely abolishing the apoptosis induced by MVC infection (Fig. 3-3-1A, Q-VD), did not change the cell cycle perturbation (data not shown). To further support the observation that MVC infection induced cell cycle arrest, we used Western blotting to probe the level of cell cycle regulatory proteins, cyclin B1, phospho-cdc2 (pY15) and cyclin A. As shown in Fig. 3-3-1C, G2/M-phase checkpoint regulators, cyclin B1 and phospho-cdc2 (pY15), were both upregulated at 24

Figure 3-1. MVC infection induces apoptosis and cell cycle arrest.

WRD cells were infected with MVC at an MOI of 3. **(A)** Cells were cultured in media supplemented with DMSO as a control or a pan-caspase inhibitor Q-VD (R&D Systems) at 40 μM immediately after infection. At indicated times p.i., infected cells were triple stained by anti-NS1, Live-Dead Violet and poly-FLICA. Anti-NS1-stained cells were selected and plotted as Live-Dead Violet *vs.* poly-FLICA florescence. The percentage of live cells (double negative) is shown in the square gate. **(B)** At the indicated times p.i., cells were double stained by anti-NS1 and DAPI. The anti-NS1-stained cells were selected and plotted as cell counts *vs.* DAPI staining. Percentages of cells at G0/G1-, S- and G2/M-phase are shown in circle graphs at the bottom of the panel. **(C)** Mock and MVC-infected WRD cells were harvested at 24 hrs and 48 hrs p.i., respectively. Cell lysates were subjected to Western blotting using anti-cyclin B1, anti-cdc2(pY15), anti-cyclin A and anti-β-actin, respectively. The levels of signals on blots, which are normalized to the level of β-actin, are shown in the bar chart to the right. The normalized value of the mock cells at 24 hrs is arbitrarily set to 1. **(D)** At 24 hrs and 48 hrs p.i., MVC- infected WRD cells were stained with DDAO and anti-NS1. Both anti-NS1 positive (NS1+) and negative [NS1(-)] populations were gated and plotted as histograms of cell counts *vs.* DDAO signal. Numbers as shown are percentage of proliferated cells. The line as shown is arbitrarily set based on the non-proliferated control cells, which were fixed immediately after infection.

A representative of two independent experiments is shown in panels A-D.

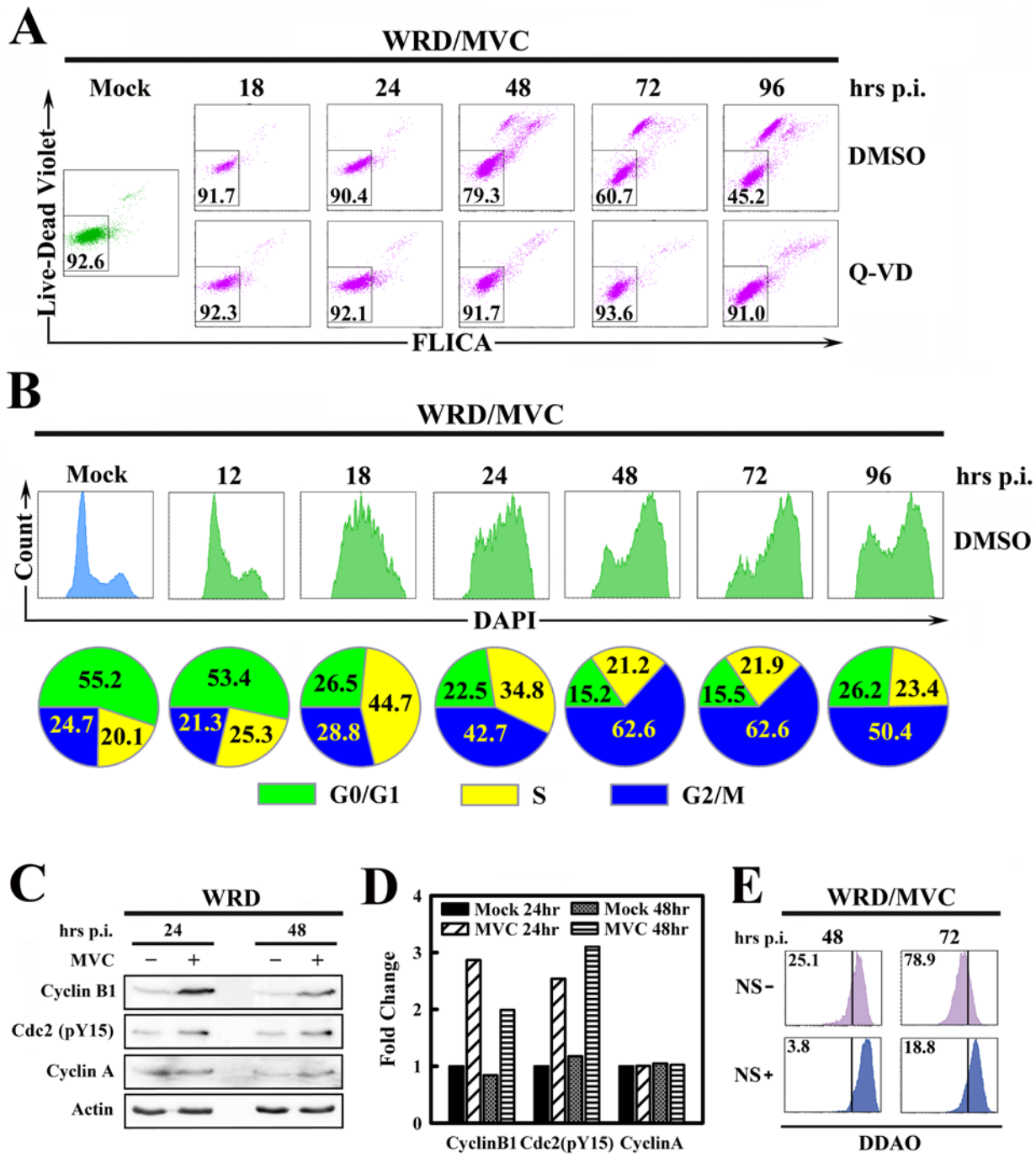
A
WRD/MVC
Mock
18
24
48
72
96
hrs p.i.
DMSO
Q-VD
Live-Dead Violet
FLICA
92.6
91.7
90.4
79.3
60.7
45.2
92.3
92.1
91.7
93.6
91.0
B
WRD/MVC
Mock
12
18
24
48
72
96
hrs p.i.
DMSO
Count
DAPI
55.2
24.7
20.1
53.4
21.3
25.3
26.5
28.8
44.7
22.5
42.7
34.8
21.2
15.2
62.6
21.9
15.5
62.6
26.2
50.4
23.4
G0/G1
S
G2/M
C
WRD
hrs p.i.
24
48
MVC
Cyclin B1
Cdc2 (pY15)
Cyclin A
Actin
D
Mock 24hr
MVC 24hr
Mock 48hr
MVC 48hr
Fold Change
CyclinB1
Cdc2(pY15)
CyclinA
E
WRD/MVC
hrs p.i.
48
72
NS-
NS+
25.1
78.9
3.8
18.8
DDAO

and 48 hrs p.i. in MVC-infected cells. Cyclin A, which is required for S-phase passage, did not differ significantly between mock- and MVC-infected cell groups.

We next stained MVC-infected cells with DDAO to evaluate cell proliferation. Consistent with the cell death and cell cycle arrest induced during MVC infection, NS1-expressing cells showed a severely impaired proliferation of approximately 4-fold compared with NS1-negative cells both in early infection (3.8% *vs.* 25.1% at 48 hrs p.i.) and later infection (18.8% *vs.* 78.9% at 72 hrs p.i.) [Fig. 3-3-1D, compare groups NS(-) with NS+].

Taken together, these results show that MVC infection induces an apoptotic cell death and a perturbation of cell cycle progression from the S-phase during early infection to the G2/M-phase during later infection.

MVC infection-induced apoptosis is mitochondrion-mediated.

We next sought to examine the potential activation of the mitochondrion-mediated apoptotic pathway in MVC infection-induced apoptosis. During mitochondrion-mediated apoptosis, the proapoptotic protein Bax translocalizes to the mitochondrion outer membrane to trigger the permeabilization of the outer membrane, which in turn results in cytochrome c release and downstream caspase activation (103). We first employed the MitoProbe™ $DiIC_1(5)$ to directly probe the level of mitochondrion outer membrane permeabilization (MOMP). During MVC infection, the degree of MOMP occurred in a time-dependent manner (Fig. 3-3-2A). NS1-expressing cells showed a clear transition from $DiIC_1(5)^{high}/PI^-$ (Live) to $DiIC_1(5)^{low}/PI^-$(Early/Middle apoptotic) and to $DiIC_1(5)^{low}/PI^+$ (Late apoptotic/Dead) populations during infection from 48 to 96 hrs p.i. The $DiIC_1(5)^{low}/PI^-$ population represents cells in which the mitochondrial outer membrane is disrupted but the cell membrane is intact, while the $DiIC_1(5)^{low}/PI^+$ population represents cells in which both the mitochondrial outer membrane and the cell membrane are disrupted. This result indicated that MOMP precedes cell death during MVC infection.

Figure 3-2. MVC infection-induced apoptosis is mitochondrion-mediated.

WRD cells were infected with MVC at an MOI of 3. **(A)** MVC-infected cells were harvested at indicated times p.i., and double stained with PI and $DilC_1(5)$. A mock infection control and a MOMP-positive control (CCCP-treated cells) were included. Stained cells were thereafter analyzed by flow cytometry and plotted as PI staining *vs.* $DilC_1(5)$ staining. The $DilC_1(5)^{high}/PI^-$ (Blue) population represents live cells; $DilC_1(5)^{low}/PI^-$ (Green) cells are in the early and middle stages of apoptosis; $DilC_1(5)^{low}/PI^+$ (Red) are late-apoptotic or dead cells. The percentage of each cell population is shown in color. A representative of two independent experiments is shown. **(B)** MVC-infected WRD cells, at 96 hrs p.i., were double stained with poly-FLICA and $DilC_1(5)$. A representative dot plot is shown. The $DilC_1(5)^{high}/FLICA^-$ (Blue) population represents live cells; $DilC_1(5)^{low}/FLICA^-$ (Green) population are cells in the initial stage of apoptosis ; $DilC_1(5)^{low}/FLICA^+$ (Red) population are both apoptotic and dead cells. The percentage of each cell population is shown in color. **(C)** At 48 hrs p.i., mock or MVC-infected WRD cells were stained with MitoTracker Red (Red) and anti-Bax (Green). Representative confocal images were taken. Nuclei were stained with DAPI. **(D)** At the indicated times p.i., MVC-infected WRD cells were stained with anti-NS1 and various FLICA peptides as shown. Anti-NS1-stained cells were selectively gated and plotted in histogram form to show the FLICA signals of NS1-expressing cells. Mock cells were all plotted as poly-FLICA staining. The percentage of FLICA positive cells is shown. A representative of two independent experiments is shown.

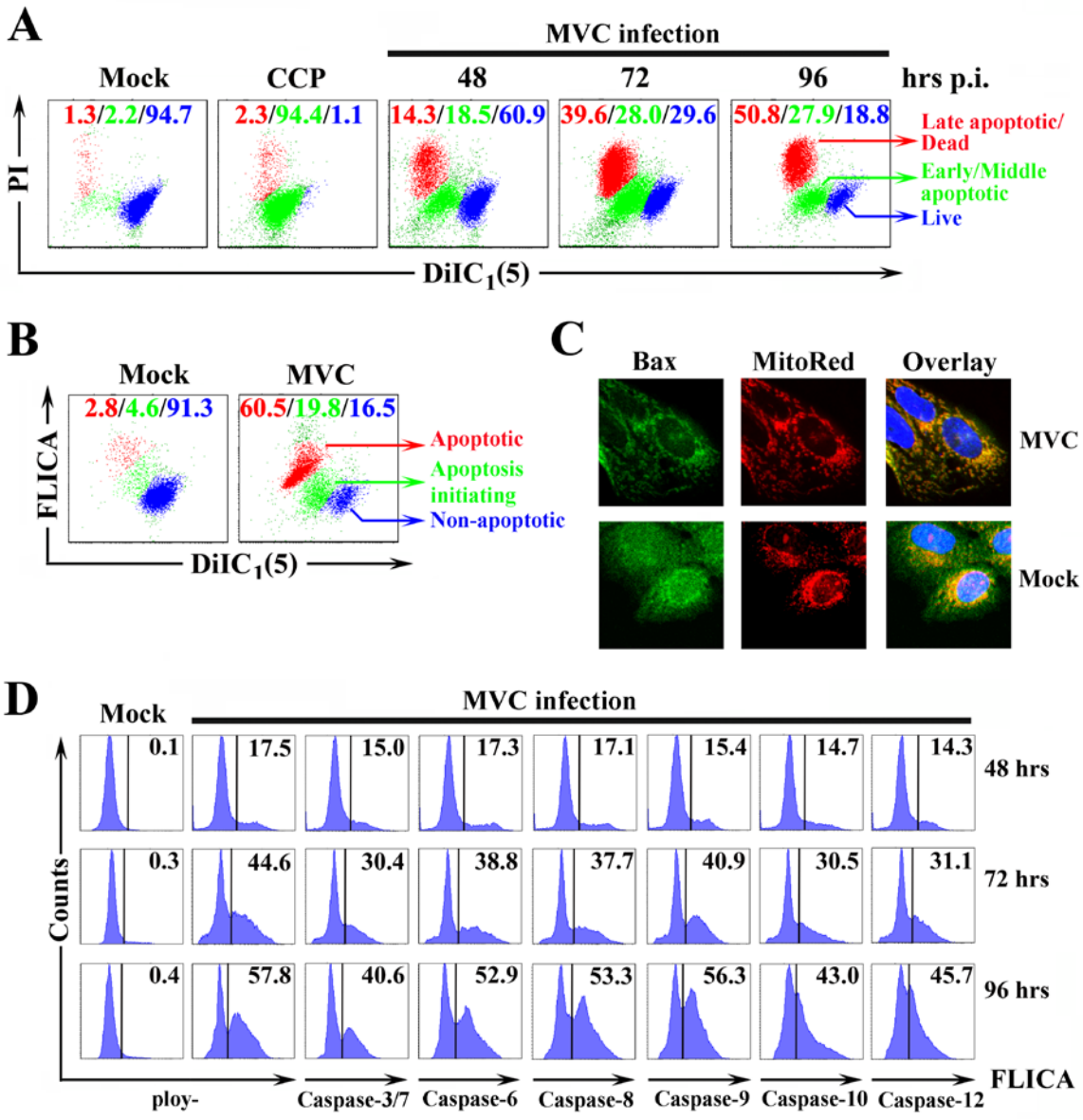
A
MVC infection
Mock
CCP
48
72
96
hrs p.i.
1.3/2.2/94.7
2.3/94.4/1.1
14.3/18.5/60.9
39.6/28.0/29.6
50.8/27.9/18.8
Late apoptotic/ Dead
Early/Middle apoptotic
Live
PI
DiIC1(5)
B
Mock
MVC
2.8/4.6/91.3
60.5/19.8/16.5
Apoptotic
Apoptosis initiating
Non-apoptotic
FLICA
DiIC1(5)
C
Bax
MitoRed
Overlay
MVC
Mock
D
Mock
MVC infection
0.1
17.5
15.0
17.3
17.1
15.4
14.7
14.3
48 hrs
0.3
44.6
30.4
38.8
37.7
40.9
30.5
31.1
72 hrs
0.4
57.8
40.6
52.9
53.3
56.3
43.0
45.7
96 hrs
Counts
FLICA
ploy-
Caspase-3/7
Caspase-6
Caspase-8
Caspase-9
Caspase-10
Caspase-12

We also co-stained MVC-infected cells with FAM-VAD-FMK (poly-FLICA) and $DilC_1(5)$ at 96 hrs p.i. The NS1-expressing cells showed three distinct populations as $DilC_1(5)^{high}$/FLICA$^-$ (Non-apoptotic), $DilC_1(5)^{low}$/FLICA$^-$ (Apoptosis initiating) and $DilC_1(5)^{low}$/FLICA$^+$ (Apoptotic), respectively (Fig. 3-3-2B). The $DilC_1(5)^{low}$/FLICA$^-$ population represents cells in which the mitochondrial outer membrane is disrupted but caspases have not yet been activated, while the $DilC_1(5)^{low}$/FLICA$^+$ population represents cells with both a disrupted mitochondrial outer membrane and activated caspases. This result supports that a transition occurs from $DilC_1(5)$ staining to poly-FLICA staining in NS1-expressing cells. Collectively, these results suggest that MOMP precedes caspase activation and cell death during infection. The fact that caspases are activated in the same population of cells with MOMP is consistent with mitochondrion-mediated apoptosis.

To further confirm that MVC infection-induced apoptosis is mitochondrion-mediated, we used anti-Bax staining and a mitochondrion-specific MitoRed staining to probe whether the Bax localizes on the mitochondrial outer membrane. We observed a precise colocalization of the anti-Bax staining (Green) with the MitoRed staining in MVC-infected cells at 48 hrs (Fig. 3-3-2C, MVC). In contrast, Bax dispersed in the uninfected cells (Fig. 3-3-2C, Mock). This result indicates translocation of the Bax to the mitochondrial outer membrane of MVC-infected cells during infection, which presumably triggers disruption of the mitochondrial outer membrane potential that in turn activates caspases.

To confirm activation of individual caspases during infection, we used poly- and individual caspase FLICA assays to determine the level of activated caspases of NS1-expressing cells. Activation of caspases increased from 48 hrs, 72 hrs and 96 hrs p.i.; however, at all three time points, similar patterns of caspase activation were detected (Fig. 3-3-2D). Among all the caspases tested, caspase-6, -8 and -9 were the most activated, followed by caspase-3/7, -10 and -12 (Fig. 3-3-2D). At 96 hrs p.i., while poly-FLICA showed an overall active caspase-positive rate of 58%, caspase-6, -8 and -9 were activated at a rate of 53%, 53%

and 56% of NS1-expressing cells, respectively (Fig. 3-3-2D, 96 hrs). Active caspase-3/7, -10 and -12 were only detected in 40%, 43% and 48% of NS1-expressing cells, respectively. The extensive activation of caspase-9 is further an evidence that supports the mitochondrion-mediated apoptosis induced during MVC infection.

Replication of the MVC genome induces caspase activation.

Next, we sought to explore which vial components were involved in MVC infection-induced apoptosis and cell cycle arrest. We transfected the MVC infectious clone, pIMVC, its derivatives pIMVCNS1(-), pIMVCNP1(-), pIMVCVP1(-), pIMVCVP2(-), pIMVCVP1/2(-) and pIMVCΔ1/2LTR, and MVC NSCap gene-containing pMVCNSCap into WRD cells, separately. At 48 hrs posttransfection, we analyzed transfected cells for apoptosis and cell cycle by poly-FLICA and DAPI staining, respectively, and co-stained cells with anti-NS1 except for pIMVCNS1(-)-transfected cells, which were co-stained with anti-NP1. The NS1-expressing or NP1-expressing cells were then selected and plotted for FLICA or DAPI florescence intensity for comparison (Fig. 3-3A&B).

Transfection of pIMVC induced 22% poly-FLICA$^+$ population in NS1-expressing cells at 48 hrs posttransfection (Fig. 3-3A, pIMVC). The NS1 knock-out construct, pIMVCNS1(-), which is replication-deficient (204), generated only 5.4% poly-FLICA$^+$ population [Fig. 3-3A, NS1(-)]. However, transfection of the NS(-) mutant did express NP1 that was used to select positive transfected cells, suggesting only expression of the NP1 does not activate caspases. The NP1 knock-out construct, pIMVCNP1(-), which replicates poorly(204), generated 9.8% poly-FLICA$^+$ population [Fig. 3-3A, NP1(-)]. Regardless of whether VP1, VP2 or both were knocked out, replication of the MVC genome was detected in pIMVCVP1(-), pIMVCVP2(-) (204) and pIMVCVP1/2(-)-transfected cells [Fig. 3-3C, VP1(-) and VP1/2(-)]; correspondingly, an average of 17% of FLICA$^+$ populations were detected in transfected cells [Fig. 3-3A, VP1(-), VP2(-) and VP1/2(-)]. Transfection of the half left terminal repeat (LTR)-deleted mutant, pIMVCΔ1/2LTR, of

Figure 3-3. Replication of the MVC genome activates caspases and the MVC genome *per se* arrests cell cycle at the G2/M-phase.

WRD cells were transfected with plasmids as shown. **(A)** At 48 hrs posttransfection, transfected cells were co-stained with anti-NS1, except for pIMVCNS1(-)-transfected cells, which were co-stained with anti-NP1, and poly-FLICA peptide. The anti-NS1 positive or anti-NP1 positive population was selectively gated and plotted as cell counts and FLICA signal. The percentage of FLICA positive cells is shown as an average with a standard deviation generated from three independent experiments. **(B)** At 48 hrs posttransfection, transfected cells were co-stained with anti-NS1, except for pIMVCNS1(-)-transfected cells, which were co-stained with anti-NP1, and DAPI. Anti-NS1- or anti-NP1-stained cells were selectively gated and plotted as cell counts and DAPI signal. The percentage of each cell cycle phase was quantified and is shown as a pie graph at the bottom of the panel. A representative of two independent experiments is shown. **(C)** Southern blotting analysis of transfected WRD cells. At 48 hrs posttransfection, transfected cells were harvested and Hirt DNA was prepared. Hirt DNA was then digested with DpnI. The blot was probed with the NSCap probe as previously described (60). Detected bands are indicated with their respective designations to the left. Lanes 1, 10 and 15 are size markers of 5.15 kb. RF: replicative form; dRF: double replicative form.

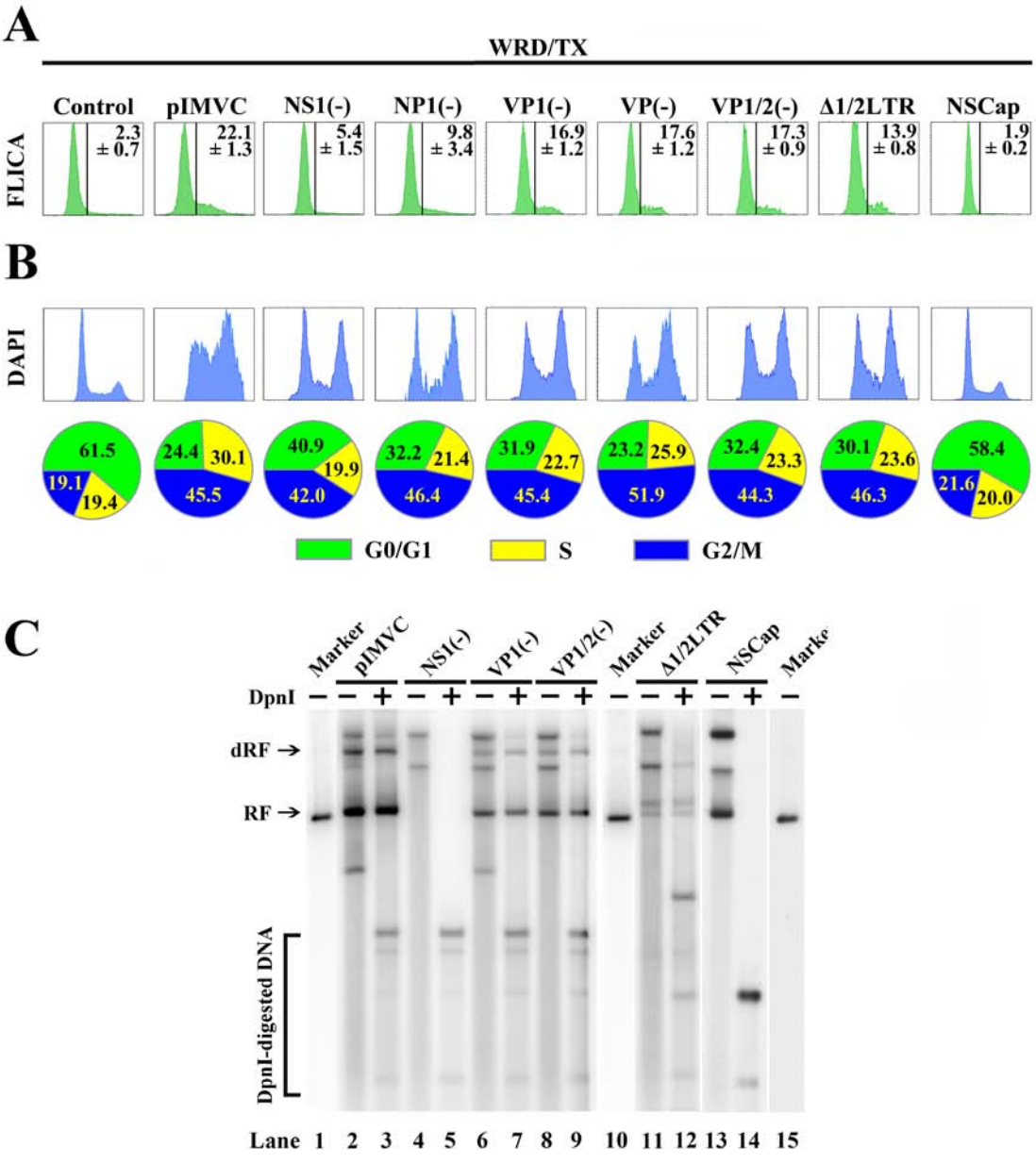
A
WRD/TX
Control
pIMVC
NS1(-)
NP1(-)
VP1(-)
VP(-)
VP1/2(-)
Δ1/2LTR
NSCap
FLICA
2.3 ± 0.7
22.1 ± 1.3
5.4 ± 1.5
9.8 ± 3.4
16.9 ± 1.2
17.6 ± 1.2
17.3 ± 0.9
13.9 ± 0.8
1.9 ± 0.2
B
DAPI
61.5
19.1
19.4
24.4
30.1
45.5
40.9
19.9
42.0
32.2
21.4
46.4
31.9
22.7
45.4
23.2
25.9
51.9
32.4
23.3
44.3
30.1
23.6
46.3
58.4
21.6
20.0
G0/G1
S
G2/M
C
Marker
pIMVC
NS1(-)
VP1(-)
VP1/2(-)
Marker
Δ1/2LTR
NSCap
Marker
DpnI
dRF
RF
DpnI-digested DNA
Lane 1 2 3 4 5 6 7 8 9 10 11 12 13 14 15

which replication was decreased (Fig. 3-3C, Δ1/2LTR), induced a reduced level, 14%, of poly-FLICA^{+} population (Fig. 3-3A, Δ1/2LTR). Transfection of the NSCap gene-containing construct, pMVCNSCap, which did not replicate (Fig. 3-3C, NSCap), failed to induce a significant level of poly-FLICA^{+} population compared with the control (Fig. 3-3A, NSCap). However, transfection of the pMVCNSCap expressed NS1, which was used to select positive transfected cells, and NP1 (Fig. 3-5B), suggesting that only expression of the NS1 and NP1 without replication of the genome does not activate caspases.

The VP1(-) and VP2(-) mutants have been shown to knock out VP1 and VP2 expression by a single burst replication of the viral genome(204). Transfection of the combined VP1/2(-) mutant resulted in a single burst replication compared with transfection of the VP1(-) mutant [Fig. 3-3C, compare VP1/2(-) with VP1(-)]. These results suggest that without expression of the VP1 and VP2 only replication of the MVC genome is sufficient to activate caspases.

Replication efficiency of these transfected constructs as shown by Southern blots was ranked as pIMVC > pIMVCVP1(-), pIMVCVP2(-) and pIMVCVP1/2(-) > pIMVCΔ1/2LTR > pIMVCNS1(-) and pMVCNSCap (Fig. 3-3C). Thus, the efficiency of replication seems to correlate directly with the level of caspase activation. Collectively, these results reveal that activation of caspases, as assayed by poly-FLICA, of transfected cells is associated with replication of the MVC genome, rather than the expression of the MVC NP1 and VP1/VP2 capsid proteins.

The MVC genome *per se* arrests cell cycle at the G2/M-phase.

With DAPI-staining, we further examined the capability of inducing cell cycle arrest through transfection of these MVC constructs. Transfection of the infectious clone (pIMVC) induced a scenario of cell cycle arrest at the G2/M-phase similar to that of MVC-infected cells with a transition of S-phase accumulation (Fig. 3-3B, pIMVC). Surprisingly, at 48 hrs posttransfection, cells transfected with pIMVCNS1(-), pIMVCNP1(-), pIMVCVP1(-), pIMVCVP2(-)

and pIMVCVP1/2(-), which all contain terminal repeats at both ends, showed an apparent G2/M arrest of approximately 42%, 46%, 45%, 52% and 44%, respectively, in comparison with 19% in the control group (Fig. 3-3B). However, no apparent S-phase accumulation was observed in cells transfected with the above pIMVC mutants even at earlier time points (data not shown). Interestingly, transfection of the left half terminal repeat (TR)-deleted mutant, pIMVCΔ1/2LTR, still induced a G2/M arrest of 46% (Fig. 3-3B, Δ1/2LTR); however, transfection of the TRs-deleted mutant, pMVCNSCap, failed to induce G2/M arrest in NS1-expressing cells compared with the control (Fig. 3-3B, NSCap).

Together with those results from Southern blotting analysis (Fig. 3-3C), our observations suggest that the terminal repeats of the MVC genome are required to induce cell cycle arrest at the G2/M-phase, and replication of the genome and expression of the NS1, NP1 and VP1/2 proteins are dispensable. The S-phase accumulation as seen during MVC infection and transfection of the infectious clone may require a status of efficient replication of the viral genome.

Expression of MVC individual viral proteins by transfection does not induce cell death or cell cycle arrest.

To further confirm that MVC proteins are not required to induce apoptosis and cell cycle arrest of transfected WRD cells, we transfected WRD cells with a set of constructs expressing GFP-fused MVC proteins, the GFP-positive population was selectively gated and quantified by AnnexinV staining for apoptosis (38). Not surprising, no significant amount of apoptosis or cell cycle disturbance was observed in cells transfected with individual or combined GFP-fused MVC protein-expressing constructs in comparison with cells transfected with the GFP control, as shown by AnnexinV/PI staining for apoptosis (Fig. 3-4A) and DAPI staining for cell cycle (Fig. 3-4B&C).

Figure 3-4. Expression of individual MVC proteins or in combination by transfection does not induce cell death or cell cycle arrest.

WRD cells were transfected with various constructs, as shown, that express GFP-fused MVC proteins. **(A)** Transfected cells were co-stained with AnnexinV/PI at 48 hrs posttransfection. The GFP-positive population was selectively gated. The percentage of non-apoptotic cells (AnnexinV^{-}/PI^{-} population) in the GFP-positive population in each transfection was then plotted. All the values were generated from three independent experiments and are shown as an average with a standard deviation. **(B)** Representative results of cell cycle analysis. Transfected cells were stained with DAPI at 48 hrs posttransfection. The GFP-positive population was selectively gated. The cell cycle analysis results are shown as GFP-negative population *vs.* GFP-positive population, respectively. **(C)**The percentage of cells at the G0/G1-phase is shown as an average with a standard deviation obtained from three independent experiments. **(D)** Transfected cells were stained with DDAO at 48 hrs posttransfection. The GFP-positive population was selectively gated and plotted. Numbers as shown are percentage of proliferated cells. The line as shown is arbitrarily set in the control cells, which were fixed immediately after transfection.

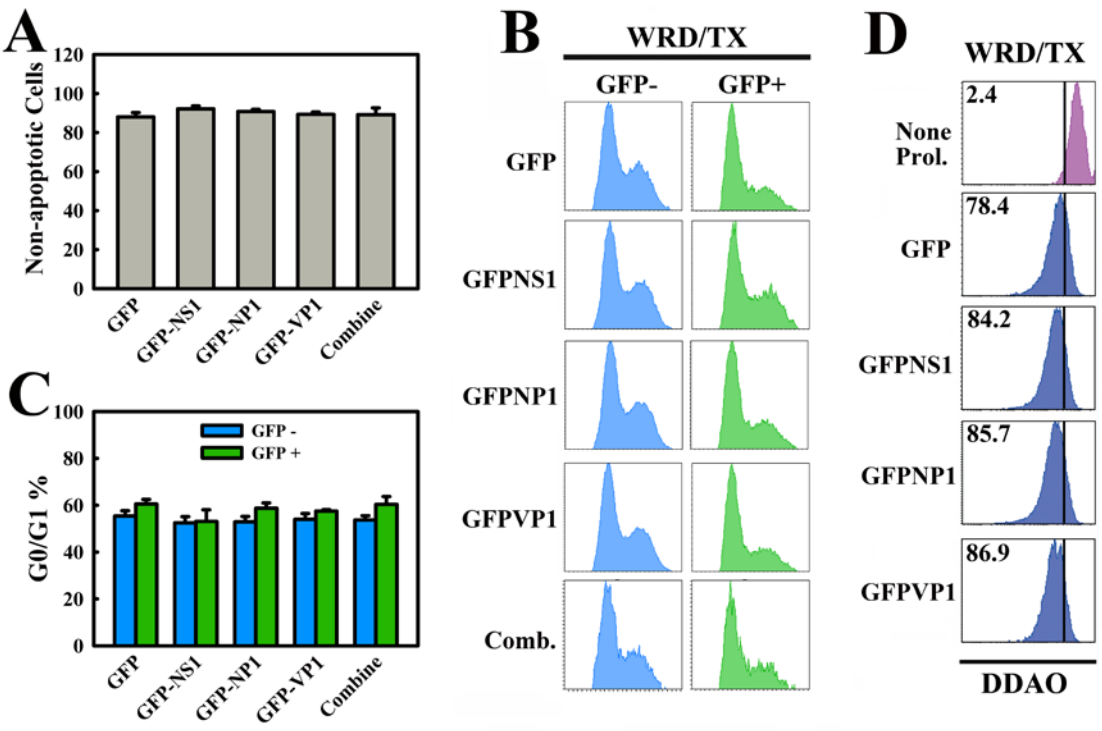
A
Non-apoptotic Cells
120
100
80
60
40
20
0
GFP
GFP-NS1
GFP-NP1
GFP-VP1
Combine
C
G0/G1 %
GFP -
GFP +
B
WRD/TX
GFP-
GFP+
GFP
GFPNS1
GFPNP1
GFPVP1
Comb.
D
WRD/TX
None Prol.
2.4
GFP
78.4
GFPNS1
84.2
GFPNP1
85.7
GFPVP1
86.9
DDAO

Expression of these GFP-fused proteins by transfection was confirmed by fluorescence microscopy (Fig. 3-5A), approximately 10% of WRD cells were GFP-positive. GFP-NS1 and -NP1 showed a similar nucleus-localization as that of the wild type NS1 and NP1 expressed from the transfection of pMVCNSCap in WRD cells (Fig. 3-5B), while transfection of the GFP-VP1 showed localization mostly in the nucleus with somewhat diffusion in the cytoplasm (Fig. 3-5A). Interestingly, during MVC infection, the NS1 was localized in distinct replication center-like foci (Fig. 3-5B, MVC/α-NS1), similar to that of other parvoviruses (9,59), while the NP1 showed a unique peri-nucleus localization (Fig. 3-5B, MVC/α-NP1). The pattern of NS1 localization was also observed in cells transfected with replicative pIMVC and pIMVCVP1/2(-) (Fig. 3-5B). We speculate that the unique localization of the NS1 is due to the replication of the viral genome. Transfection of the pIMVCNP1(-) and pMVCNSCap did not show clear NS1-localized foci in the nucleus (Fig. 3-5B). We did not observe the peri-nucleus localization of NP1 in cells transfected with both replicative and non-replicative MVC constructs (Fig. 3-5B). Thus, we believe that the difference of the localization pattern of the NS1 and NP1 in the nucleus is less likely to result in the inability of the NS1 and NP1 to induce apoptosis. In addition to these observations, we also observed that expression of individual GFP-fused MVC proteins or those combined by transfection did not inhibit cell proliferation compared with the control GFP transfection group (Fig. 3-4D).

Collectively, our results suggest that unlike the non-structural proteins of other parvoviruses, the MVC proteins, especially the NS1 and NP1, expressed by transfection of WRD cells, do not induce an apparent cell death or a perturbation of cell cycle progression.

UV-inactivated MVC induces cell cycle arrest but not cell death.

To further confirm the role of the MVC genome in inducing apoptosis and cell cycle arrest, we inactivated purified MVC by UV irradiation. WRD cells were either infected with untreated (MVC) or inoculated with UV-irradiated MVC (UV-MVC). Apoptosis and cell cycle

Figure 3-5. Cellular localization of MVC proteins during infection and in transfection.

(A) WRD cells were transfected with constructs expressing GFP-fused MVC proteins as shown. Cells were treated at 48 hrs posttransfection. **(B)** WRD cells were infected with MVC at an MOI of 3 or transfected with the MVC constructs as indicated. At 48 hrs p.i. or posttransfection, cells were stained with anti-NS1 and anti-NP1, respectively. Confocal images were taken at × 60 magnification. Nuclei were stained with DAPI.

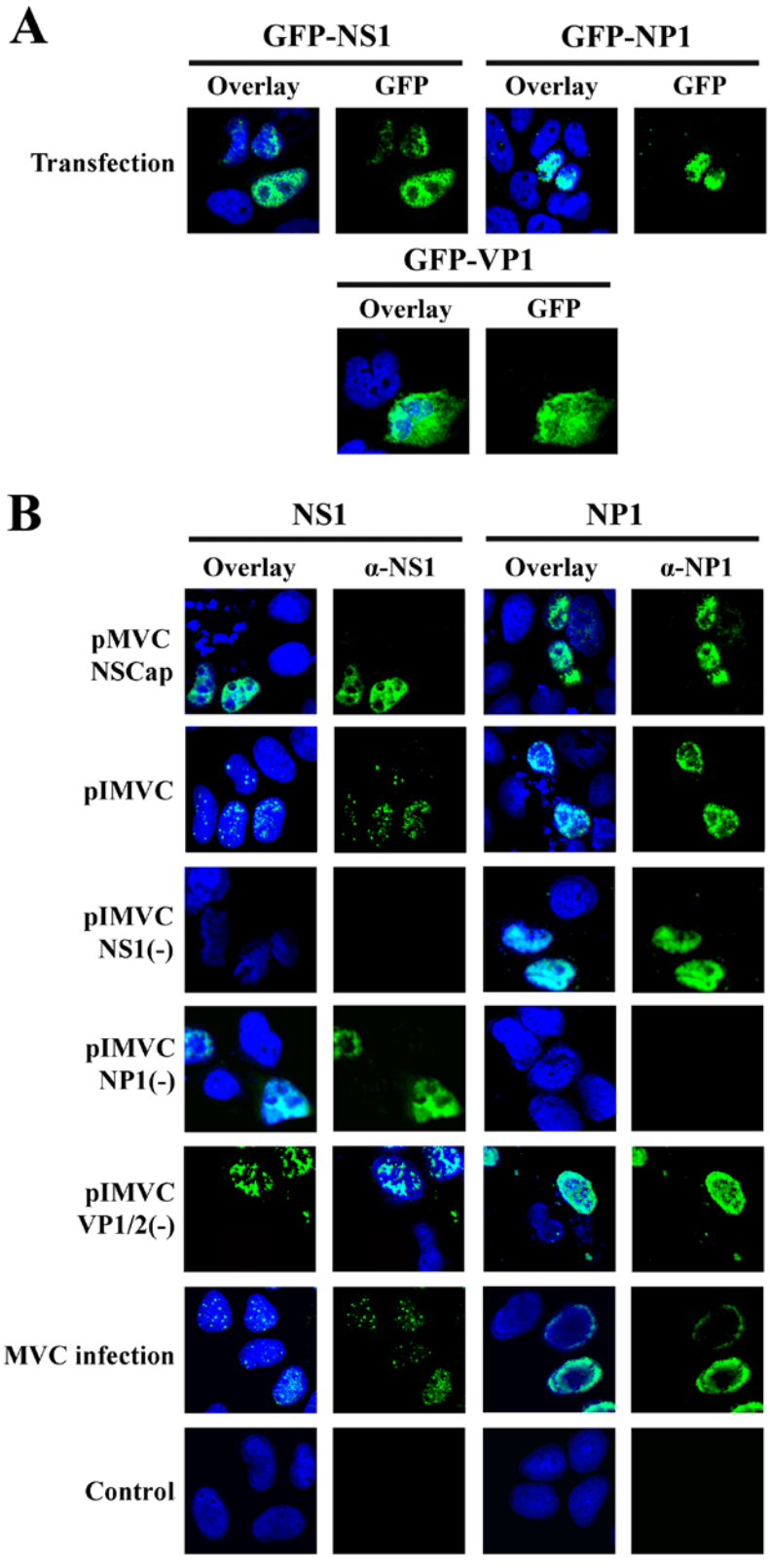
A
GFP-NS1
GFP-NP1
Overlay
GFP
Overlay
GFP
Transfection
GFP-VP1
Overlay
GFP
B
NS1
NP1
Overlay
α-NS1
Overlay
α-NP1
pMVC NSCap
pIMVC
pIMVC NS1(-)
pIMVC NP1(-)
pIMVC VP1/2(-)
MVC infection
Control

Figure 3-6. UV-MVC inoculation induces cell cycle arrest at G2/M but not cell death.

WRD cells were infected by MVC or inoculated with UV-MVC at an MOI of 9. **(A)** Infected or inoculated cells were co-stained with Live-Dead Violet and poly-FLICA peptide at indicated times p.i. Stained cells were plotted in histograms as Live-Dead Violet and FLICA signals. The numbers in the square show percentages of live cells (double negative). **(B)** At 48 hrs p.i., mock or UV-MVC-infected cells were stained with DAPI and plotted as cell counts and DAPI signal. The percentage of each cell cycle phase was quantified and is shown as a pie graph at the bottom of the panel. **(C)** UV-MVC-infected cells were harvested at indicated times p.i. Cell lysates were subjected to Western blotting analysis using anti-cyclin B1, -cdc2 (pY15), -cyclin A and -β-actin, respectively. The level of signals on blots is normalized to the level of β-actin and is shown in the bar chart. The normalized value of the mock cells is arbitrarily set to 1.

A representative of two independent experiments is shown in panels A&B.

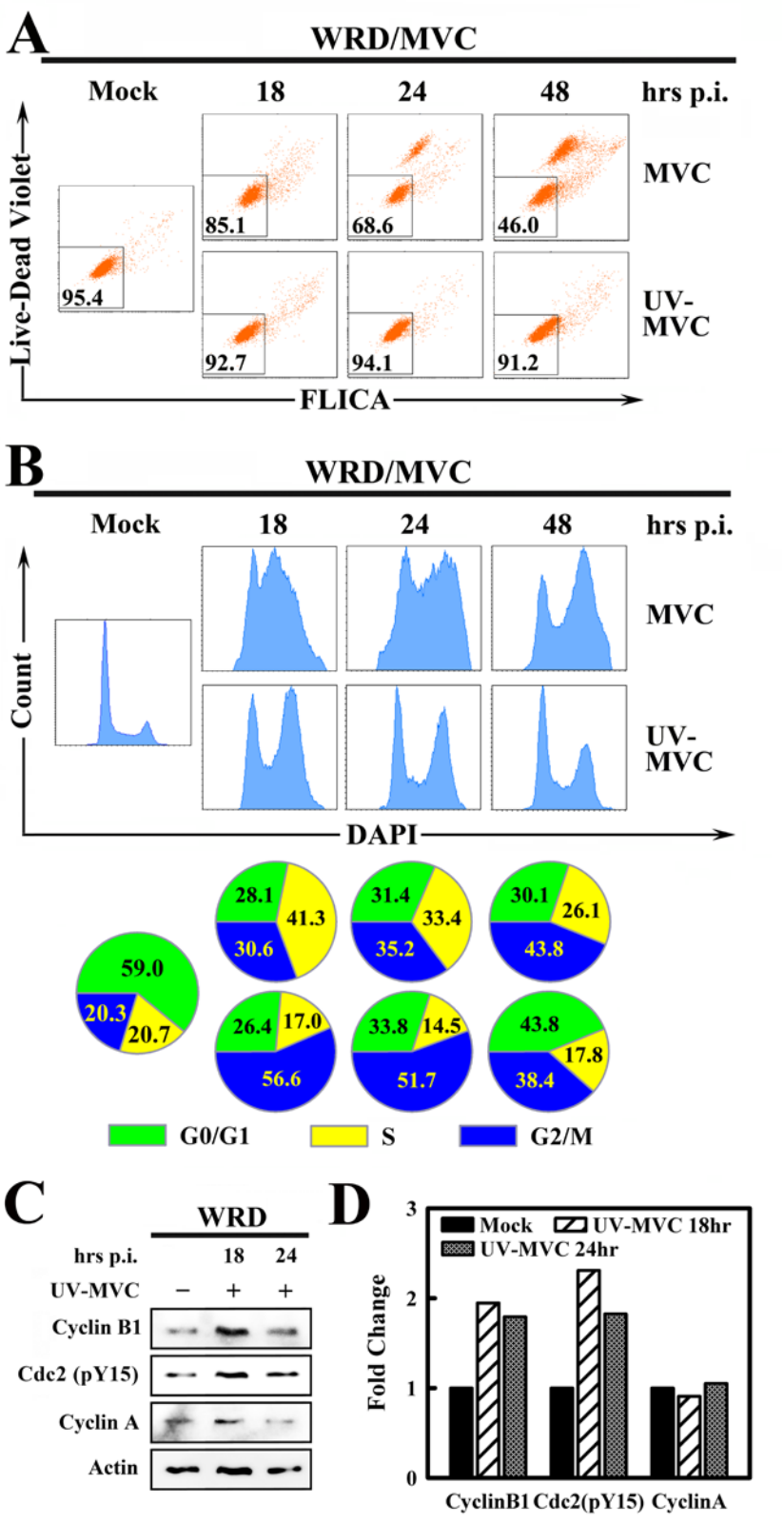
A
WRD/MVC
Mock
18
24
48
hrs p.i.
MVC
UV-MVC
Live-Dead Violet
FLICA
95.4
85.1
68.6
46.0
92.7
94.1
91.2
B
WRD/MVC
Count
DAPI
59.0
20.3
20.7
28.1
41.3
30.6
31.4
33.4
35.2
30.1
26.1
43.8
26.4
17.0
56.6
33.8
14.5
51.7
43.8
17.8
38.4
G0/G1
S
G2/M
C
WRD
hrs p.i.
UV-MVC
Cyclin B1
Cdc2 (pY15)
Cyclin A
Actin
D
Mock
UV-MVC 18hr
UV-MVC 24hr
Fold Change
CyclinB1
Cdc2(pY15)
CyclinA

status were evaluated by Live-Dead Violet/FLICA co-staining and DAPI staining, respectively. Since NS1 was not expressed in WRD cells inoculated with UV-MVC (data not shown), we used an MOI of 9 for inoculation. We gated total cells and plotted them in Fig. 3-6A&B. At this MOI, MVC infection induced apoptosis more drastically, which was observed as early as 18 hrs p.i. and progressed over the course of infection (Fig. 3-6A, MVC). At 48 hrs p.i., only 46% of MVC-infected cells were still alive (Live-Dead Violet^{-}/FLICA^{-}). In contrast, UV-MVC inoculation failed to induce a significant level of cell death at all three times p.i. (Fig. 3-6A, UV-MVC)

Meanwhile, we compared the cell cycle regulation of MVC-infected and UV-MVC-inoculated WRD cells at the same MOI. Consistent with the findings shown in Fig. 3-3-1B, the S-phase accumulation transitioned to the G2/M arrest during MVC infection (Fig. 3-6B, MVC). While most of the WRD cells were at the S-phase at 18 hrs p.i., the majority of MVC-infected cells were arrested at the G2/M-phase at late time points. Interestingly, UV-MVC induced a significant cell cycle arrest at G2/M as early as 18 hrs p.i. (Fig. 3-6B, UV-MVC). Consistent with the transfection experiments shown in Fig. 3-3, we did not observe an S-phase accumulation during UV-MVC inoculation (Fig. 3-6B). Moreover, to confirm the G2/M arrest induced by UV-MVC inoculation, we determined the protein level of the G2/M-phase checkpoint regulators in UV-MVC-inoculated cells. A significant increase of both cyclin B1 and cdc2 (pY15) was observed at both 18 and 24 hrs p.i. (Fig. 3-6C). However, the fold of increase was less than that of the MVC-infected cells shown in Fig. 3-3-1C. The level of cyclin A remained unchanged in UV-MVC inoculated cells.

Collectively, these lines of evidence further support that the MVC viral genome alone can induce cell cycle arrest at the G2/M-phase, but not the S-phase accumulation or cell death.

Discussion

***Bocavirus* MVC infection induces a mitochondrion-mediated apoptosis:** Parvovirus infection often causes cell death of infected cells either by apoptosis or by various mechanisms

of non-apoptotic cell death. Novel mechanisms of non-apoptotic cell death induced by parvovirus infection have been revealed recently. MVM infection-induced cell death is mediated by NS1 interference with intracellular CKII signaling (54, 149, 150). On the other hand, parvovirus H-1 can induce a non-apoptotic cell death of glioma cells that is dependent on accumulation of cathepsin B/L (63). However, the mechanisms underlying parvovirus infection-induced apoptosis have not been elucidated in detail. Apoptosis is defined mechanistically as three pathways of regulated cell death involving the sequential activation of caspases, the extrinsic pathway is involved in the engagement of particular “death” receptors (e.g., Fas) and through the formation of the death-inducing-signaling-complex (DISC) (9). The mitochondrion-mediated (intrinsic) pathway is activated by “BH3-only” proteins such as tBid, Bad, Bim and PUMA; these activated proteins are subsequently translocated to the mitochondrial membrane, where they activate the proapoptotic proteins, Bax and Bak (103). Bax/Bak activation results in mitochondrial outer membrane permeabilization (MOMP), with consequent release of cytochrome c and other mitochondrial proteins with the consequent activation of caspase-9 (40). Activated caspase-8/-10 is also able to cleave Bid to tBid which activates Bax/Bak. In endoplasmic reticulum (ER)-stress-mediated apoptosis, caspase-12 is localized to the ER and activated by ER stress (141).

We have shown in our studies that MVC infection induces an apoptotic cell death, represented by the presence of activated caspases in infected cells. Consistently, the specific pan-caspase inhibitor Q-VD completely blocked MVC infection-induced cell death. Moreover, the translocalization of the proapoptotic Bax to the mitochondrial outer membrane and consequently the time-dependent disruption of mitochondrial outer membrane potential indicated the activation of mitochondrion-mediated apoptosis during MVC infection. This mechanism is further supported by the extensive activation of caspases, especially the activated caspase-9, during MVC infection. We also detected the activation of the initiator caspase-8, -10

and -12; however, whether the extrinsic pathway or the ER-stress-mediated pathway is also involved in MVC infection-induced apoptosis to some extent warrants further investigation.

Replication of the viral genome induces apoptosis of MVC-infected cells: In our results, expression of the non-structural protein NS1 and NP1 of MVC did not induce cell death in transfected cells, which contrasts with the function of the large nonstructural protein of other parvoviruses, e.g., the NS1 of MVM (44), H-1 (52) and B19V (58), the Rep78 of AAV2 (56), and the small nonstructural protein 11kDa of B19V (16). Thus, our results suggest that the non-cytotoxic nature of the MVC NS1 is novel in parvoviruses, and might be a general feature of the NS1 among other members in the genus *Bocavirus*.

Surprisingly, our studies showed that activation of caspases coincided with the replication of the viral gnome. The efficiency of replication correlated well with the level of caspase activation in cells transfected with pIMVC and its mutants (Fig. 3-3A&C). In the scenario in which replication of the MVC genome occurs either during MVC infection or in transfection of the replicative MVC constructs, apoptosis is induced in infected or transfected cells. However, when DNA replication is abolished either by knocking out NS1 expression or deleting both terminal repeats, transfection of these non-replicative mutants does not induce apoptosis. When DNA replication is significantly reduced either by knocking out the NP1 expression or deleting the left half terminal repeats, transfection of these replication-reduced mutants induces a decreased degree of apoptosis. These observations strongly suggest that the apoptosis induced from transfection of the MVC infectious clone and its replicative derivatives is dependent on the replication of the MVC genome. We know that only expression of the viral proteins by transfection (Fig. 3-4) does not induce apoptosis; however, NS1 is essential for the replication of the viral genome. Thus, we cannot rule out an indirect role of the NS1 in inducing apoptosis during MVC infection.

It is reasonable to speculate that a DNA damage response could be induced in WRD cells upon MVC infection or simply by replication of the viral genome. A DNA damage response

induced by AAV2 infection has been extensively explored (51,61,64). AAV2 DNA, which is single stranded with hairpin loops at both ends, can be sensed as abnormal DNA by the cell, triggering a DNA damage response independent of p53 (51). We have evidence that MVC infection induced a DNA damage response represented by phosphorylation of H2AX, p53 and ATM (data not shown). DNA damage response induces apoptosis when the damage is not repairable through upregulation of the proapoptotic proteins such as tBid, Fas, Bax or PUMA (5,35,54). It is also possible that an initial DNA damage response induced by the MVC genome incurs cell cycle arrest, and later, during viral DNA replication, accumulated MVC genomes trigger an irreversible DNA damage response that results in apoptotic cell death. On the other hand, the DNA damage response signals the DNA repair machinery, which may be helpful in replicating the single stranded genome of MVC. These novel mechanisms have never been studied in autonomous parvovirus infection and warrants further investigation. Therefore, we have provided an excellent model to study how the viral genome and its replication induce cellular responses that favor virus DNA replication at an early stage of infection and egress of progeny virus at a later stage of infection. The apoptosis induced by replication of the MVC genomes may be a common mechanism underlying parvovirus infection-induced apoptosis.

***Bocavirus* MVC infection induces cell cycle arrest:** Parvovirus infection induces cell cycle arrest (30,33,42,47,65) most often at the S/G2-phase, which favors virus DNA replication. However, a G2/M-phase arrest is clearly observed as early as 6 hrs after B19V infection (42). Nevertheless, we have shown here that MVC infection incurs an apparent S-phase accumulation at early infection followed by an arrest of the G2/M phase in late infection (Fig. 3-3-1). The DAPI staining in our study presents the authentic cell cycle of host cells. We quantified the MVC genomic copy number per cell at 48 hrs p.i. The genomic copy number per cell, which includes the replicative form (RF) DNA of MVC, was approximately 0.1 million, which equals 0.55 billion bases. The human genome contains approximately 3.4 billion base pairs per cell (http://www.genome.gov/18016863). Thus, assuming the canine genome is similar in size to the

human genome, the DAPI staining contributed by the replicated MVC genomes and RF DNA is less than 8% of the total DAPI staining in an infected cell, which is not sufficient to change the pattern of the cell cycle represented by DAPI staining. Based on evidence showing the critical cell cycle proteins and inhibition of cell proliferation during MVC infection (Fig. 3-3-1C&D), we believe that the DAPI staining presents the authentic cell cycle of MVC-infected cells in our studies.

Cell cycle arrest at the G2/M-phase often precedes the onset of apoptosis (22,31,63). We did not observe an apparent G2/M-phase arrest preceding apoptosis during MVC infection. In contrast, G2/M arrest by transfection of the NS1-knock-out mutant [pMVCNS1(-)] or UV-irradiated MVC did not induce apoptosis (Fig. 3-3 and Fig. 3-6), and inhibition of apoptosis by Q-VD did not release cell cycle arrest (data not shown). Thus, we believe that the cell cycle arrest and apoptosis of MVC infection are induced through independent pathways in parallel.

In transfecting the mutant MVC infectious clones, as shown in Fig. 3-3, we tested cell cycle arrest at early time points of transfection. We were not able to detect any S-phase accumulation in transfection of these mutants than the infectious clone *per se* (data not shown). Nevertheless, we consistently observed the G2/M arrest at 48 hrs posttransfection in all the transfections of the mutant infectious clones that contain the viral terminal repeats. Thus, the S-phase accumulation appears only when highly efficient replication occurs, e.g., transfection of the infectious clone or MVC infection. The S-phase has been emphasized to be important for parvovirus replication. For example, parvovirus H-1 protein synthesis coincides with cellular DNA synthesis (62), and MVM replication apparently requires mitotically active cells (28). Efficient replication of the MVC genome could possibly trigger the S-phase accumulation which loops back to further facilitate MVC DNA replication.

The genome of MVC induces cell cycle arrest at G2/M: Using UV-MVC, we were able to show a significant level of G2/M arrest of UV-MVC-inoculated WRD cells as early as 18 hrs p.i. UV-MVC infection-induced cell cycle arrest at G2/M is consistent with previous reports of

other parvoviruses (41,51,53). The genome of AAV2 that contains an identical inverted terminal repeat at both ends has been shown to induce cell cycle arrest at the G2/M-phase (51). Infection of UV-irradiated B19V has been shown to induce a G2/M arrest as early as at 24 hrs p.i. (41). The G2/M-phase arrest by the MVC genome alone was also reproduced by transfection of the NS1 knock-out mutant of the MVC infectious clone. The MVC genome that lacks half of the left terminal repeat still induced a clear G2/M arrest by transfection. Only the MVC genome that does not contain both terminal repeats, the NSCap gene, lost its ability to induce cell cycle arrest. These observations suggest that the terminal repeats of the MVC genome, which form strong secondary structures (60), play an important role in inducing cell cycle arrest at the G2/M-phase during MVC infection. It may be true that the structure of the terminal repeats of parvoviruses acts as a perfect trigger to induce DNA damage response, which in turn, induces cell cycle arrest.

Chapter 4

Role of erythropoietin receptor signaling in parvovirus B19 infection of human erythroid progenitor cells

Abstract

Human parvovirus B19 (B19V) infection is highly restricted to human erythroid progenitors. In this study, firstly, we have shown that erythroid progenitor cells *ex vivo* expanded from $CD34^+$ hematopoietic cells (HSCs) in the absence of erythropoietin (Epo) [$CD36^+$/Epo(-) EPCs)] did not support B19V replication, even though B19V did enter these cells. Epo exposure either prior to infection or after virus entry tuned the $CD36^+$/Epo(-) EPCs to accommodate active B19V replication. Secondly, a Janus kinase 2 (Jak2) inhibitor, AG490, inhibited phosphorylation of Jak2 and thereafter phosphorylation of Epo receptor (EpoR), and subsequently abolished replication of B19V in *ex vivo* expanded erythroid progenitor cells in the presence of Epo ($CD36^+$/Epo+ EPCs), at a final concentration of 5 μM. Moreover, expression of a constitutively active EpoR in $CD36^+$/Epo(-) EPCs conferred an efficient B19V replication. Finally, we provide evidence that B19V replication in $CD36^+$/Epo+ EPCs required Epo in a dose-dependent manner. In conclusion, we have demonstrated that the EpoR signaling is absolutely required for B19V infection of *ex vivo* expanded erythroid progenitor cells after initial virus entry, which in part explains the remarkable tropism of B19V infection to human erythroid progenitors.

Introduction

Parvovirus B19 (B19V) is pathogenic to humans. It is an autonomously replicating virus with a remarkable tropism to human erythroid progenitors of bone marrow (163, 199). Clinical manifestations of B19V infection vary among different health conditions. The most common one is erythema infectiosum. However, B19V infection often results in bone marrow failure in the following conditions. In patients with increased destruction of erythrocytes and a high turnover of erythrocytes (e.g., sickle cell disease patients), acute B19V infection can cause transient aplastic crisis. In immunocompromised patients, persistent B19V infection may develop manifestations as pure red-cell aplasia, a chronic anemia. B19V fetal infection, however, can cause severe anemia in fetus, resulting in non-immune hydrops fetalis and fetal death (2, 57). Erythropoiesis is the process whereby a fraction of primitive multipotent hematopoietic stem cells ($CD34^+$) commit to the erythroid lineage, forming burst-forming units-erythroid (BFU-Es, earlier erythroid progenitors), colony-forming units-erythroid (CFU-Es, later erythroid progenitors), normoblasts, erythroblasts, reticulocytes, and ultimately the mature erythrocytes. B19V infection shows a remarkable tropism to human erythroid progenitors with the $CD36^+$ marker of both BFU-Es and CFU-Es (163, 199). Clinical manifestations of B19V infection, as seen in aplastic crisis and pure red-cell aplasia, are due to the direct cytotoxicity of the virus infection (29), a direct outcome of the cell death of erythroid progenitors that are targets of B19V replication. A progressive host cell apoptosis has been observed during B19V infection of primary erythroid progenitor cells (195, 225), which is likely induced by the abundantly expressed 11kDa non-structural protein during infection (38). Erythroid progenitors in the tissues of fetuses who exhibited hydrops fetalis caused by B19V infection also were characteristic of apoptotic cell death (225).

Polyadenylation at the proximal site in the center of the B19V genome [(pA)p] precludes the inclusion of the capsid-coding open reading frame, and so alternative polyadenylation plays a key role in B19V capsid protein production (160, 226). We have recently shown that replication

of the B19V genome enhances read-through of the proximal polyadenylation site and the polyadenylation of B19V transcripts at the distal site. Therefore, replication of the B19V genome facilitates the generation of sufficient full-length transcripts to encode the viral capsid proteins (79).

The remarkable tropism of B19V to human erythroid progenitors was believed to be due to the blood-group P antigen (Globoside), the cellular receptor for B19V (28). However, the recent finding of co-receptors (138, 218) suggests that erythrocyte P antigen is necessary, but not sufficient, for B19V binding and entry; the expression level of the P antigen does not correlate with the efficiency of viral binding (219). In addition to the native target cells for B19V infection in human bone marrow and fetal livers, a few cell lines (basically myeloblastoid cell line like UT7/Epo-S1 (135) and KU812Ep6 (127)) do support B19V replication but in a limited efficiency (23, 222). Recently, *ex vivo* expanded $CD36^+$ erythroid progenitor cells ($CD36^+$ EPCs) have been proven to be highly permissive to B19V infection and support active B19V replication (at least 100-fold increase of the B19V genome) (195, 206). All the myeloblastoid cell line cells and primary $CD36^+$ EPCs require Epo to sustain proliferation, suggesting that Epo is required for B19V infection. Epo has been confirmed to be required for susceptibility of human bone marrow cells to B19V infection (206), from which a conclusion was drawn that the target cells of B19V are in erythroid lineage from BFU-Es to erythroblasts, with susceptibility to B19V increasing along differentiation (206). Thus, the role of Epo in B19V permissiveness was thought mainly to differentiate bone marrow hematopoietic stem cells (HSCs) to the stage of erythroid progenitor. In this study, we have shown a direct role of Epo and its pathway in supporting replication of the B19V genome. We prepared $CD36^+$ EPCs by *ex vivo* expanding $CD34^+$ HSCs in two formulated media with or without Epo. In the absence of Epo, the $CD36^+$ EPCs expanded in StemCell medium (Tab. 4-1), namely $CD36^+$/Epo(-) EPCs, were not permissive to B19V infection, though the virus entered the cells. However, upon addition of Epo either prior to or after virus infection, Epo-pulsed $CD36^+$/Epo(-) EPCs became permissive to B19V replication.

Moreover, inhibiting EpoR signaling, either by the Jak2 inhibitor AG490 or Jak2 shRNA, decreased B19V replication in $CD36^+$ EPCs expanded in Wong medium (Tab. 4-1) with Epo ($CD36^+$/Epo+ EPCs). More importantly, expression of a constitutively active EpoR in $CD36^+$/Epo(-) EPCs rescued B19V replication to a level comparable to that in $CD36^+$/Epo+ EPCs. Thus, our study elucidates an indispensible role of Epo and its pathway in B19V replication, which was not appreciated previously, and can partially illuminate why B19V prefers to propagate in cells which take Epo as an essence to proliferate.

Materials and Methods

Generation of $CD36^+$ EPCs: $CD34^+$ HSCs were purchased from National Disease Research Interchange (NDRI), Philadelphia, PA. One million cells were cultured in two different expansion media as described in Table 4-1. $CD34^+$ HSCs were *ex vivo* expanded in Wong medium from day 0 and stored in liquid nitrogen at day 4 as described previously (14,45). Large numbers of $CD36^+$ EPCs were expanded in StemCell medium continuously until day 6 or day 8 for purification, and day 8 for B19V infection where indicated.

Construction and production of retroviral and lentiviral vectors:

Retroviral vector expressing Epo-R(R129C): Plasmid pMSCV-EpoR(R129C)-IRES-GFP was constructed by inserting EpoR(R129C) gene (13) into BamH-Xba-digested pMSCV-MCS-IRES-GFP-WRE vector. Retroviruses (Retro-EpoR and Retro-GFP) were produced by transfecting pMSCV-EpoR(R129C)-IRES-GFP and pMSCV-IRES-GFP, respectively, with pCMV-VSVG in GP293 cells (Clontech). Concentration of retroviral vectors was carried out following the manufacturer's instructions (Clontech, cat. No.:PT3132-1).

Lentiviral vectors expressing shRNA: We obtained pLKO.1 cloning vector and pLKO-Scrambe-shRNA vector from Addgene Inc. (Cambridge, MA). The puromycin resistance gene in

pLKO vectors was replaced by the GFP ORF from pC1GFP (Clontech) through BamHI/KpnI sites, resulting in pLKO-GFP and pLKO-GFP-Scramble-shRNA, respectively. The validated JAK2 shRNA1 sequence (TRCN0000003181, NM_004972, Sigma) was cloned into pLKO-GFP through AgeI and EcoRI sites, which resulted in pLKO-GFP-Jak2-shRNA. Lentivirus was generated and concentrated following Addgene's instructions (http://www.addgene.org/plko).

Purification of $CD36^+$ EPCs cultured in StemCell medium: 3×10^6 of $CD34^+$ HSCs were cultured in StemCell medium. At day 6 or 8, approximately $2\text{-}3 \times 10^7$ expanded cells were spun down at 300 g for 10 min, resuspended in 1 ml of autoMACS rinsing buffer (Miltenyi Biotec, Auburn, CA), and incubated with mouse anti-human CD36 antibody (BD Biosciences, 10^6 cells/μl) for 15 min at 4 °C. Then cells were spun down at 2, 250 rpm for 2 min and washed three times with the autoMACS rinsing buffer. After incubation with anti-mouse IgM magnetic microbeads (Miltenyi Biotec) for 15 min at 4 °C, cells were loaded onto MS column and labeled cells were eluted following the manufacturer's instructions. Purified $CD36^+$ EPCs expanded in the absence of Epo were named as $CD36^+$/Epo(-) EPCs.

Virus and infection:

We obtained B19V viremic plasma samples, P20 (14) and P32, from ViraCor Laboratories (Lee's Summit, MO), and quantified for B19V genomic copies [10^{12} genomic copies (gc)/ml] as previously described (14). Infection was performed at a multiplicity of infection (MOI) of 5,000 genomic copies (gc)/cell [approximately 1 fluorescent foci-forming unit (fffu)/cell]. Except for Fig. 4-1, for which P20 was used, all other figures were generated by using P32 for consistency. For retroviral transduction, concentrated retrovirus was added to $CD36^+$/Epo(-) EPCs purified at day 6 of culture at an MOI of 4 fffu/cell. B19V infection was carried out at 48 hrs posttransduction (p.t.).

Viral entry assay and replication quantification: For Viral entry assay (2), cells were infected with B19V at an MOI of 5,000 gc/cell. At 2 hrs after incubation with the virus, the cells were washed with AMEM (Alpha Modification of Eagles Medium, Mediatech, Manassas, VA), and spun down at 2,200 rpm for 3 min. The cell pellet was then resuspended in 0.5 million cells per 100 µl of trypsin/*versene (0.25% trypin in 20mM EDTA buffer)* for 5 min at 37 ºC. Total DNA was extracted following instructions of the Blood DNA Mini Kit (Qiagen) with modification. Extracted DNA was then used to quantify B19V genomic copies by quantitative real time PCR (qPCR) as described previously (15). The replicated B19V genome was extracted as described above and quantified by qPCR at 48 hrs p.i., except Fig. 4-3C at 24 hrs p.i.

Southern blot analysis: At 48 hrs p.i., cells were harvested for Hirt DNA extraction, and Hirt DNA samples were analyzed by Southern blot as described previously (14,15). Blots were exposed to a GE phosphor imaging screen, and quantified by a phosphor imager (Storm 856) using Image Quant TL software v2005 (GE Healthcare).

Reverse transcription (RT) and quantitative real time PCR (RT-qPCR): We extracted mRNA using TurboCapture mRNA kit (Qiagen) following manufacturer's instructions. We then performed reverse transcription directly in the TurboCapture tubes using random hexamers (Promega) and MMLV-RT (Invitrogen). A multiplex RT-qPCR was performed to detect B19V VP2-encoding mRNA and B19V mRNA spliced from D1 donor site to A1-2 acceptor site (D1/A1-2-spliced mRNA) (14), with β-actin mRNA serving as an internal control as previously reported (14,15).

Immunofluorescence: Infected cells were cytocentrifuged at 1, 500 rpm for 5 min and fixed in a mixture of acetone and methanol (1:1) at - 20°C for 15 min. The staining was performed as previously described using anti-B19V capsid (clone 521-5D) and FITC- conjugated anti-mouse IgG (15).

Western blot analysis: Cell lysates were prepared at 48 hrs post-treatment, and used for Western blotting analysis as previously described (34).

Cell viability assay: We examined cell viability using CellTiter-Glo® kit (Promega) to determine the number of viable cells in culture based on quantifying the ATP presence following manufacturer's instructions.

Flow cytometry analysis:

For surface staining, 10^5 cells were incubated with the first antibody at 1: 100 dilution in a volume of 100 µl of PBS containing 2% FCS (PBS-FCS) for 30 min at room temperature (RT). Washed twice with PBS-FCS, cells were incubated with FITC-conjugated secondary antibody at a dilution of 1: 100 for 30 min at RT. After washing, the cells were fixed in 1% paraformaldehyde before analysis. The intracellular staining was basically performed as previously described (7).

Results

$CD36^+$ EPCs differentiated from $CD34^+$ HSCs in the absence of Epo are not permissive to B19V infection.

To distinguish the role of Epo in differentiating HSCs and supporting B19V replication, we generated erythroid progenitor cells, which possess erythroid progenitor marker CD36 (60, 154) through differentiating human bone marrow derived-HSCs ($CD34^+$ cells) in two expansion media. They contain different combination of cytokines as described in Tab. 4-1.

At day 8 in culture, cells in different expansion media were analyzed by flow cytometry with antibodies to erythroid markers (CD36, GPA, EpoR, and CD71), B19V receptor (Globoside) and co-receptors (CD49e and KU80), and the CD41 megakaryoblastic marker (214) as well as the CD34 HSC marker for specific lineage differentiation of the cells. The *ex vivo* expanded cells

both in Wong and StemCell media expressed CD36 marker at 99.4% and 41.5%, respectively (Fig. 4-1A). Expanded cells in StemCell medium (without Epo) retained a considerable level of CD34 maker at 23.3%, and a low level of CD41 marker at 7.4% (Fig. 4-1A), indicating their lineage differentiation toward erythroid progenitor cells. CD71, the transferrin receptor, was expressed at levels of 96.8%

Table 4-1. Formula of expansion media for $CD36^+$ EPCs.

Serum-free expansion media (SFEM) and BIT9500 (BIT) were obtained from StemCell Technologies Inc. (Vancouver, BC, Canada). All the cytokines were purchased from Invitrogen except for the Epo from Amgen. SCF=Stem cell factor; IL-6=Interleukin 6; IL-3=Interleukin 3; Flt-3-L=Flt-3 ligand; TPO=T*hrombopoietin; Epo=Erythropoietin. Wong medium also contains* 900 ng/ml of $Fe^{2+,}$ 90 ng/ml of Fe^{3+} and 1μM of Hydrocortisone as *described previously (79, 222).*

Name of medium	StemCell	Wong
Serum-free base:	SFEM	BIT in AMEM
Cytokines (ng/ml):		
SCF	100	100
IL-6	20	x
IL-3	20	5
Flt-3-L	20	x
TPO	50	x
Epo	x	3 (unit/ml)

Figure 4-1. CD36$^+$ EPCs expanded in StemCell medium without Epo are not permissive to B19V infection.

CD34$^+$ HSCs were cultured in StemCell medium shown in Tabel 1. **(A)** At day 8 of culture, the indicated surface markers of cells from different cultures were analyzed and presented in histogram. For surface staining, antibodies against cell surface antigen CD34, CD36, CD41, GPA, CD71 and CD49e (all obtained from BD Biosciences, San Jose, CA), and antibodies against globoside (Matreya, Pleasant Gap, PA), KU80 (Calbiochem, San Diego, CA) and EpoR (Abcam, Cambridge, MA) were used to characterize cell phenotype. Numbers in each panel indicate the percentage of positive population. A representative result from two independent experiments is shown. **(B)** At day 8 of culture, B19V infection was carried out as described in Materials and Methods. Immunofluorescence staining was performed at 48 hrs p.i. using antibody against B19V capsid antibody. DAPI was used to stain nucleus. Images were acquired by an Eclipse C1 Plus confocal microscope (Nikon) at a magnification of x 40.

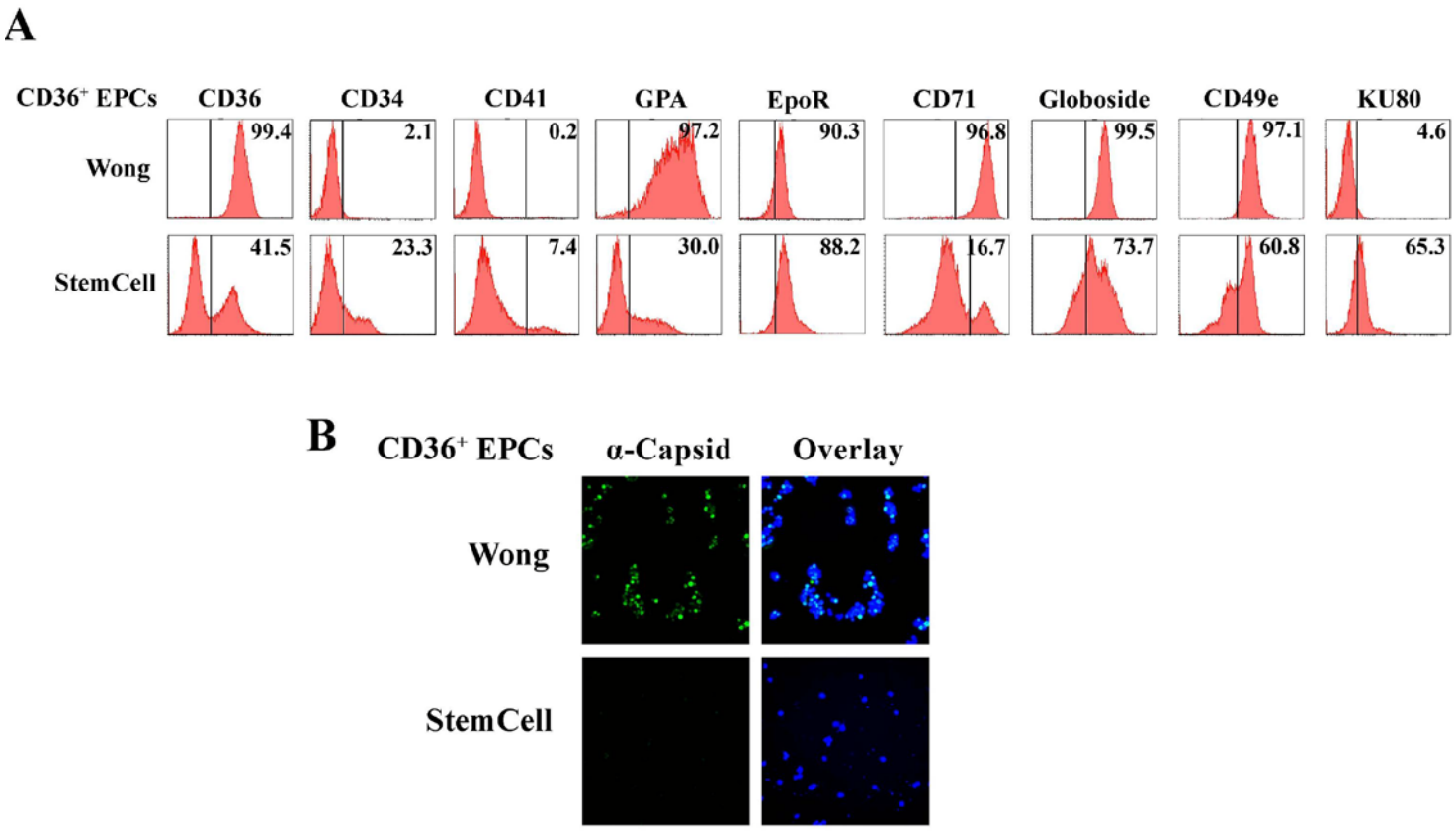
A
CD36+ EPCs
CD36
CD34
CD41
GPA
EpoR
CD71
Globoside
CD49e
KU80
Wong
99.4
2.1
0.2
97.2
90.3
96.8
99.5
97.1
4.6
StemCell
41.5
23.3
7.4
30.0
88.2
16.7
73.7
60.8
65.3
B
CD36+ EPCs
α-Capsid
Overlay
Wong
StemCell

and 16.7% (Fig. 4-1A), respectively, on cells expanded in Wong and StemCell media. Cells gained the GPA (CD235a) marker at a high extent, 97.2%, on $CD36^+$ EPCs expanded in Wong medium, while only 30.0% on cells expanded in StemCell medium (Fig. 4-1A). Cells expanded in both media expressed a high level of globoside and CD49e, the primary receptor and co-receptor for B19V infection (4,44), as well as the EpoR (Fig. 4-1A). Interestingly, KU80, which was proposed as a co-receptor of B19V (24), was expressed on the most of cells (65.3%) expanded in StemCell medium, but only on 4.6% of the cells expanded in Wong medium (Fig. 4-1A).

We then infected these two types of $CD36^+$ EPCs with B19V in their respective media for two days. B19V infectivity was examined by immunofluorenscence with anti-B19V capsid antibody (Fig. 4-1B). Surprisingly, $CD36^+$ EPCs expanded in StemCell medium, which did not contain Epo, were not permissive to B19V infection as shown by negative anti-capsid staining. Conversely, $CD36^+$ EPCs expanded in Wong medium, which contained Epo at 3 units/ml, showed more than 80% of cells positive with anti-capsid staining, indicating an effective infection (222). This result suggests that the committed erythroid progenitor cells cultured in the absence of Epo are not permissive to B19V infection, and Epo is required not only for differentiation of erythroid progenitor cells but also may be necessary for B19V infection of erythroid progenitor cells.

Epo confers permissiveness of B19V infection to $CD36^+$/Epo(-) EPCs by turning on viral genome replication.

We next chose to purify $CD36^+$ EPCs from the cells expanded in StemCell medium. Purified cells, named as $CD36^+$/Epo(-) EPCs, were analyzed by flow cytometry, expressing uniform erythroid progenitor markers, i.e., $CD36^+$ at 87.5%, GPA^+ at 88.2% and $EpoR^+$ at 84.5%, as well as high levels of B19V receptor ($Globoside^+$ at 87.9%) and co-receptors ($CD49e^+$ at 39.4% and $KU80^+$ at 85.7%). Interestingly, these purified cells were mostly (82.5%) both $CD34^+$ and $CD36^+$

(Fig. 4-2B, 0 hr), indicating they were at the stage of BFU-E (154). Similar to unpurified cells expanded in StemCell medium (Fig. 4-1B), purified $CD36^+$/Epo(-) EPCs were not susceptible to B19V infection as shown by negative anti-capsid staining and undetectable B19V mRNAs (Fig. 4-2C, D&E).

To examine whether Epo is absolutely required for B19V infection, we pretreated purified $CD36^+$/Epo(-) EPCs with Epo at 3 unit/ml for 2 hrs and overnight (approximately 16 hrs), respectively, followed by B19V infection. Interestingly, cells treated with Epo for 2 hrs or overnight clearly became susceptible to B19V infection to some extent (Fig. 4-2C, D&E). With overnight Epo treatment, approximately 10% of purified $CD36^+$/Epo(-) EPCs expressed B19V capsid, as well as B19V VP2-encoding mRNA (at a level of 0.7% of β-actin mRNA copy) and D1/A1-2-spliced mRNA (at a level of 0.4% of β-actin mRNA copy), respectively. As demonstrated by virus entry assay and DNA replication quantification, while purified $CD36^+$/Epo(-) EPCs without Epo treatment did not show any increase of the B19V genome, Epo treatment for 2 hrs and overnight facilitated replication of the B19V genome for approximately 2.5-fod and 13-fold, respectively (Fig. 4-3A). As control, $CD36^+$/Epo+ EPCs supported approximately 93-fold increase of entered B19V genome. Interestingly, we also

Figure 4-2. Epo pulse confers B19V viral protein expression in CD36^{+}/Epo(-) EPCs.

Purified CD36^{+}/Epo(-) EPCs were pulsed with Epo (3 U/ml) for different length of time. **(A)** Indicated surface markers were determined on cells with different treatments. **(B)** Double staining of CD34 and CD36 markers on cells with different Epo treatments. **(C)** Cells were treated with Epo as indicated, and infected with B19V. At 48 hrs p.i., immunofluorescence staining of B19V capsid was performed with costaining of DAPI to show nucleus. Images were acquired by an Eclipse C1 Plus confocal microscope (Nikon) at a magnification of x 40. **(D&E)** At 48 hrs p.i., VP2-encoding mRNA **(D)** and D1/A1-2-spliced mRNA **(E)** were quantified by multiplex RT-qPCR and presented as copy number per β-actin mRNA (internal control) with average and standard deviation as shown.

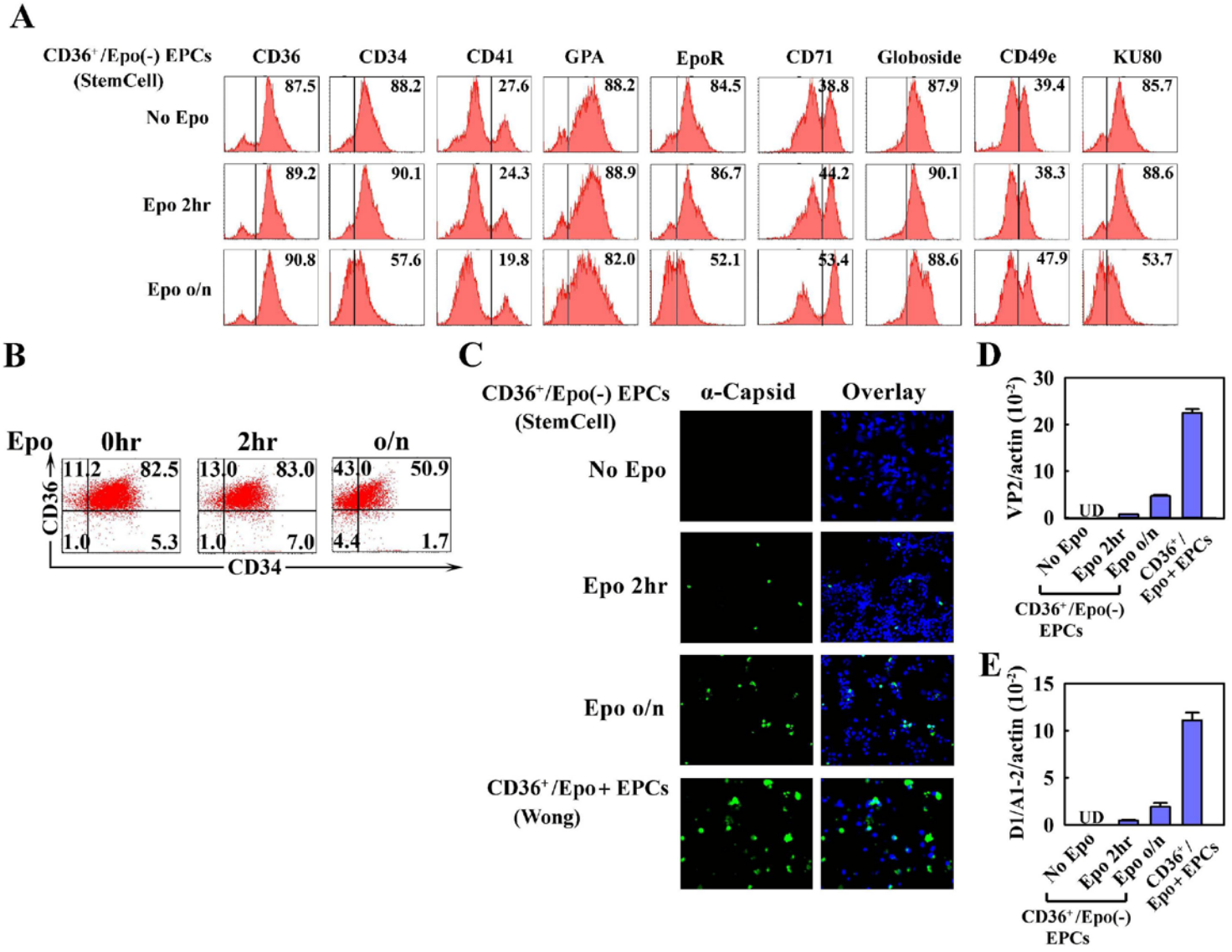
A
CD36+/Epo(-) EPCs (StemCell)
CD36
CD34
CD41
GPA
EpoR
CD71
Globoside
CD49e
KU80
No Epo
87.5
88.2
27.6
88.2
84.5
38.8
87.9
39.4
85.7
Epo 2hr
89.2
90.1
24.3
88.9
86.7
44.2
90.1
38.3
88.6
Epo o/n
90.8
57.6
19.8
82.0
52.1
53.4
88.6
47.9
53.7
B
Epo
0hr
2hr
o/n
CD36
CD34
11.2
82.5
1.0
5.3
13.0
83.0
1.0
7.0
43.0
50.9
4.4
1.7
C
CD36+/Epo(-) EPCs (StemCell)
α-Capsid
Overlay
No Epo
Epo 2hr
Epo o/n
CD36+/Epo+ EPCs (Wong)
D
VP2/actin (10-2)
30
20
10
0
UD
No Epo
Epo 2hr
Epo o/n
CD36+/Epo+EPCs
CD36+/Epo(-) EPCs
E
D1/A1-2/actin (10-2)
15
10
5
0
UD
No Epo
Epo 2hr
Epo o/n
CD36+/Epo+EPCs
CD36+/Epo(-) EPCs

observed that $CD36^+/Epo^+$ EPCs allowed B19V entry to the most extent, approximately 17 times more than that into purified $CD36^+$/Epo(-) EPCs without Epo treatment, and approximately 5-8 times more than that into the cells treated with Epo for either 2 hrs or overnight (Fig. 4-3A). This indicates that B19V virus entry of $CD36^+$ EPCs is affected by Epo stimulation.

Cell surface markers on purified $CD36^+$/Epo(-) EPCs treated with Epo for 2 hrs and overnight revealed slight shift toward the profile presented on $CD36^+$/Epo+ EPCs, especially the CD34, CD41 and CD71 markers (Fig. 4-2A). This result indicates that Epo treatment does differentiate the cells from BFU-E- to CFU-E-type cells which loose both CD34 and CD41 markers (154). Taken together, we demonstrated that susceptibility of $CD36^+$/Epo(-) EPCs to B19V infection is not due to the blockage of viral entry; instead, these cells do not facilitate replication of the B19V genome, and Epo treatment turned on B19V replication in these cells. As markers of Epo treatment (18), increased levels of phosphorylated Jak2 (pJak2) and phosphorylated Epo receptor (pEpoR) were detected in cells treated with Epo for 2 hrs and overnight (Fig. 4-3B) compared with cells without Epo treatment. Thus our results suggest that the Epo/EpoR signaling is likely essential to B19V replication.

To rule out the potential interference from viral entry, we performed B19V entry assay prior to Epo stimulation. In such a condition, at the time of Epo treatment, the cells in different groups have exactly the same amount of entered viral genome. Again, $CD36^+$/Epo+ EPCs

Figure 4-3. Epo stimulation is a switch of B19V replication in CD36$^+$/Epo(-) EPCs.

(A&B) We pulsed purified CD36$^+$/Epo(-) EPCs with Epo (3 U/ml) for different lengths of time prior to B19V infection. CD36$^+$/Epo+ EPCs expanded in Wong medium were used as control. **(A)** B19V entry and DNA replication were determined as described in Materials and Methods. The number in the panel indicated the fold difference between replication and entry. The "No Epo" group bars were enlarged to better present the results with scale. **(B)** We determined the phosphorylation of EpoR and Jak2 by flow cytometry in cells with different treatment immediately before B19V infection. We used anti-pEpoR (Tyr 456) (Santa Cruz Biotech, Inc., Santa Cruz, CA), anti-pJak2 (Tyr 1007) (Genscript, Piscataway, NJ) and anti-B19V NS1 (8) for staining pJak2, pEpoR and B19V NS1, respectively. We used Cy5-conjugated anti-mouse or rabbit secondary antibodies for intracellular staining. Quantification of Mean Fluorescence Intensity (MFI) with the reference line indicating the background is shown in bar figures to the right in panel B.

(C, D&E) We recovered purified CD36$^+$/Epo(-) EPCs in StemCell medium for 1 hr, then we infected cells with B19V. While one fifth of the cells were used to quantify viral entry, the other four-fifths of the cells were evenly divided into four groups for Epo treatment for 0, 2, 8 and 24 hrs, respectively. CD36$^+$/Epo+ EPCs expanded in Wong medium were used as control. B19V entry and replication were quantified by qPCR and presented as B19V genome copy number per cell (gc/cell). **(C)**. B19V VP2-encoding mRNA **(D)** and D1/A1-2-spliced mRNA **(E)** were quantified by RT-qPCR and presented as copy number per β-actin mRNA (internal control). Average and standard deviation are shown in panel A, C, D and E, and were calculated from at least three independent experiments.

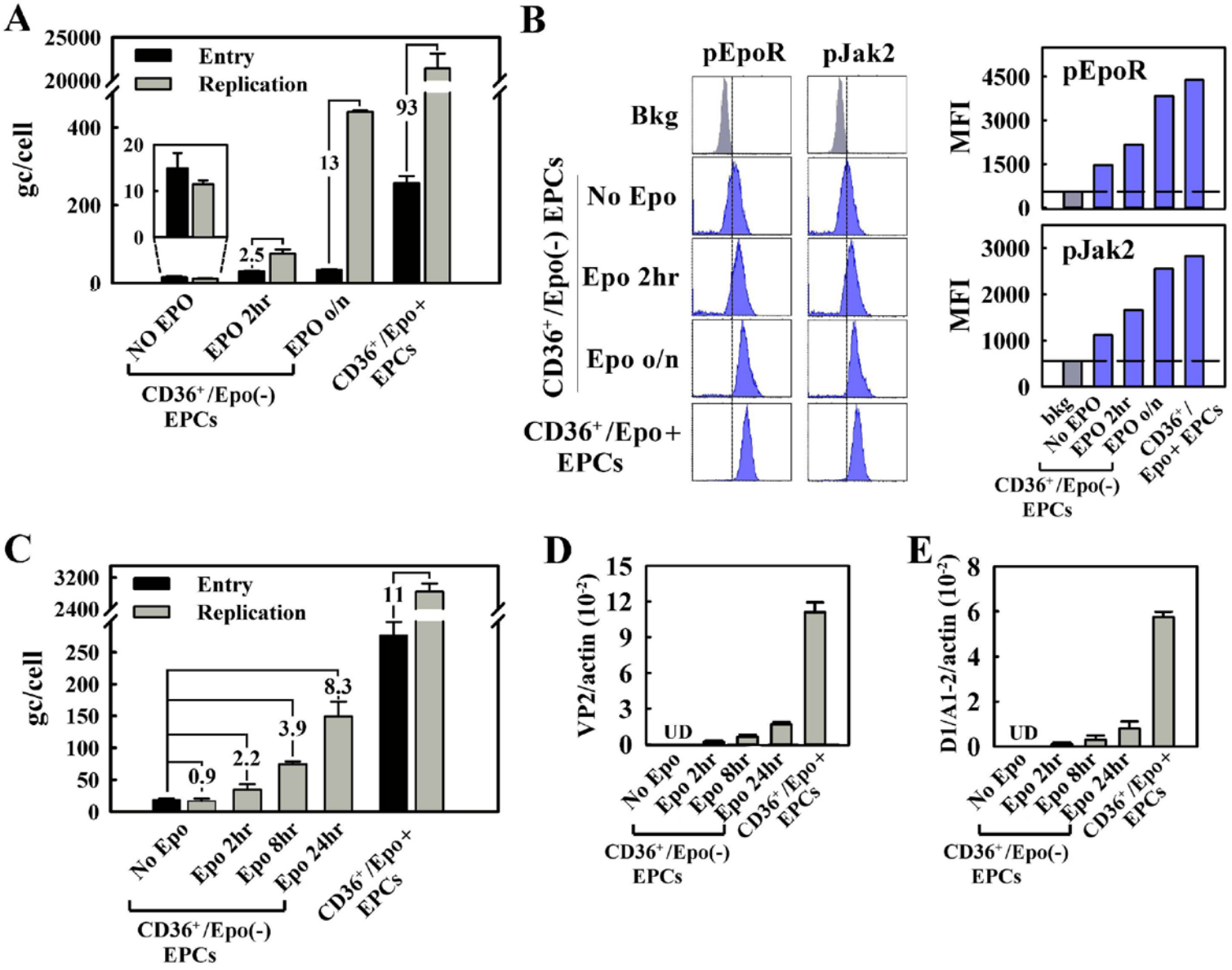
A
25000
20000
400
200
0
gc/cell
Entry
Replication
20
10
0
2.5
13
93
NO EPO
EPO 2hr
EPO o/n
CD36+/Epo+ EPCs
CD36+/Epo(-) EPCs
B
pEpoR
pJak2
Bkg
No Epo
Epo 2hr
Epo o/n
CD36+/Epo(-) EPCs
CD36+/Epo+ EPCs
MFI
4500
3000
1500
0
pEpoR
3000
2000
1000
0
pJak2
bkg
No EPO
EPO 2hr
EPO o/n
CD36+/ Epo+ EPCs
CD36+/Epo(-) EPCs
C
3200
2400
250
200
150
100
50
0
gc/cell
Entry
Replication
0.9
2.2
3.9
8.3
11
No Epo
Epo 2hr
Epo 8hr
Epo 24hr
CD36+/Epo+ EPCs
CD36+/Epo(-) EPCs
D
VP2/actin (10-2)
15
12
9
6
3
0
UD
No Epo
Epo 2hr
Epo 8hr
Epo 24hr
CD36+/Epo+ EPCs
CD36+/Epo(-) EPCs
E
D1/A1-2/actin (10-2)
8
6
4
2
0
UD
No Epo
Epo 2hr
Epo 8hr
Epo 24hr
CD36+/Epo+ EPCs
CD36+/Epo(-) EPCs

were used as control. While no replication was observed at 24 hrs p.i. without Epo stimulation, Epo treatment for 2, 8 and 24 hrs increased B19V DNA replication 2.2-, 3.9- and 8.3-fold of entered viral genome, respectively (Fig. 4-3C). As control, $CD36^+$/Epo+ EPCs replicated viral genome for approximately 11-fold of the entered B19V genome at 24 hrs p.i. In terms of the B19V mRNAs, no VP2-encoding mRNA and D1/A1-2-spliced mRNA were detected from infected cells without Epo stimulation (Fig. 4-3D&E). Increasing amounts of Epo pulse conferred increasingly detectable levels of both VP2-encoding and D1/A1-2-spliced mRNAs from infected $CD36^+$/Epo(-) EPCs, though the level was still lower than that in $CD36^+$/Epo(+) EPCs.
Thus, our results indicate a pivotal role of Epo in B19V replication. Epo is absolutely required to turn on replication of B19V genome and thus confers the permissiveness of $CD36^+$/Epo(-) EPCs to B19V infection.

Inhibiting phosphorylation of Jak2 blocks B19V replication in $CD36^+$/Epo+ EPCs.

Epo ligation triggers EpoR dimerization and in turn phosphorylates Jak2 that is associated with EpoR (115). Phosphorylated Jak2 then phosphorylates tyrosine residues in the cytoplasmic tail of EpoR. We decided to investigate whether this phosphorylated Jak2 (pJak2)-mediated Epo/EpoR signaling is involved in facilitating B19V replication. To this end, we used a Jak2-specific inhibitor, AG490 (125), to inhibit Jak2 phosphorylation. The inhibitory effect of AG490 was examined by detecting pJak2 and phosphorylated EpoR (pEpoR) as shown (Fig. 4-4A). At 2 and 5 μM, AG490 effectively decreased the phosphorylation of both

Figure 4-4. Jak2 inhibitor abolishes B19V replication in CD36^{+}/Epo+ EPCs.

CD36^{+}/Epo+ EPCs at day 7 were treated with inhibitors at concentrations as indicated. Twenty four hours later (day 8), inhibitor-treated cells were infected with B19V. **(A)** At 48 hrs post-treatment, a part of the cells were harvested and analyzed by Western blot using antibodies as indicated. Quantification of bands on blots is shown as relative levels to DMSO control (0.5% DMSO). **(B)** The cytotoxicity of inhibitor treatment was evaluated using CellTiter-Glo® kit at 48 hrs post-treatment. The luminescence readings are normalized by the value of cell control group (Non-treated). **(C)** The level of cell death of cells treated with indicated concentrations of AG490 was evaluated by AnnexinV/PI double staining. The numbers indicate the percentage of cells in each gate versus parental population. In the bottom panel, AG490-treated cells were stained with DAPI to show the cell cycle pattern. The numbers indicated percentage of cells in G0/G1, S and G2/M phase respectively. **(D)** At 48 hrs p.i., Hirt DNA was extracted from infected cells and analyzed by Southern Blot. Double replication form (dRF), replication form (RF) and single-stranded DNA (ssDNA) of B19V are indicated. At 48 hrs p.i., mRNAs encoding VP2 **(E)** and spiced from D1 to A1-2 sites **(F)** were quantified by RT-qPCR and presented as copy number per β-actin mRNA (as internal control). **(G)** B19V entry and replication were quantified by qPCR as described in Materials and Methods and presented as B19V genome copy number per cell. Average and standard deviation are shown in panel A, B, D, E and F were calculated from at least three independent experiments.

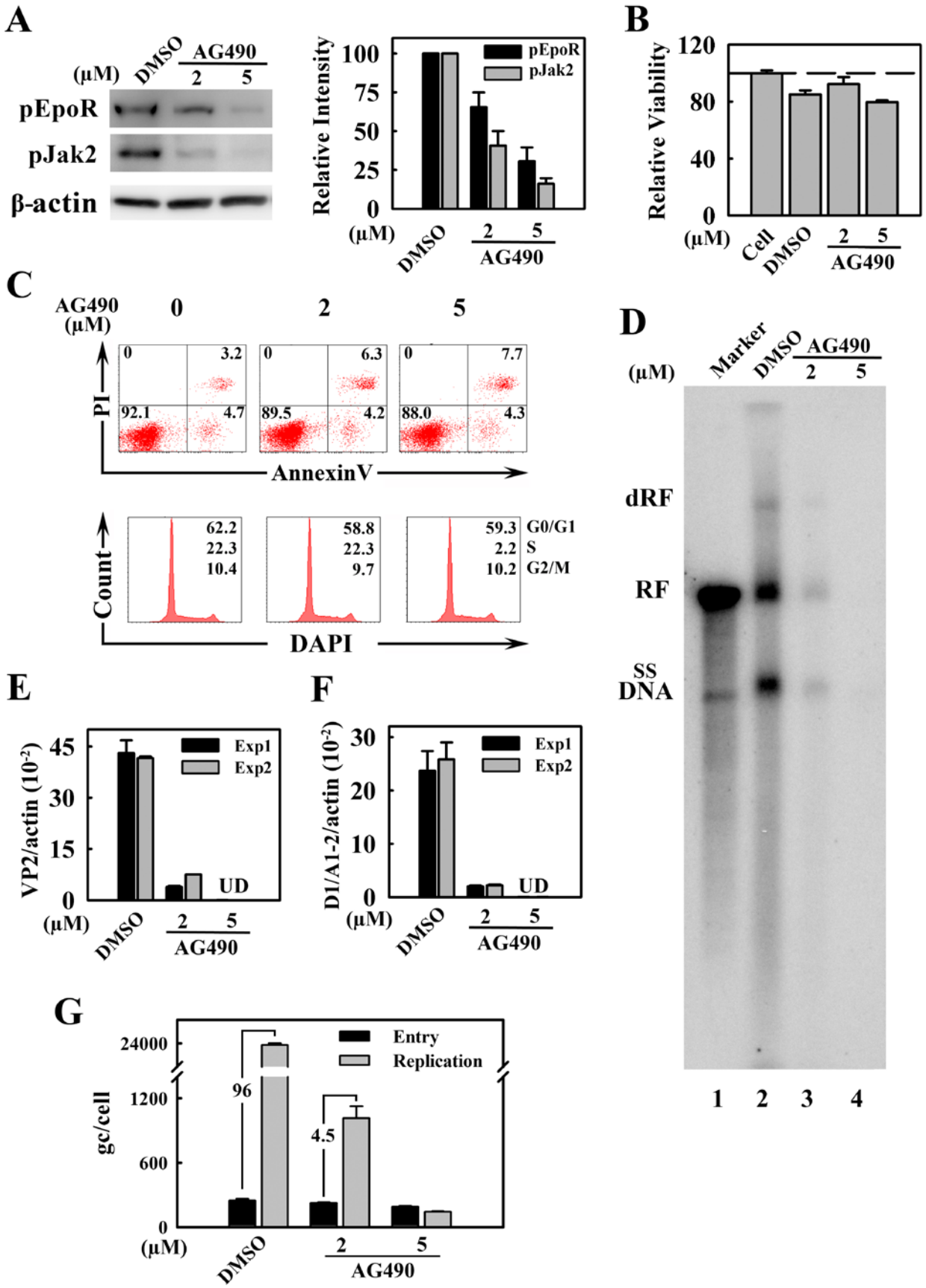
A
(μM)
DMSO
AG490
2
5
pEpoR
pJak2
β-actin
Relative Intensity
100
75
50
25
0
pEpoR
pJak2
(μM)
DMSO
2
5
AG490
B
Relative Viability
120
80
40
0
(μM)
Cell
DMSO
2
5
AG490
C
AG490 (μM)
0
2
5
PI
AnnexinV
0
3.2
92.1
4.7
0
6.3
89.5
4.2
0
7.7
88.0
4.3
Count
DAPI
62.2
22.3
10.4
58.8
22.3
9.7
59.3
2.2
10.2
G0/G1
S
G2/M
D
Marker
DMSO
AG490
2
5
(μM)
dRF
RF
SS DNA
1
2
3
4
E
VP2/actin (10-2)
45
30
15
0
Exp1
Exp2
UD
(μM)
DMSO
2
5
AG490
F
D1/A1-2/actin (10-2)
30
20
10
0
Exp1
Exp2
UD
(μM)
DMSO
2
5
AG490
G
gc/cell
24000
1200
600
0
Entry
Replication
96
4.5
(μM)
DMSO
2
5
AG490

Jak2 and EpoR in a dose-dependent manner. Particularly, at 5 μM, pJak2 and pEpoR were decreased to approximately 20% and 30% of those in the DMSO control, respectively. The cytotoxicity of AG490 in $CD36^+$/Epo+ EPCs was monitored by using the Titer-Glo™ kit, AnnexinV/PI and DAPI staining (Fig. 4-4B&C). No significant retardation of cell viability was observed at either concentration. However, at 2 μM, AG490 inhibited B19V infection significantly with a decrease of approximately 20-fold in B19V DNA replication as shown by Southern blot analysis (Fig. 4-4D, lane 3 vs. 2) as well as expression of B19V VP2-encodig mRNA and D1/A1-2-spliced mRNA (Fig. 4-4E&F). Strikingly, using AG490 at 5 μM, both B19V DNA replication and expression of VP2-encoding and D1/A1-2-spliced mRNAs were undetectable (Fig. 4-4D, lane 4, and Fig. 4-4E, F&G), indicating that B19V infection of $CD36^+$/Epo+ EPCs is sensitive to AG490 treatment. As control, AG490 treatment did not affect B19V entry to the cells (Fig. 4-4G).

To confirm the role of Jak2, we next sought to use Jak2-specifc shRNA to knock down Jak2 expression. We generated a lentivirus expressing shRNA to Jak2 (Lenti-GFP-Jak2-shRNA) and a lentivirus expressing scramble shRNA (Lenti-GFP-Scramble-shRNA). $CD36^+$/Epo+ EPCs were pretreated with lentiviruses two days prior to B19V infection. At 2 days p.i., GFP-expressing cells were gated and analyzed by flow cytometry using anti-Jak2 and anti-B19V NS1 staining. In agreement with the decreased level of Jak2, approximately 50% knock-down, in GFP-Jak2-shRNA-expressing cells, the level of anti-B19V NS1 was significantly decreased approximately 50%, compared to that in GFP-Scramble-shRNA-expressing cells (Fig. 4-5A). Replication of the B19V genome, as

Figure 4-5. Jak2 shRNA reduces B19V infection of CD36$^+$/Epo+ EPCs.

CD36$^+$/Epo+ EPCs at day 6 were transduced with Lenti-GFP-Jak2-shRNA and Lenti-GFP-Scramble-shRNA, respectively. At 48 hrs p.t., transduced cells were infected with B19V. **(A)** At 48 hrs p.i., cells were harvested and stained intracellularly for antigen as indicated. GFP-expressing cells were selectively gated to quantify expression levels of Jak2 and B19V NS1. The percentage of B19V NS1-expressing cells in each group is shown in the histograms, and the MFI of Jak2 expression was quantified and presented in the bar figure to the right in panel A. **(B&C)** At 48 hrs p.i., cells were harvested for mRNA isolation using the Turbo mRNA kit as described in section Materials and Methods. RT-qPCR was carried out to determine B19V VP2-encoding mRNA/β-actin mRNA **(B)** and B19V D1/A1-2-spliced mRNA/β-actin mRNA **(C).** Average and standard deviation are shown in panel B and C, and were calculated from at least three independent experiments.

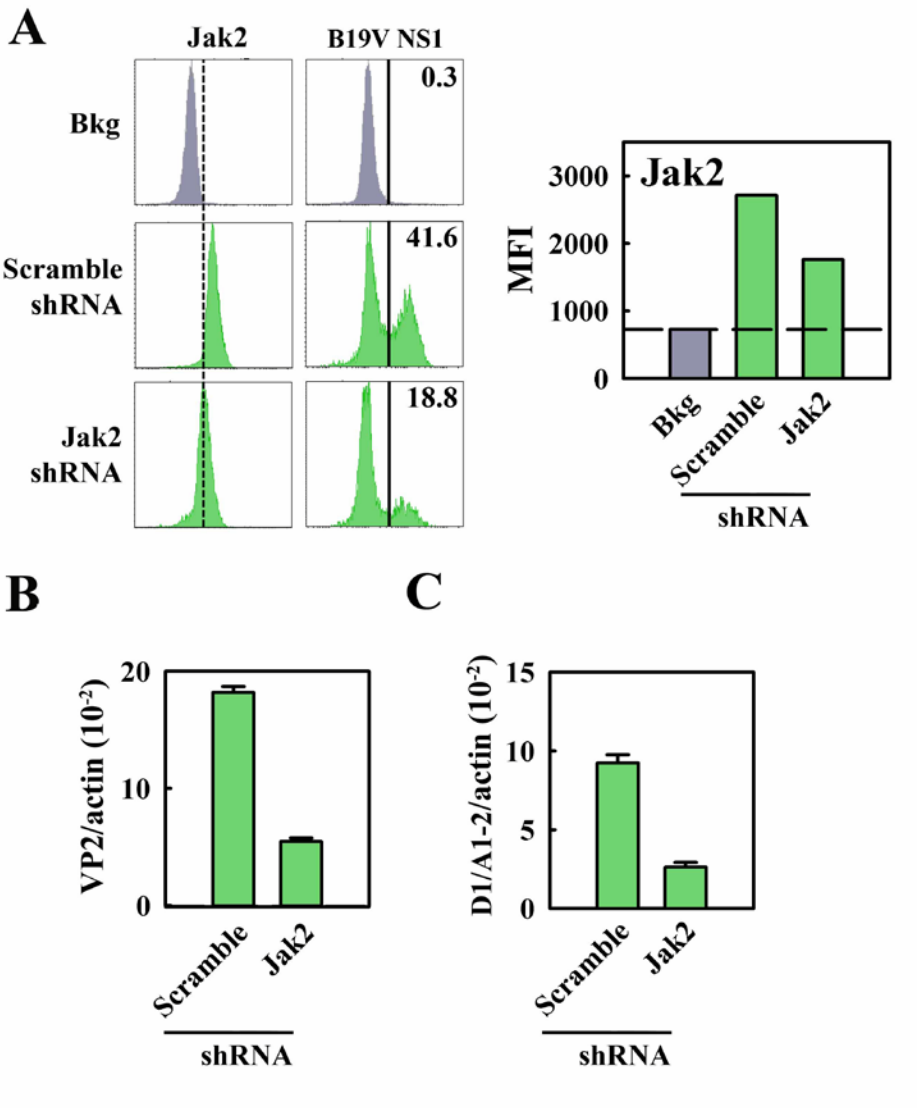
A
Jak2
B19V NS1
Bkg
Scramble shRNA
Jak2 shRNA
0.3
41.6
18.8
MFI
Jak2
3000
2000
1000
0
Bkg
Scramble
Jak2
shRNA
B
VP2/actin (10-2)
20
10
0
Scramble
Jak2
shRNA
C
D1/A1-2/actin (10-2)
15
10
5
0
Scramble
Jak2
shRNA

assayed by the levels of B19V VP2-encoding mRNA and D1/A1-2-spliced mRNA, decreased by approximately 3-fold in cells expressing GFP-Jak2-shRNA (Fig. 4-5B&C), confirming the important role of Jak2 in facilitating B19V infection of $CD36^+$/Epo+ EPCs.

Taken together, these results indicate that the Epo/EpoR/pJak2/pEpoR signaling pathway is crucial in facilitating B19V infection of $CD36^+$/Epo+ EPCs.

Expression of constitutively active EpoR activates B19V infection of $CD36^+$/Epo(-) EPCs.

To further confirm the role of EpoR signaling pathway during B19V infection, we generated a retroviral vector that expresses a constitutively active EpoR gene (75). Purified $CD36^+$/Epo(-) EPCs were transduced with Retro-EpoR or Retro-GFP (as control) 48 hrs prior to B19V infection. At 48 hrs p.i., GFP-expressing cells (approximately 50%) were gated and analyzed by flow cytometry using intracellular staining of anti-pEpoR, anti-pJak2 and anti-B19V NS1 antibodies, respectively. Retro-EpoR-transduced cells successfully expressed constitutively activated Epo-R, as shown by an increased level of anti-pEpoR staining, which presumably was phosphorylated by the active Jak2 as detected, compared to those staining in Retro-GFP-transduced cells (Fig. 4-6A). Correspondingly, Retro-EpoR-transduced cells showed a higher level of anti-B19V NS1 staining by approximately 40%, compared to nearly negative staining of anti-B19V NS1 (1.1%) in Retro-GFP-transduced cells (Fig. 4-6A). Levels of B19V mRNAs and replication of the B19V

Figure 4-6. Retroviral transduction of constitutively active EpoR confers CD36$^+$/Epo(-) EPCs permissive to B19V infection.

Purified CD36$^+$/Epo(-) EPCs were transduced with GFP control retrovirus (Retro-GFP) and constitutively active EpoR-expressing retrovirus (Retro-EpoR). At 48 hrs p.t., cells were infected with B19V. **(A)** At 48 hrs p.i., infected cells were harvested and stained intracellularly for antigens as indicated. GFP-expressing cells were selectively gated to quantify expression levels of pJak2, pEpoR and B19V NS1. The percentage of B19V NS1-expressing cells is shown in histograms. The MFI of pEpoR and pJak2 expression was quantified and presented in the bar figure to the right in panel A. **(B&C)** At 48 hrs p.i., cells were harvested for mRNA isolation. RT-qPCR was carried out to determine B19V VP2-encoding mRNA/β-actin mRNA **(B)** and B19V D1/A1-2-spliced mRNA/β-actin mRNA **(C)**, respectively. **(D)** B19V entry and genome replication levels in cells with indicated treatment were quantified by qPCR and presented as genomic copy number per cell (gc/cell). Fold changes between replication and virus entry are shown. The bars of "Retro-GFP" group are enlarged to scale for better presentation. Average and standard deviation are shown in panel B, C and D, and were calculated from at least three independent experiments. **(E)** Several key cell surface markers of erythroid progenitors were stained as indicated at 48 hrs p.t., prior to B19V infection. GFP-expressing cells were selectively gated in Retro-GFP and Retro-EpoR groups, respectively. Cy5-conjugated secondary antibodies were used for flow cytometry analysis to generate this panel. A representative result from two independent experiments is shown.

Two groups of cells, CD36$^+$/Epo(-) EPCs treated with Epo overnight (Epo o/n) and CD36$^+$/Epo+ EPCs, were set up as controls.

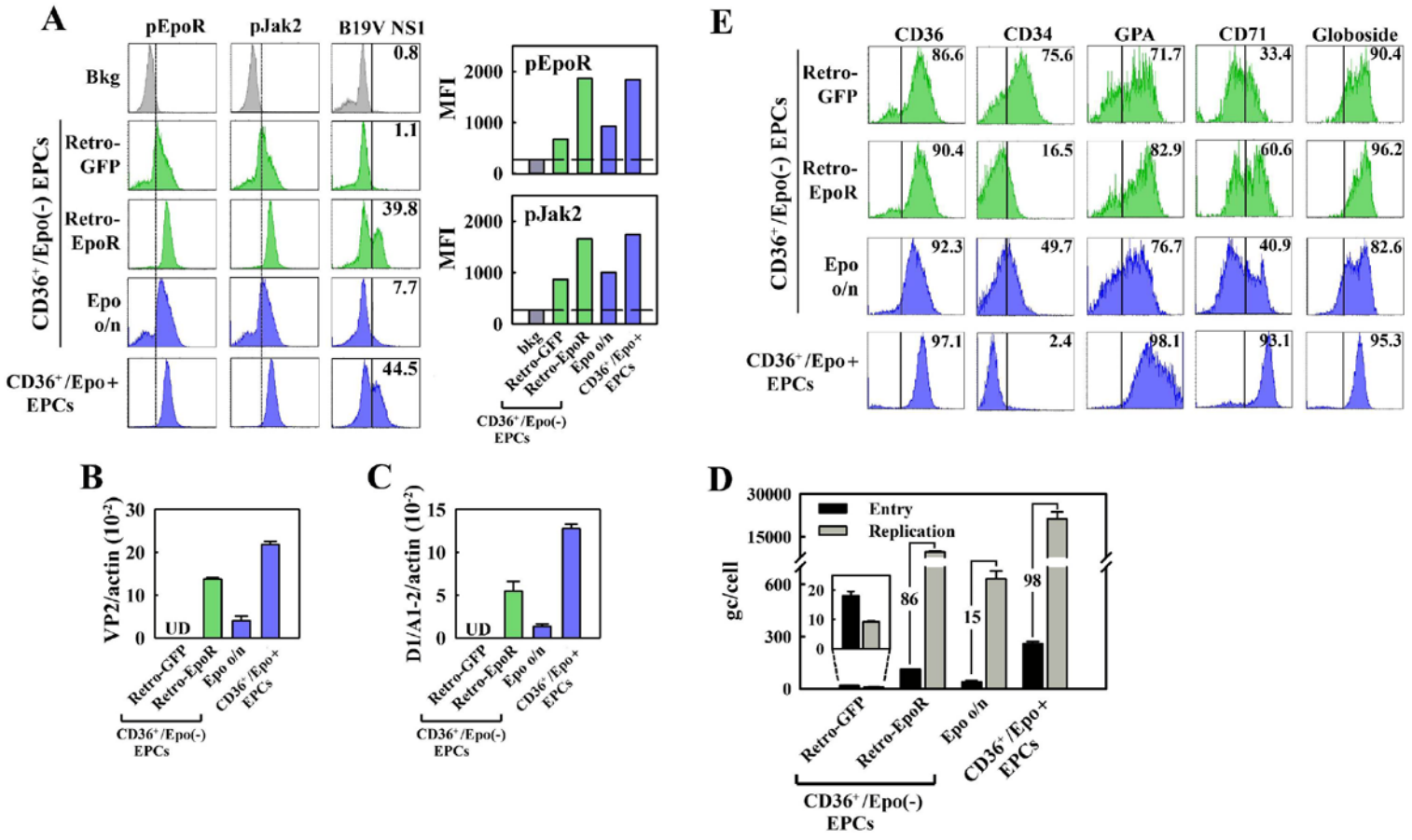
A
pEpoR
pJak2
B19V NS1
Bkg
Retro-GFP
Retro-EpoR
Epo o/n
CD36+/Epo+ EPCs
CD36+/Epo(-) EPCs
0.8
1.1
39.8
7.7
44.5
MFI
2000
1000
0
bkg
Retro-GFP
Retro-EpoR
Epo o/n
CD36+/Epo+ EPCs
B
VP2/actin (10-2)
30
20
10
UD
C
D1/A1-2/actin (10-2)
15
10
5
D
Entry
Replication
gc/cell
30000
15000
600
300
86
15
98
E
CD36
CD34
GPA
CD71
Globoside
86.6
75.6
71.7
33.4
90.4
90.4
16.5
82.9
60.6
96.2
92.3
49.7
76.7
40.9
82.6
97.1
2.4
98.1
93.1
95.3

genome were further confirmed to be significantly high in Retro-EpoR-transduced cells, but were not detectable in the control Retro-GFP-transduced cells (Fig. 4-6B, C&D).

Expression of a constitutively active EpoR differentiated transduced cells in erythroid lineage toward $CD36^+$/Epo+ EPCs as shown by the profile of these major cell surface markers, which typically include the decreased level of CD34 and increased levels of GPA and CD71 (Fig. 4-6E). In consistence, B19V entry was increased approximately 6.2-fold in Retro-EpoR-transduced cells; however, B19V genome in these cells was replicated by approximately 86-fold (Fig. 4-6D), suggesting that expression of the constitutively active EpoR accommodates replication of the B19V genome. Thus, we have provided direct evidence that expression of the constitutively active EpoR renders B19V-nonpermisisve $CD36^+$/Epo(-) EPCs to be permissive, confirming the role of EpoR/Jak2 signaling in B19V infection of erythroid progenitor cells.

B19V infection of $CD36^+$/Epo+ EPCs responds to Epo concentration.

We next sought to confirm the role of Epo in B19V infection of $CD36^+$/Epo+ EPCs expanded in Wong medium. To this end, we cultured cells from day 4 stock in Wong medium but with various concentrations of Epo. These cells were infected at day 8 and analyzed at 48 hrs p.i. We found that, with the increase of Epo concentration from 0.1, 0.5 to 2 U/ml, NS1-expressing cells were increased from approximately 12, 30 to 50% as determined by flow cytometry using anti-NS1 staining (Fig. 4-7A). No significant difference was observed in groups with 2 and 10 U/ml of Epo. Consequently, phosphorylation of both EpoR and Jak2

Figure 4-7. B19V infection of CD36^{+}/Epo+ EPCs responds to the Epo concentration in culture.

CD34^{+} HSCs were *ex vivo* expanded in Wong expansion medium from day 0 and stored at day 4. From day 4 stock in liquid nitrogen, thawed cells were cultured in Wong medium containing Epo at concentrations as indicated until day 8 when B19V infection was carried out. **(A)** At 48 hrs p.i., cells were harvested and stained for antigens intracellularly as indicated. The percentage of B19V NS1-expressing cells is shown. MFI of the anti-pEpoR and anti-pJak2 staining was quantified and is presented in the bar figures to the right in panel A. **(B&C)** At 48 hrs p.i., cells were harvested for mRNA isolation. RT-qPCR was carried out to determine the level of B19V VP2-encoding mRNA per β-actin mRNA **(B)** and the level of B19V D1/A1-2-spliced mRNA per β-actin mRNA **(C)**, respectively. **(D)** At 48 hrs p.i., total DNA was extracted from infected cells. The B19V genomic copy numbers in each group were determined and expressed as gc/cell. Levels of virus entry were determined as described in Materials and Methods, and fold changes between replication and virus entry are shown. Average and standard deviation are shown in panel B, C and D, and were calculated from at least three independent experiments.

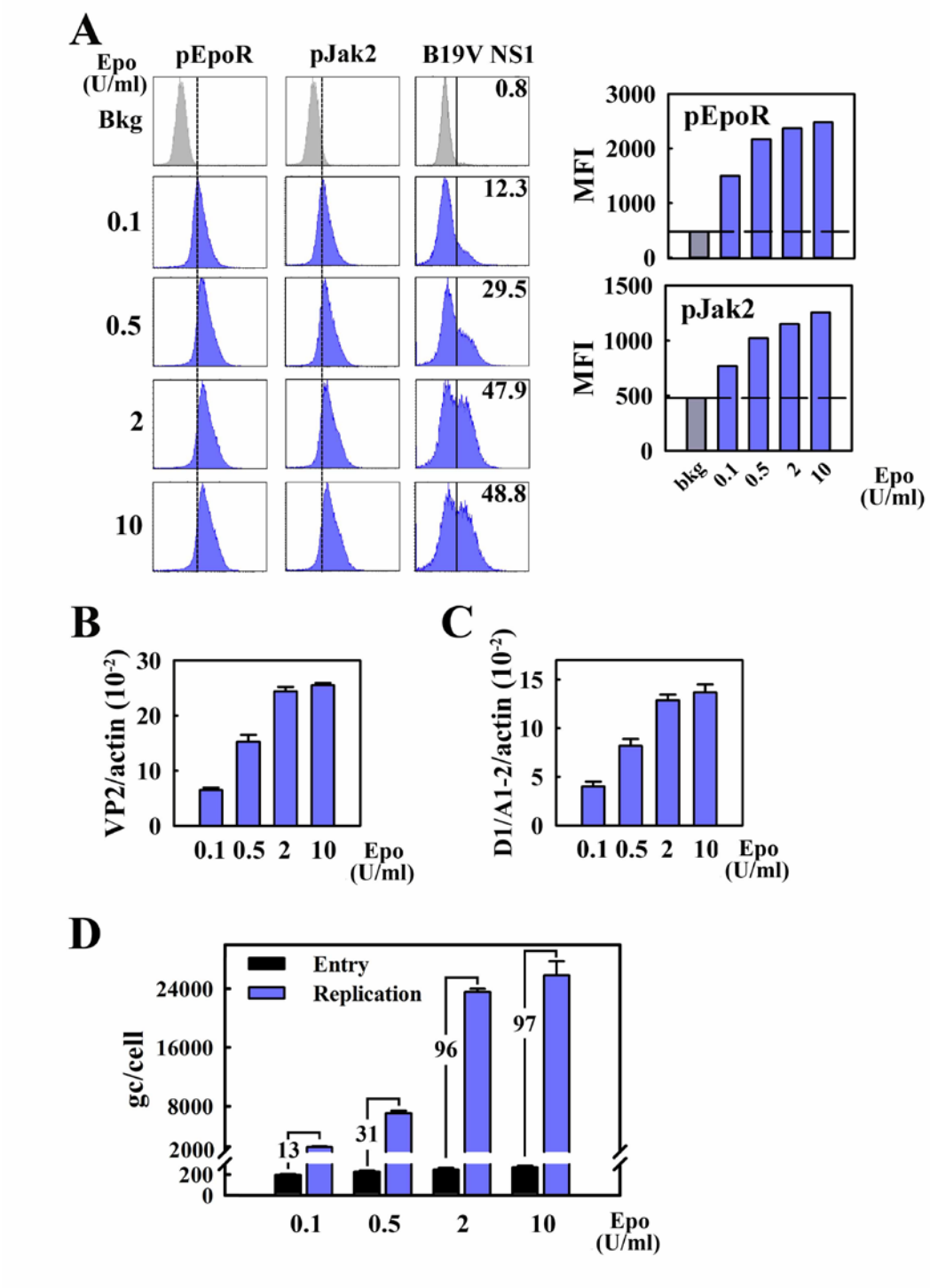
A
Epo (U/ml)
pEpoR
pJak2
B19V NS1
Bkg
0.1
0.5
2
10
0.8
12.3
29.5
47.9
48.8
MFI
pEpoR
pJak2
bkg
Epo (U/ml)
B
VP2/actin (10-2)
C
D1/A1-2/actin (10-2)
D
Entry
Replication
gc/cell
13
31
96
97

was increased proportionally in groups with Epo from 0.1 to 0.5 and 2 U/ml, but remained at a similar level between groups with Epo of 2 and 10 U/ml (Fig. 4-7A). In addition, we observed an increase of B19V infection in these groups with Epo from 0.1 to 0.5 and 2 U/ml as confirmed by the levels of B19V VP2-encoding mRNA, D1/A1-2-spliced mRNA, and B19V DNA replication (Fig. 4-7B, C&D). However, B19V virus entry to cells in all groups with different Epo concentrations was determined to be similar (Fig. 4-7D). Collectively, we have shown that the level of B19V infection in $CD36^{+}$/Epo+ EPCs is dependent on Epo concentration, again confirming the role of Epo in B19V replication.

Discussion

B19V is highly tropic to human erythroid progenitor cells, which was previously thought to be simply due to the presence of the P antigen (Globoside), the B19V receptor (28). We have recently demonstrated that replication of B19V genome is a limiting step during B19V infection of erythroid progenitors (79). Expression of B19V capsid-encoding mRNA requires reading through the proximal polyadenylation site, which is affiliated by replication of the genome. In this study, we provide strong evidence showing that the EpoR signaling pathway is important for B19V replication in erythroid progenitor cells. Our study thus further supports the hypothesis that the limiting step of B19V infection is the replication of the B19V genome rather than the virus entry.

Erythropoiesis and B19V infection: Previous study has shown that Epo is essential to differentiate human hematopoietic stem cells to be susceptible to B19V (206). But the role of Epo in B19V infection was thought to be only for directing differentiation of the hematopoietic stem cells to erythroid progenitor cells at the stages of BFU-E, CFU-E and erythroblasts (206). Erythropoiesis is a regulated process whereby hematopoietic progenitor cells give rise to committed erythroid progenitor cells, differentiate and proliferate to mature red blood cells. It includes the Epo-independent early phase of erythropoiesis, the commitment of pluripotent

hematopoietic stem cells to erythroid lineage, and the Epo-dependent late phase that facilitates terminal maturation of precursors into circulation enucleated erythrocytes. The commitment of hematopoietic stem cells to both early and late erythroid progenitors (BFU-E and CFU-E) is independent of Epo (152, 164, 223, 224). Stem cell factor (SCF) (55, 140, 164, 224), interleukin-6 (IL-6) (202) and IL-3 (164) have been reported to stimulate early erythropoiesis or generation of erythroid progenitors. In contrast, Epo is a late-acting factor of erythropoiesis, which is erythroid-lineage-specific and supports proliferation and maturation of committed erythroid progenitors (152). Epo acts on committed erythroid progenitors to stimulate the later phase of erythroid differentiation (106). Interestingly, Epo-independent erythrocyte production also has been reported (202).

In this study, we used key markers of erythroid progenitors (70), i.e., CD36, CD71, EpoR and GPA, and B19V receptors to profile $CD36^{+}$ EPCs expanded in media with or without Epo. CD36 is detected early on erythroid progenitors, and has been used to monitor hematopoietic differentiation (60, 69, 142, 154). EpoR is the cellular receptor for Epo presented on erythroid progenitors; it appears on erythroid progenitors at BFU-E stage and highly expresses on the most Epo-sensitive CFU-Es (70). Similar to EpoR, CD71, transferrin receptor, is expressed on cells at the BFU-E stage and disappears at late reticulocyte stage (69, 154). GPA is a specific membrane component of mature erythrocytes. GPA is expressed on cells from erythroid progenitors at CFU-E stage (116) to proerythroblast (55, 69, 154, 194). CD41 is a cell surface marker for megakaryocyte, and is not present on erythroid progenitors (154). As judged by these key markers of erythroid progenitors, the cells expanded on day 8 in Wong medium were basically CFU-E-type cells. Using StemCell medium, we obtained highly pure $CD36^{+}$/Epo(-) EPCs by stimulating $CD34^{+}$ HSCs with SCF, IL3, IL6, Flt-3 and TPO. Purified $CD36^{+}$/Epo(-) EPCs process a marker of $CD36^{+87.5\%}$ $GPA^{+88.2\%}$$EpoR^{+84.5\%}$, which have no significant difference from that of $CD36^{+}$/Epo+ EPCs expanded in Wong medium ($CD36^{+97.5\%}$$GPA^{+97.2\%}$$EpoR^{+90.3\%}$); however, the majority of $CD36^{+}$/Epo(-) EPCs retain CD34 marker. BFU-Es contain CD34 marker

(154), and are devoid of CD71 (92, 205), indicating that the $CD36^+$/Epo(-) EPCs are presumably at BFU-E stage. However, these erythroid progenitor cells are sensitive to Epo stimulation, which confers their permissiveness to B19V replication.

P-antigen (Globoside), a glycosphingolipid found on erythroid cells, is a cellular receptor for B19V (4). CD49e and KU80 have been reported to be co-receptors of B19V infection (24,44). Interestingly, $CD36^+$/Epo+ EPCs expanded in Wong medium allow B19V to enter cells at a high efficiency, approximately 17 times higher than that of the $CD36^+$/Epo(-) EPCs. This could be due to the increasing expression of CD49e, the co-receptor of B19V (44), or as yet unidentified co-receptors, but may not be the KU80 (24). The mechanism by which B19V enters cells warrants further investigation. Nevertheless, without Epo stimulation, entered B19V genomes did not replicate. We believe that the blockage of B19V infection of $CD36^+$/Epo(-) EPCs is most likely at the step of B19V DNA replication, rather than intracellular trafficking of the entered viral genomes to the nucleus. Together with our previous finding that expression of adenovirus genes confers replication of B19V genome in B19V-nonpermisisve 293 cells (80), we hypothesize that replication of the B19V genome requires a unique microenviroment in nucleus, which is created upon Epo stimulation in erythroid progenitor cells.

Epo/EpoR/pJAK2/pEpoR signaling pathway is required for B19V replication: Jak2 plays a pivotal role in Epo signal transduction (144, 165). Jak2 associates with EpoR at a membrane proximal region of the cytoplasmic domain. It is hypothesized that binding Epo to EpoR induces a conformational alternation of the EpoR cytoplasmic domain, and allows the juxtaposition of Jak2 molecules in a manner that facilitates their transphosphorylation within the activation loop, resulting in activation of the Jak2. Upon activation, Jak2 phosphorylates 8 tyrosine residues in the cytoplasmic domain of EpoR as well as a number of additional sites on itself (115). Phosphorylated EpoR further recruits and mediates activation of SH2-bidning factors including STAT5, Grb2 and PI3K, which signal Jak2/STAT5, Ras/MARK and PI3K/AKT pathways.

Activating these pathways synergistically prevents apoptosis of committed erythroid progenitors, allowing them to undergo a predetermined program of terminal proliferation and erythroid differentiation. We have shown here that inhibition of Jak2 kinase and thereafter EpoR phosphorylation abolished B19V replication of infected erythroid progenitor cells. Together with the Jak2 shRNA experiment, we believe that signaling transduction pathways under the Jak2/pEpoR must be involved in B19V replication, which function individually or synergistically. In fact, STAT5A, a downstream signaling molecule of Jak2, was observed to be phosphorylated at higher level in $CD36^+$/Epo+ EPCs, but not in $CD36^+$/Epo(-) EPCs that have been stimulated by cytokines SCF, IL3, IL6, Flt-3 and TPO (data not shown). STAT5 is a transcription activator in nucleus that has a profound effect on expression of a set of genes (31), which might be required for efficient replication of the B19V genome. Further investigation apparently is necessary to understand the mechanism underlying B19V replication of erythroid progenitors. Expression of the constitutively active EpoR has been shown to activate Jak2 in condition without Epo binding (117). And in our experiment, Jak2 was apparently phosphorylated upon expression of the EpoR(R129C) in $CD36^+$/Epo(-) EPCs (Fig. 4-6), and phosphorylated EpoR was further regulated by exposing cells with Epo at various concentrations (Fig. 4-7). As a result, Retro-EpoR-expressing cells facilitated B19V infection. In agreement, treatment of $CD36^+$/Epo(-) EPCs with Epo only for 2 hrs turned on B19V infection of treated cells; while overnight Epo treatment conferred treated cells to be infected by B19V at a relatively higher level (Fig. 4-2&3). Accordingly, both Jak2 and EpoR are phosphorylated upon Epo treatment. Therefore, our results strongly suggest the chain of signal transduction of EpoR→activation of Jak2→phosphorylation of EpoR→B19V replication.

In conclusion, our study has provided evidence that EpoR signaling is essential to B19V replication. Activation of EpoR either by addition of Epo or expressing constitutively active EpoR(R129C), confers permissiveness to B19V infection to previously non-permissive but committed erythroid progenitors, $CD36^+$/Epo(-) EPCs, by turning on replication of the B19V

genome. Conversely, inhibition of Jak2 reduced phosphorylation of EpoR, which in turn decreased/blocked B19V DNA replication. Thus, our study reveals a previously unappreciated role of EpoR signaling in supporting B19V replication, which can explain the unique tropism of B19V infection of human erythroid progenitors.

Chapter 5

Conclusions and Discussion

The studies presented in this thesis for my PhD degree are composed of two parts: 1) investigation of the molecular mechanisms underlying the cytopathic effects induced during infection of parvovirus B19V and MVC; and 2) identifying the cellular microenvironment that facilitates B19V replication. For the first part, we took advantage of a recently developed in vitro permissive B19V infection system, and demonstrate that the small nonstructural protein 11kDa of B19V is a novel pro-apoptotic protein, which plays a key role in inducing apoptosis during B19V infection of erythroid progenitor cells. In contrast, apoptotic cell death during MVC infection appears to be viral DNA replication-associated rather than viral protein-induced. In addition, a G2/M cell cycle arrest during MVC infection is caused by the viral genome *per se* rather than its replication. For the second part, we demonstrate that Epo/EpoR/Jak2 signaling is essential for B19V DNA replication.

Virus infection-induced cytopathic effects are often related to disease outcomes, particularly in the case of B19V. B19V encodes two small non-structural proteins 11kDa and 7.5kDa, of which the 11kDa is essential to the viral life cycle. Knocking out the 11kDa protein resulted in a significant decrease of infectious virion production (229). However the precise role of 11kDa in B19V infection is unknown. In our study (Chapter 2), we have demonstrated clearly that the cytoplasm-localized 11kDa is a novel apoptosis inducer and is expressed abundantly during B19V infection of erythroid progenitor cells. It plays a key role in B19V infection-induced apoptosis of erythroid progenitor cells (38). Mechanistically, the 11kDa-induced apoptosis is mediated by caspase-10, an initiator caspase of the extrinsic apoptosis pathway; and is similar

to B19V infection-induced apoptosis. Though caspase-8, the other initiator caspase in the extrinsic pathway, was thought to be the ortholog of caspase-10 (22), it could not substitute the function of caspase-10 in either B19V- or 11kDa-induced apoptosis. Increasing evidence shows that capase-10 and caspase-8, though they sometimes work interchangeably, can function differently in other situations (104, 217). Inhibition of 11kDa by antisense oligos during B19V infection significantly reduced the level of apoptotic cells as evidenced by decreased TUNEL-positive cells. Thus, it is reasonable to speculate that the apoptosis induced by 11kDa may be important for the release of progeny virus from the nucleus, which warrants further investigation. Our continued work on this part shows that the pro-apoptotic activity of 11kDa may reside in the C-terminus (Chen AY & Qiu J, unpublished). More experiments are needed to further support this observation.

Our finding of the novel pro-apoptotic activity of 11kDa provides new insights into B19V infection-induced cytopathic effects. It "breaks new ground on various fronts, from the basic biology of erythroid cells to the mechanisms of B19 parvovirus–induced anemia, and suggests an assay that will predict the efficacy of drugs in the treatment of the associated anemia" (126).

HBoVs are newly emergent parvoviruses that are infectious to humans. They have been associated with clinical symptoms, e.g., pneumonia, in children. Without an infectious clone and an efficient in vitro culture system, the study of HBoV is difficult (64). MVC belongs to the same genus *bocavirus* as HBoVs and they share high similarity in both genome organization and expressed proteins. Thus, we used MVC as a model system to investigate the molecular mechanisms underlying *bocavirus* infection (Chapter 3). Taking advantage of the MVC infectious clone and productive culture system established in our lab (204), we examined the nature of CPE induced during MVC infection (37). Our results indicate that MVC viral proteins do not possess pro-apoptotic activity. Apoptosis induced during MVC infection is tightly associated with replication of the viral genome. In contrast to the extrinsic pathway induced during B19V infection (caspase-10-mediated), MVC infection triggered an intrinsic apoptosis

pathway, as evidenced by Bax translocation and permeabilization of the mitochondrion outer membrane. The cell cycle of the host cells was affected by MVC infection, showing an S-phase plateau during early stages of infection, which progressed into prolonged G2/M arrest at a later stage. The G2/M arrest can be reproduced by transfecting terminal repeats-containing viral genomes into host cells. The S-phase plateau, however, only appears when active replication takes place. Similarly, expression of HBoV viral proteins individually or together by transfection did not induce appreciable levels of cell death or cell cycle arrest (36). Thus our results suggest that the DNA replication-associated apoptosis and viral genome-induced cell cycle arrest could be a common feature among members in the genus *Bocavirus*.

Our work in this part represents the first study looking into the mechanisms underlying the cytopathic effect induced during bocavirus infection. It may provide a direct molecular basis of bocavirus infection-associated disease. Understanding these mechanisms sheds light on the future direction to further delineates the molecular basis of cell cycle arrest and apoptosis induced by DNA viruses. Results from other members in our lab have shown that a DNA damage response may be one of the bridges connecting viral infection with host cell cycle arrest and apoptosis. Active investigation is currently being undertaken in our lab to further understand the molecular details.

Epo has been clearly shown to be essential for the differentiation and proliferation of determined erythroid progenitor cells. In Chapter 4, we demonstrate that Epo/EpoR/Jak2 signaling is also crucial for B19V infection, particularly viral DNA replication. Erythroid progenitor cells cultured in Epo-depleted medium were not permissive to B19V unless treated with Epo. Using different approaches either to down- or up-regulate EpoR and Jak2, we show that EpoR and Jak2 phosphorylation correlated directly with B19V replication. It is worth emphasizing that the inhibition of Jak2 by the specific inhibitor AG490, at no/low toxic levels, significantly blocked B19V replication. However, the extent of viral entry was not affected. AG490 and its analogs could serve as potential candidates for anti-B19V drugs.

Our unpublished work indicates that STAT5A, which is activated by Jak2 via phosphorylation in erythroid progenitor cells, plays an important role in B19V infection. Knocking down STAT5A significantly impaired B19V NS1 expression. STAT5A has been clearly shown to play a crucial role in differentiation of erythroid progenitor cells, further supporting the importance that the differentiation status of erythroid progenitor cells corresponds to B19V permissiveness. In other words, the cellular environment that possesses active differentiation potential may also be the condition favoring B19V DNA replication.

Our work in this part represents the first attempt to explore the Epo/EpoR/Jak2 signaling and its role during B19V infection. Our results not only establish a direct connection of the Epo/EpoR signaling with B19V DNA replication, but also propose a drug candidate for B19V infection. In addition, our findings promote a novel concept that the cellular microenvironment determines the exclusive tropism of B19V for erythroid progenitor cells, in addition to the B19V receptor and co-receptors (138, 218). It opens up a gate toward deeply understanding how cellular signal transduction controls B19V permissiveness. This exact signaling network, which we believe to be regulated under Epo/EpoR signaling, is unique to erythroid progenitor cells.

B19V 11kDa protein interacts with cellular Grb2 via proline-rich SH3-binding motifs (71) (Chen AY and Qiu J, unpublished). Grb2 is an important adaptor protein mediating receptor (EpoR, in the case of erythroid progenitor cells) triggered Ras-MAPK activation (115). MAPK has been implicated in a variety of cellular interactions, including phospholipases, transcription factors, and cytoskeletal proteins (151, 185). Our preliminary findings also indicate a crucial role of MEK/MAPK in B19V replication (unpublished data). Hence, we speculate that 11kDa facilitates B19V progeny virus production via interfering with the MEK/MAPK signaling pathway.

In conclusion, the work presented in this thesis represents several novel advances in understanding the molecular mechanisms underlying parvovirus infection. Those results provide molecular-level insights into virus-host interaction during both early and late stages of infection. Exploration of cytopathic effects induced during infection shows that distinct mechanisms can

be employed effectively by parvoviruses from different genera. In addition, we have introduced a novel concept that a unique cellular microenvironment in erythroid progenitor cells is a prerequisite to B19V DNA replication, and thus determines the permissiveness to and tropism of B19V.

Reference List

1. **Abdel-Latif, L., B. K. Murray, R. L. Renberg, K. L. O'Neill, H. Porter, J. B. Jensen, and F. B. Johnson.** 2006. Cell death in bovine parvovirus-infected embryonic bovine tracheal cells is mediated by necrosis rather than apoptosis. J Gen Virol **87:**2539-48.

2. **Al-Khan, A., A. Caligiuri, and J. Apuzzio.** 2003. Parvovirus B-19 infection during pregnancy. Infect Dis Obstet Gynecol **11:**175-9.

3. **Allander, T.** 2008. Human bocavirus. J.Clin.Virol. **41:**29-33.

4. **Allander, T., T. Jartti, S. Gupta, H. G. Niesters, P. Lehtinen, R. Osterback, T. Vuorinen, M. Waris, A. Bjerkner, A. Tiveljung-Lindell, B. G. van den Hoogen, T. Hyypia, and O. Ruuskanen.** 2007. Human bocavirus and acute wheezing in children. Clin.Infect.Dis. **44:**904-910.

5. **Allander, T., M. T. Tammi, M. Eriksson, A. Bjerkner, A. Tiveljung-Lindell, and B. Andersson.** 2005. Cloning of a human parvovirus by molecular screening of respiratory tract samples. Proc.Natl.Acad.Sci.U.S.A **102:**12891-12896.

6. **Anderson, M. J., M. N. Khousam, D. J. Maxwell, S. J. Gould, L. C. Happerfield, and W. J. Smith.** 1988. Human parvovirus B19 and hydrops fetalis. Lancet **1:**535.

7. **Anouja, F., R. Wattiez, S. Mousset, and P. Caillet-Fauquet.** 1997. The cytotoxicity of the parvovirus minute virus of mice nonstructural protein NS1 is related to changes in the synthesis and phosphorylation of cell proteins. J Virol **71:**4671-8.

8. **Arthur, J. L., G. D. Higgins, G. P. Davidson, R. C. Givney, and R. M. Ratcliff.** 2009. A novel bocavirus associated with acute gastroenteritis in Australian children. PLoS.Pathog. **5:**e1000391.

9. **Ashkenazi, A., and V. M. Dixit.** 1998. Death receptors: signaling and modulation. Science **281:**1305-1308.

10. **Astell, C. R., W. Luo, J. Brunstein, and J. Amand.** 1997. B19 parvovirus:biochemical and molecular features, p. 16-41. *In* L. J. Anderson and N. Young (ed.), Human parvovirus B19. Karger.

11. **Basu, A., V. P. Castle, M. Bouziane, K. Bhalla, and S. Haldar.** 2006. Crosstalk between extrinsic and intrinsic cell death pathways in pancreatic cancer: synergistic action of estrogen metabolite and ligands of death receptor family. Cancer Res **66:**4309-18.

12. **Bauder, B., A. Suchy, C. Gabler, and H. Weissenbock.** 2000. Apoptosis in feline panleukopenia and canine parvovirus enteritis. J Vet Med B Infect Dis Vet Public Health **47:**775-84.

13. **Berns, K. I., and C. Giraud.** 1996. Biology of adeno-associated virus. Curr Top Microbiol Immunol **218:**1-23.

14. **Berthet, C., K. Raj, P. Saudan, and P. Beard.** 2005. How adeno-associated virus Rep78 protein arrests cells completely in S phase. Proc Natl Acad Sci U S A **102:**13634-9.

15. **Best, S. M.** 2008. Viral subversion of apoptotic enzymes: escape from death row. Annu Rev Microbiol **62:**171-92.

16. **Best, S. M., J. F. Shelton, J. M. Pompey, J. B. Wolfinbarger, and M. E. Bloom.** 2003. Caspase cleavage of the nonstructural protein NS1 mediates replication of Aleutian mink disease parvovirus. J Virol **77:**5305-12.

17. **Best, S. M., J. B. Wolfinbarger, and M. E. Bloom.** 2002. Caspase activation is required for permissive replication of Aleutian mink disease parvovirus in vitro. Virology **292:**224-34.

18. **Binn, L. N., E. C. Lazar, G. A. Eddy, and M. Kajima.** 1970. Recovery and Characterization of a Minute Virus of Canines. Infect.Immun. **1:**503-508.

19. **Binn, L. N., R. H. Marchwicki, E. H. Eckermann, and T. E. Fritz.** 1981. Viral antibody studies of laboratory dogs with diarrheal disease. Am J Vet Res **42:**1665-7.

20. **Blachon, S., S. Bellanger, C. Demeret, and F. Thierry.** 2005. Nucleo-cytoplasmic shuttling of high risk human Papillomavirus E2 proteins induces apoptosis. J Biol Chem **280:**36088-98.

21. **Bloom, M. E., R. E. Race, and J. B. Wolfinbarger.** 1980. Characterization of Aleutian disease virus as a parvovirus. J.Virol. **35:**836-843.

22. **Boatright, K. M., and G. S. Salvesen.** 2003. Mechanisms of caspase activation. Curr Opin Cell Biol **15:**725-31.

23. **Bonvicini, F., C. Filippone, S. Delbarba, E. Manaresi, M. Zerbini, M. Musiani, and G. Gallinella.** 2006. Parvovirus B19 genome as a single, two-state replicative and transcriptional unit. Virology **347:**447-54.

24. **Bonvicini, F., C. Filippone, E. Manaresi, M. Zerbini, M. Musiani, and G. Gallinella.** 2008. Functional analysis and quantitative determination of the expression profile of human parvovirus B19. Virology **381:**168-77.

25. **Brandenburger, A., D. Legendre, B. Avalosse, and J. Rommelaere.** 1990. NS-1 and NS-2 proteins may act synergistically in the cytopathogenicity of parvovirus MVMp. Virology. **174:**576-584.

26. **Branzei, D., and M. Foiani.** 2008. Regulation of DNA repair throughout the cell cycle. Nat Rev Mol Cell Biol **9:**297-308.

27. **Brown, K. E.** 2005. The genus Erythrovirus, p. 25-45. *In* J. Kerr, S. F. Cotmore, M. E. Bloom, R. M. Linden, and C. R. Parrish (ed.), Parvoviruses. Hodder Arnold, London.

28. **Brown, K. E., S. M. Anderson, and N. S. Young.** 1993. Erythrocyte P antigen: cellular receptor for B19 parvovirus. Science **262:**114-7.

29. **Brown, K. E., and N. Young.** 1997. Human parvovirus B19: Pathogenesis of disease, p. 105-119. *In* L. J. Anderson and N. Young (ed.), Human parvovirus B19, vol. 20. Karger, Basel, Switzerland.

30. **Brown, K. E., N. S. Young, and J. M. Liu.** 1994. Molecular, cellular and clinical aspects of parvovirus B19 infection. Crit Rev Oncol Hematol **16:**1-31.

31. **Bunting, K. D.** 2007. STAT5 signaling in normal and pathologic hematopoiesis. Front Biosci **12:**2807-20.

32. **Burrer, R., B. W. Neuman, J. P. Ting, D. A. Stein, H. M. Moulton, P. L. Iversen, P. Kuhn, and M. J. Buchmeier.** 2007. Antiviral effects of antisense morpholino oligomers in murine coronavirus infection models. J.Virol. **81:**5637-5648.

33. **Carmichael, L. E., D. H. Schlafer, and A. Hashimoto.** 1991. Pathogenicity of minute virus of canines (MVC) for the canine fetus. Cornell Vet. **81:**151-171.

34. **Caserta, T. M., A. N. Smith, A. D. Gultice, M. A. Reedy, and T. L. Brown.** 2003. Q-VD-OPh, a broad spectrum caspase inhibitor with potent antiapoptotic properties. Apoptosis. **8:**345-352.

35. **Chauvier, D., S. Ankri, C. Charriaut-Marlangue, R. Casimir, and E. Jacotot.** 2007. Broad-spectrum caspase inhibitors: from myth to reality? Cell Death Differ **14:**387-91.

36. **Chen, A. Y., F. Cheng, S. Lou, Y. Luo, Z. Liu, E. Delwart, D. Pintel, and J. Qiu.** 2010. Characterization of the gene expression profile of human bocavirus. Virology **[Epub ahead of print]**.

37. **Chen, A. Y., Y. Luo, F. Cheng, Y. Sun, and J. Qiu.** 2010. Bocavirus infection induces mitochondrion-mediated apoptosis and cell cycle arrest at G2/M phase. J Virol **84:**5615-26.

38. **Chen, A. Y., E. Y. Zhang, W. Guan, F. Cheng, S. Kleiboeker, T. M. Yankee, and J. Qiu.** 2010. The small 11 kDa nonstructural protein of human parvovirus B19 plays a key role in inducing apoptosis during B19 virus infection of primary erythroid progenitor cells. Blood **115:**1070-80.

39. **Chen, K. C., B. C. Shull, E. A. Moses, M. Lederman, E. R. Stout, and R. C. Bates.** 1986. Complete nucleotide sequence and genome organization of bovine parvovirus. J.Virol. **60:**1085-1097.

40. **Chen, M., and J. Wang.** 2002. Initiator caspases in apoptosis signaling pathways. Apoptosis **7:**313-319.

41. **Chen, Y. Q., F. de Foresta, J. Hertoghs, B. L. Avalosse, J. J. Cornelis, and J. Rommelaere.** 1986. Selective killing of simian virus 40-transformed human fibroblasts by parvovirus H-1. Cancer Res **46:**3574-9.

42. **Cheng, F., A. Y. Chen, S. M. Best, M. E. Bloom, D. Pintel, and J. Qiu.** 2010. The capsid proteins of Aleutian mink disease virus activate caspases and are specifically cleaved during infection. J Virol **84:**2687-96.

43. **Chipuk, J. E., L. Bouchier-Hayes, and D. R. Green.** 2006. Mitochondrial outer membrane permeabilization during apoptosis: the innocent bystander scenario. Cell Death Differ **13:**1396-1402.

44. **Chisaka, H., E. Morita, K. Murata, N. Ishii, N. Yaegashi, K. Okamura, and K. Sugamura.** 2002. A transgenic mouse model for non-immune hydrops fetalis induced by the NS1 gene of human parvovirus B19. J Gen Virol **83:**273-81.

45. **Chisaka, H., E. Morita, N. Yaegashi, and K. Sugamura.** 2003. Parvovirus B19 and the pathogenesis of anaemia. Rev Med Virol **13:**347-59.

46. **Clarke, P. R., and L. A. Allan.** 2009. Cell-cycle control in the face of damage--a matter of life or death. Trends Cell Biol **19:**89-98.

47. **Collaco, R. F., J. M. Bevington, V. Bhrigu, V. Kalman-Maltese, and J. P. Trempe.** 2009. Adeno-associated virus and adenovirus coinfection induces a cellular DNA damage and repair response via redundant phosphatidylinositol 3-like kinase pathways. Virology **392:**24-33.

48. **Corbau, R., V. Duverger, J. Rommelaere, and J. P. Nuesch.** 2000. Regulation of MVM NS1 by protein kinase C: impact of mutagenesis at consensus phosphorylation sites on replicative functions and cytopathic effects. Virology **278:**151-67.

49. **Cornelis, J. J., P. Becquart, N. Duponchel, N. Salome, B. L. Avalosse, M. Namba, and J. Rommelaere.** 1988. Transformation of human fibroblasts by ionizing radiation, a chemical carcinogen, or simian virus 40 correlates with an increase in susceptibility to the autonomous parvoviruses H-1 virus and minute virus of mice. J Virol **62:**1679-86.

50. **Cornelis, J. J., N. Spruyt, P. Spegelaere, E. Guetta, T. Darawshi, S. F. Cotmore, J. Tal, and J. Rommelaere.** 1988. Sensitization of transformed rat fibroblasts to killing by parvovirus minute virus of mice correlates with an increase in viral gene expression. J Virol **62:**3438-44.

51. **Cossart, Y. E., A. M. Field, B. Cant, and D. Widdows.** 1975. Parvovirus-like particles in human sera. Lancet **1:**72-3.

52. **Cotmore, S. F., and P. Tattersall.** 1984. Characterization and molecular cloning of a human parvovirus genome. Science. **226:**1161-1165.

53. **Cotmore, S. F., and P. Tattersall.** 2006. A rolling-hairpin strategy: basic mechanisms of DNA replication in the parvoviruses. *In* J. R. Kerr, S. F. Cotmore, M. E. Bloom, R. m. linden, and C. R. Parrish (ed.), Parvoviruses. A Hodder Arnold Publication.

54. **Daeffler, L., R. Horlein, J. Rommelaere, and J. P. Nuesch.** 2003. Modulation of minute virus of mice cytotoxic activities through site-directed mutagenesis within the NS coding region. J.Virol. **77:**12466-12478.

55. **Dai, C. H., S. B. Krantz, and K. M. Zsebo.** 1991. Human burst-forming units-erythroid need direct interaction with stem cell factor for further development. Blood. **78:**2493-2497.

56. **Davy, C., and J. Doorbar.** 2007. G2/M cell cycle arrest in the life cycle of viruses. Virology **368:**219-26.

57. **de Jong, E. P., T. R. de Haan, A. C. Kroes, M. F. Beersma, D. Oepkes, and F. J. Walther.** 2006. Parvovirus B19 infection in pregnancy. J.Clin.Virol. **36:**1-7.

58. **De Maria, R., A. Zeuner, A. Eramo, C. Domenichelli, D. Bonci, F. Grignani, S. M. Srinivasula, E. S. Alnemri, U. Testa, and C. Peschle.** 1999. Negative regulation of erythropoiesis by caspase-mediated cleavage of GATA-1. Nature **401:**489-93.

59. **De, M. R., U. Testa, L. Luchetti, A. Zeuner, G. Stassi, E. Pelosi, R. Riccioni, N. Felli, P. Samoggia, and C. Peschle.** 1999. Apoptotic role of Fas/Fas ligand system in the regulation of erythropoiesis. Blood. **93:**796-803.

60. **de Wolf, J. T., E. W. Muller, D. H. Hendriks, R. M. Halie, and E. Vellenga.** 1994. Mast cell growth factor modulates CD36 antigen expression on erythroid progenitors from human bone marrow and peripheral blood associated with ongoing differentiation. Blood. **84:**59-64.

61. **Degterev, A., M. Boyce, and J. Yuan.** 2003. A decade of caspases. Oncogene. **22:**8543-8567.

62. **Degterev, A., and J. Yuan.** 2008. Expansion and evolution of cell death programmes. Nat.Rev.Mol.Cell Biol. **9:**378-390.

63. **Di Piazza, M., C. Mader, K. Geletneky, Y. C. M. Herrero, E. Weber, J. Schlehofer, L. Deleu, and J. Rommelaere.** 2007. Cytosolic activation of cathepsins mediates parvovirus H-1-induced killing of cisplatin and TRAIL-resistant glioma cells. J Virol **81:**4186-98.

64. **Dijkman, R., S. M. Koekkoek, R. Molenkamp, O. Schildgen, and L. van der Hoek.** 2009. Human bocavirus can be cultured in differentiated human airway epithelial cells. J Virol **83:**7739-48.

65. **Doerig, C., B. Hirt, J. P. Antonietti, and P. Beard.** 1990. Nonstructural protein of parvoviruses B19 and minute virus of mice controls transcription. J Virol **64:**387-96.

66. **Durham, P. J., and R. H. Johnson.** 1985. Studies on the replication of a bovine parvovirus. Vet Microbiol **10:**165-77.

67. **Durham, P. J., A. Lax, and R. H. Johnson.** 1985. Pathological and virological studies of experimental parvoviral enteritis in calves. Res Vet Sci **38:**209-19.

68. **Duverger, V., U. Sartorius, P. Klein-Bauernschmitt, P. H. Krammer, and J. R. Schlehofer.** 2002. Enhancement of cisplatin-induced apoptosis by infection with adeno-associated virus type 2. Int J Cancer **97:**706-12.

69. **Edelman, P., G. Vinci, J. L. Villeval, W. Vainchenker, A. Henri, R. Miglierina, P. Rouger, J. Reviron, J. Breton-Gorius, and C. Sureau.** 1986. A monoclonal antibody against an erythrocyte ontogenic antigen identifies fetal and adult erythroid progenitors. Blood. **67:**56-63.

70. **Elliott, S., M. Foote, and G. Molineux.** 2009. Erythropoiesis: an overview. *In* S. G. Elliott, M. A. Foote, and G. Molineux (ed.), Erythropoietins, Erythropoietic Factors, and Erythropoiesis, 2nd ed. Birkhäuser Verlag.

71. **Fan, M. M., L. Tamburic, C. Shippam-Brett, D. B. Zagrodney, and C. R. Astell.** 2001. The small 11-kDa protein from B19 parvovirus binds growth factor receptor-binding protein 2 in vitro in a Src homology 3 domain/ligand-dependent manner. Virology **291:**285-91.

72. **Foghsgaard, L., D. Wissing, D. Mauch, U. Lademann, L. Bastholm, M. Boes, F. Elling, M. Leist, and M. Jaattela.** 2001. Cathepsin B acts as a dominant execution protease in tumor cell apoptosis induced by tumor necrosis factor. J Cell Biol **153:**999-1010.

73. **Fragkos, M., M. Breuleux, N. Clement, and P. Beard.** 2008. Recombinant adeno-associated viral vectors are deficient in provoking a DNA damage response. J Virol **82:**7379-87.

74. **Fragkos, M., J. Jurvansuu, and P. Beard.** 2009. H2AX is required for cell cycle arrest via the p53/p21 pathway. Mol Cell Biol **29:**2828-40.

75. **Fu, P., X. Jiang, and M. O. Arcasoy.** 2009. Constitutively active erythropoietin receptor expression in breast cancer cells promotes cellular proliferation and migration through a MAP-kinase dependent pathway. Biochem.Biophys.Res.Commun. **379:**696-701.

76. **Gareus, R., A. Gigler, A. Hemauer, M. Leruez-Ville, F. Morinet, H. Wolf, and S. Modrow.** 1998. Characterization of cis-acting and NS1 protein-responsive elements in the p6 promoter of parvovirus B19. J Virol **72:**609-16.

77. **Garner, E., F. Martinon, J. Tschopp, P. Beard, and K. Raj.** 2007. Cells with defective p53-p21-pRb pathway are susceptible to apoptosis induced by p84N5 via caspase-6. Cancer Res **67:**7631-7.

78. **Gloning, K. P., T. Schramm, E. Brusis, T. Schwarz, and M. Roggendorf.** 1990. Successful intrauterine treatment of fetal hydrops caused by parvovirus B19 infection. Behring Inst Mitt**:**79-85.

79. **Guan, W., F. Cheng, Y. Yoto, S. Kleiboeker, S. Wong, N. Zhi, D. J. Pintel, and J. Qiu.** 2008. Block to the production of full-length B19 virus transcripts by internal polyadenylation is overcome by replication of the viral genome. J Virol **82:**9951-63.

80. **Guan, W., S. Wong, N. Zhi, and J. Qiu.** 2009. The genome of human parvovirus B19 virus can replicate in non-permissive cells with the help of adenovirus genes and produces infectious virus. J Virol **83:**9541-9553.

81. **Guetta, E., D. Ron, and J. Tal.** 1986. Development-dependent replication of minute virus of mice in differentiated mouse testicular cell lines. J Gen Virol **67 (Pt 11):**2549-54.

82. **Guicciardi, M. E., J. Deussing, H. Miyoshi, S. F. Bronk, P. A. Svingen, C. Peters, S. H. Kaufmann, and G. J. Gores.** 2000. Cathepsin B contributes to TNF-alpha-mediated hepatocyte apoptosis by promoting mitochondrial release of cytochrome c. J Clin Invest **106:**1127-37.

83. **Guo, Y. M., K. Ishii, M. Hirokawa, H. Tagawa, H. Ohyagi, Y. Michishita, K. Ubukawa, J. Yamashita, T. Ohteki, N. Onai, K. Kawakami, W. Xiao, and K. Sawada.** 2010. CpG-ODN 2006 and human parvovirus B19 genome consensus sequences selectively inhibit growth and development of erythroid progenitor cells. Blood.

84. **Haanen, C., and I. Vermes.** 1995. Apoptosis and inflammation, p. 5-15, Mediators of Inflammation, vol. 4.

85. **Hanayama, R., M. Tanaka, K. Miyasaka, K. Aozasa, M. Koike, Y. Uchiyama, and S. Nagata.** 2004. Autoimmune disease and impaired uptake of apoptotic cells in MFG-E8-deficient mice. Science. **304:**1147-1150.

86. **Harrison, L. R., E. L. Styer, A. R. Pursell, L. E. Carmichael, and J. C. Nietfeld.** 1992. Fatal disease in nursing puppies associated with minute virus of canines. J.Vet.Diagn.Invest. **4:**19-22.

87. **Hermanns, J., A. Schulze, P. Jansen-Db1urr, J. A. Kleinschmidt, R. Schmidt, and H. zur Hausen.** 1997. Infection of primary cells by adeno-associated virus type 2 results in a modulation of cell cycle-regulating proteins. J Virol **71:**6020-7.

88. **Hristov, G., M. Kramer, J. Li, N. El-Andaloussi, R. Mora, L. Daeffler, H. Zentgraf, J. Rommelaere, and A. Marchini.** 2010. Parvovirus H-1 through its non-structural protein NS1 induces apoptosis via accumulation of reactive oxygen species. J Virol **[Epub ahead of print]**.

89. **Hsu, T. C., W. J. Wu, M. C. Chen, and G. J. Tsay.** 2004. Human parvovirus B19 non-structural protein (NS1) induces apoptosis through mitochondria cell death pathway in COS-7 cells. Scand J Infect Dis **36:**570-7.

90. **Ingemarsdotter, C., D. Keller, and P. Beard.** 2010. The DNA damage response to non-replicating adeno-associated virus: Centriole overduplication and mitotic catastrophe independent of the spindle checkpoint. Virology **400:**271-86.

91. **Jarplid, B., H. Johansson, and L. E. Carmichael.** 1996. A fatal case of pup infection with minute virus of canines (MVC). J.Vet.Diagn.Invest. **8:**484-487.

92. **Jelkmann, W.** 2004. Molecular biology of erythropoietin. Intern Med **43:**649-59.

93. **Johnson, D. G., and C. L. Walker.** 1999. Cyclins and cell cycle checkpoints. Annu Rev Pharmacol Toxicol **39:**295-312.

94. **Johnson, N. A., M. Boyle, A. Bashashati, S. Leach, A. Brooks-Wilson, L. H. Sehn, M. Chhanabhai, R. R. Brinkman, J. M. Connors, A. P. Weng, and R. D. Gascoyne.** 2008. Diffuse large B cell lymphoma: reduced CD20 expression is associated with an inferior survival. Blood.

95. **Jurvansuu, J., M. Fragkos, C. Ingemarsdotter, and P. Beard.** 2007. Chk1 instability is coupled to mitotic cell death of p53-deficient cells in response to virus-induced DNA damage signaling. J Mol Biol **372:**397-406.

96. **Jurvansuu, J., K. Raj, A. Stasiak, and P. Beard.** 2005. Viral transport of DNA damage that mimics a stalled replication fork. J Virol **79:**569-80.

97. **Kahn, J.** 2008. Human bocavirus: clinical significance and implications. Curr.Opin.Pediatr. **20:**62-66.

98. **Kapoor, A., P. Simmonds, E. Slikas, L. Li, L. Bodhidatta, O. Sethabutr, H. Triki, O. Bahri, B. S. Oderinde, M. M. Baba, D. N. Bukbuk, J. Besser, J. Bartkus, and E. Delwart.** 2010. Human bocaviruses are highly diverse, dispersed, recombination prone, and prevalent in enteric infections. J Infect Dis **201:**1633-43.

99. **Kapoor, A., E. Slikas, P. Simmonds, T. Chieochansin, A. Naeem, S. Shaukat, M. M. Alam, S. Sharif, M. Angez, S. Zaidi, and E. Delwart.** 2009. A Newly Identified Bocavirus Species in Human Stool. J.Infect.Dis. **199:**196-200.

100. **Kaufmann, S. H., S. Desnoyers, Y. Ottaviano, N. E. Davidson, and G. G. Poirier.** 1993. Specific proteolytic cleavage of poly(ADP-ribose) polymerase: an early marker of chemotherapy-induced apoptosis. Cancer Res. **53:**3976-3985.

101. **Keen, J., L. Serghides, K. Ayi, S. N. Patel, J. Ayisi, E. A. van, R. Steketee, V. Udhayakumar, and K. C. Kain.** 2007. HIV impairs opsonic phagocytic clearance of pregnancy-associated malaria parasites. PLoS.Med. **4:**e181.

102. **Kerr, J. R., S. F. Cotmore, M. E. Bloom, R. m. linden, and C. R. Parrish.** 2006. Parvoviruses, 1st ed. A Hodder Arnold Publication.

103. **Kim, H., H. C. Tu, D. Ren, O. Takeuchi, J. R. Jeffers, G. P. Zambetti, J. J. Hsieh, and E. H. Cheng.** 2009. Stepwise activation of BAX and BAK by tBID, BIM, and PUMA initiates mitochondrial apoptosis. Mol.Cell. **36:**487-499.

104. **Kischkel, F. C., D. A. Lawrence, A. Tinel, H. LeBlanc, A. Virmani, P. Schow, A. Gazdar, J. Blenis, D. Arnott, and A. Ashkenazi.** 2001. Death receptor recruitment of endogenous caspase-10 and apoptosis initiation in the absence of caspase-8. J Biol Chem **276:**46639-46.

105. **Knipe, D. M., P. M. Howley, D. E. Griffin, R. A. Lamb, M. A. Martin, B. Roizman, and S. E. Straus.** 2007. Parvoviruses, Field's Virology, 5th ed. Lippincott Williams & Wilkins.

106. **Koury, M. J., and M. C. Bondurant.** 1992. The molecular mechanism of erythropoietin action. Eur.J.Biochem. **210:**649-663.

107. **Krantz, S. B.** 1991. Erythropoietin. Blood. **77:**419-434.

108. **Kroemer, G., L. Galluzzi, P. Vandenabeele, J. Abrams, E. S. Alnemri, E. H. Baehrecke, M. V. Blagosklonny, W. S. El-Deiry, P. Golstein, D. R. Green, M. Hengartner, R. A. Knight, S. Kumar, S. A. Lipton, W. Malorni, G. Nunez, M. E. Peter, J. Tschopp, J. Yuan, M. Piacentini, B. Zhivotovsky, and G. Melino.** 2009. Classification of cell death: recommendations of the Nomenclature Committee on Cell Death 2009. Cell Death Differ **16:**3-11.

109. **Kurtzman, G. J., P. Gascon, M. Caras, B. Cohen, and N. S. Young.** 1988. B19 parvovirus replicates in circulating cells of acutely infected patients. Blood **71:**1448-54.

110. **Lazebnik, Y. A., S. H. Kaufmann, S. Desnoyers, G. G. Poirier, and W. C. Earnshaw.** 1994. Cleavage of poly(ADP-ribose) polymerase by a proteinase with properties like ICE. Nature. **371:**346-347.

111. **Li, P., D. Nijhawan, I. Budihardjo, S. M. Srinivasula, M. Ahmad, E. S. Alnemri, and X. Wang.** 1997. Cytochrome c and dATP-dependent formation of Apaf-1/caspase-9 complex initiates an apoptotic protease cascade. Cell. **91:**479-489.

112. **Liu, J., Z. H. Ran, S. D. Xiao, and J. Rommelaere.** 2005. Changes in gene expression profiles induced by parvovirus H-1 in human gastric cancer cells. Chin J Dig Dis **6:**72-81.

113. **Liu, J. M., S. W. Green, T. Shimada, and N. S. Young.** 1992. A block in full-length transcript maturation in cells nonpermissive for B19 parvovirus. J Virol **66:**4686-92.

114. **Liu, Z., J. Qiu, F. Cheng, Y. Chu, Y. Yoto, M. G. O'Sullivan, K. E. Brown, and D. J. Pintel.** 2004. Comparison of the transcription profile of simian parvovirus with that of the human erythrovirus B19 reveals a number of unique features. J Virol **78:**12929-39.

115. **Lodish, H. F., S. Ghaffari, M. Socolovsky, W. Tong, and J. Zhang.** 2009. Intracellular signaling by the erythropoietin receptor. *In* S. G. Elliott, M. A. Foote, and G. Molineux (ed.), Erythropoietins, Erythropoietic Factors and Erythropoiesis. Birkhäuser Verlag.

116. **Loken, M. R., V. O. Shah, K. L. Dattilio, and C. I. Civin.** 1987. Flow cytometric analysis of human bone marrow: I. Normal erythroid development. Blood. **69:**255-263.

117. **Longmore, G. D., and H. F. Lodish.** 1991. An activating mutation in the murine erythropoietin receptor induces erythroleukemia in mice: a cytokine receptor superfamily oncogene. Cell **67:**1089-102.

118. **Luo, W., and C. R. Astell.** 1993. A novel protein encoded by small RNAs of parvovirus B19. Virology. **195:**448-455.

119. **Lytle, C. D., and J. L. Sagripanti.** 2005. Predicted inactivation of viruses of relevance to biodefense by solar radiation. J.Virol. **79:**14244-14252.

120. **Manteufel, J., and U. Truyen.** 2008. Animal bocaviruses: a brief review. Intervirology **51:**328-34.

121. **Martin, E. T., M. P. Fairchok, J. Kuypers, A. Magaret, D. M. Zerr, A. Wald, and J. A. Englund.** 2010. Frequent and prolonged shedding of bocavirus in young children attending daycare. J Infect Dis **201:**1625-32.

122. **Meikrantz, W., and R. Schlegel.** 1995. Apoptosis and the cell cycle. J Cell Biochem **58:**160-74.

123. **Mercille, S., and B. Massie.** 1999. Apoptosis-resistant E1B-19K-expressing NS/0 myeloma cells exhibit increased viability and chimeric antibody productivity under perfusion culture conditions. Biotechnol.Bioeng. **63:**529-543.

124. **Metcalf, J. B., R. C. Bates, and M. Lederman.** 1990. Interaction of virally coded protein and a cell cycle-regulated cellular protein with the bovine parvovirus left terminus ori. J Virol **64:**5485-90.

125. **Meydan, N., T. Grunberger, H. Dadi, M. Shahar, E. Arpaia, Z. Lapidot, J. S. Leeder, M. Freedman, A. Cohen, A. Gazit, A. Levitzki, and C. M. Roifman.** 1996. Inhibition of acute lymphoblastic leukaemia by a Jak-2 inhibitor. Nature **379:**645-8.

126. **Migliaccio, G., and A. R. Migliaccio.** 2010. Getting personal with B19 parvovirus. Blood **115:**922-3.

127. **Miyagawa, E., T. Yoshida, H. Takahashi, K. Yamaguchi, T. Nagano, Y. Kiriyama, K. Okochi, and H. Sato.** 1999. Infection of the erythroid cell line, KU812Ep6 with human parvovirus B19 and its application to titration of B19 infectivity. J Virol Methods **83:**45-54.

128. **Mochizuki, M., M. Hashimoto, T. Hajima, M. Takiguchi, A. Hashimoto, Y. Une, F. Roerink, T. Ohshima, C. R. Parrish, and L. E. Carmichael.** 2002. Virologic and serologic identification of minute virus of canines (canine parvovirus type 1) from dogs in Japan. J.Clin.Microbiol. **40:**3993-3998.

129. **Moehler, M., B. Blechacz, N. Weiskopf, M. Zeidler, W. Stremmel, J. Rommelaere, P. R. Galle, and J. J. Cornelis.** 2001. Effective infection, apoptotic cell killing and gene transfer of human hepatoma cells but not primary hepatocytes by parvovirus H1 and derived vectors. Cancer Gene Ther. **8:**158-167.

130. **Moffatt, S., N. Tanaka, K. Tada, M. Nose, M. Nakamura, O. Muraoka, T. Hirano, and K. Sugamura.** 1996. A cytotoxic nonstructural protein, NS1, of human parvovirus B19 induces activation of interleukin-6 gene expression. J Virol **70:**8485-91.

131. **Moffatt, S., N. Yaegashi, K. Tada, N. Tanaka, and K. Sugamura.** 1998. Human parvovirus B19 nonstructural (NS1) protein induces apoptosis in erythroid lineage cells. J Virol **72:**3018-28.

132. **Morey, A. L., and K. A. Fleming.** 1992. Immunophenotyping of fetal haemopoietic cells permissive for human parvovirus B19 replication in vitro. Br.J.Haematol. **82:**302-309.

133. **Morita, E., A. Nakashima, H. Asao, H. Sato, and K. Sugamura.** 2003. Human parvovirus B19 nonstructural protein (NS1) induces cell cycle arrest at G(1) phase. J Virol **77:**2915-21.

134. **Morita, E., and K. Sugamura.** 2002. Human parvovirus B19-induced cell cycle arrest and apoptosis. Springer Semin Immunopathol **24:**187-99.

135. **Morita, E., K. Tada, H. Chisaka, H. Asao, H. Sato, N. Yaegashi, and K. Sugamura.** 2001. Human parvovirus B19 induces cell cycle arrest at G(2) phase with accumulation of mitotic cyclins. J Virol **75:**7555-63.

136. **Mousset, S., Y. Ouadrhiri, P. Caillet-Fauquet, and J. Rommelaere.** 1994. The cytotoxicity of the autonomous parvovirus minute virus of mice nonstructural proteins in FR3T3 rat cells depends on oncogene expression. J Virol **68:**6446-53.

137. **Mousset, S., and J. Rommelaere.** 1982. Minute virus of mice inhibits cell transformation by simian virus 40. Nature **300:**537-9.

138. **Munakata, Y., T. Saito-Ito, K. Kumura-Ishii, J. Huang, T. Kodera, T. Ishii, Y. Hirabayashi, Y. Koyanagi, and T. Sasaki.** 2005. Ku80 autoantigen as a cellular coreceptor for human parvovirus B19 infection. Blood **106:**3449-56.

139. **Murray, A.** 1994. Cell cycle checkpoints. Curr Opin Cell Biol **6:**872-6.

140. **Muta, K., S. B. Krantz, M. C. Bondurant, and C. H. Dai.** 1995. Stem cell factor retards differentiation of normal human erythroid progenitor cells while stimulating proliferation. Blood. **86:**572-580.

141. **Nakagawa, T., H. Zhu, N. Morishima, E. Li, J. Xu, B. A. Yankner, and J. Yuan.** 2000. Caspase-12 mediates endoplasmic-reticulum-specific apoptosis and cytotoxicity by amyloid-beta. Nature. **403:**98-103.

142. **Nakahata, T., and N. Okumura.** 1994. Cell surface antigen expression in human erythroid progenitors: erythroid and megakaryocytic markers. Leuk.Lymphoma. **13:**401-409.

143. **Nash, K., W. Chen, and N. Muzyczka.** 2008. Complete in vitro reconstitution of adeno-associated virus DNA replication requires the minichromosome maintenance complex proteins. J Virol **82:**1458-64.

144. **Neubauer, H., A. Cumano, M. Muller, H. Wu, U. Huffstadt, and K. Pfeffer.** 1998. Jak2 deficiency defines an essential developmental checkpoint in definitive hematopoiesis. Cell. **93:**397-409.

145. **Nguyen, M. L., and J. A. Blaho.** 2007. Apoptosis during herpes simplex virus infection. Adv Virus Res **69:**67-97.

146. **Nuesch, J. P., R. Corbau, P. Tattersall, and J. Rommelaere.** 1998. Biochemical activities of minute virus of mice nonstructural protein NS1 are modulated In vitro by the phosphorylation state of the polypeptide. J Virol **72:**8002-12.

147. **Nuesch, J. P., S. Dettwiler, R. Corbau, and J. Rommelaere.** 1998. Replicative functions of minute virus of mice NS1 protein are regulated in vitro by phosphorylation through protein kinase C. J Virol **72:**9966-77.

148. **Nuesch, J. P., S. Lachmann, and J. Rommelaere.** 2005. Selective alterations of the host cell architecture upon infection with parvovirus minute virus of mice. Virology **331:**159-74.

149. **Nuesch, J. P., and J. Rommelaere.** 2006. NS1 interaction with CKII alpha: novel protein complex mediating parvovirus-induced cytotoxicity. J Virol **80:**4729-4739.

150. **Nuesch, J. P., and J. Rommelaere.** 2007. A viral adaptor protein modulating casein kinase II activity induces cytopathic effects in permissive cells. Proc Natl Acad Sci U S A **104:**12482-7.

151. **O'Malley, D., and J. Harvey.** 2007. MAPK-dependent actin cytoskeletal reorganization underlies BK channel activation by insulin. Eur J Neurosci **25:**673-82.

152. **Ogawa, M.** 1993. Differentiation and proliferation of hematopoietic stem cells. Blood. **81:**2844-2853.

153. **Ohshima, T., M. Iwama, Y. Ueno, F. Sugiyama, T. Nakajima, A. Fukamizu, and K. Yagami.** 1998. Induction of apoptosis in vitro and in vivo by H-1 parvovirus infection. J Gen Virol **79 (Pt 12):**3067-71.

154. **Okumura, N., K. Tsuji, and T. Nakahata.** 1992. Changes in cell surface antigen expressions during proliferation and differentiation of human erythroid progenitors. Blood. **80:**642-650.

155. **Oleksiewicz, M. B., and S. Alexandersen.** 1997. S-phase-dependent cell cycle disturbances caused by Aleutian mink disease parvovirus. J Virol **71:**1386-96.

156. **Op De, B. A., F. Anouja, S. Mousset, J. Rommelaere, and P. Caillet-Fauquet.** 1995. The nonstructural proteins of the autonomous parvovirus minute virus of mice interfere with the cell cycle, inducing accumulation in G2. Cell Growth Differ. **6:**781-787.

157. **Op De Beeck, A., and P. Caillet-Fauquet.** 1997. The NS1 protein of the autonomous parvovirus minute virus of mice blocks cellular DNA replication: a consequence of lesions to the chromatin? J Virol **71:**5323-9.

158. **Op De Beeck, A., J. Sobczak-Thepot, H. Sirma, F. Bourgain, C. Brechot, and P. Caillet-Fauquet.** 2001. NS1- and minute virus of mice-induced cell cycle arrest: involvement of p53 and p21(cip1). J Virol **75:**11071-8.

159. **Ow, Y. P., D. R. Green, Z. Hao, and T. W. Mak.** 2008. Cytochrome c: functions beyond respiration. Nat Rev Mol Cell Biol **9:**532-542.

160. **Ozawa, K., J. Ayub, Y. S. Hao, G. Kurtzman, T. Shimada, and N. Young.** 1987. Novel transcription map for the B19 (human) pathogenic parvovirus. J.Virol. **61:**2395-2406.

161. **Ozawa, K., J. Ayub, S. Kajigaya, T. Shimada, and N. Young.** 1988. The gene encoding the nonstructural protein of B19 (human) parvovirus may be lethal in transfected cells. J Virol **62:**2884-9.

162. **Ozawa, K., G. Kurtzman, and N. Young.** 1987. Productive infection by B19 parvovirus of human erythroid bone marrow cells in vitro. Blood. **70:**384-391.

163. **Ozawa, K., G. Kurtzman, and N. Young.** 1986. Replication of the B19 parvovirus in human bone marrow cell cultures. Science. **233:**883-886.

164. **Papayannopoulou, T., M. Brice, and C. A. Blau.** 1993. Kit ligand in synergy with interleukin-3 amplifies the erythropoietin-independent, globin-synthesizing progeny of normal human burst-forming units-erythroid in suspension cultures: physiologic implications. Blood. **81:**299-310.

165. **Parganas, E., D. Wang, D. Stravopodis, D. J. Topham, J. C. Marine, S. Teglund, E. F. Vanin, S. Bodner, O. R. Colamonici, J. M. van Deursen, G. Grosveld, and J. N. Ihle.** 1998. Jak2 is essential for signaling through a variety of cytokine receptors. Cell. **93:**385-395.

166. **Parrish, C. R.** 1995. Pathogenesis of feline panleukopenia virus and canine parvovirus. Baillieres Clin Haematol **8:**57-71.

167. **Parrish, C. R.** 2010. Pathogenesis of feline panleukopenia vrius and canine parvovirus. *In* K. J. R., C. S. F., B. M. E., L. M. E., and P. C. R. (ed.), Parvoviruses. Hodder Arnold, London, UK.

168. **Parrish, C. R., C. W. Leathers, R. Pearson, and J. R. Gorham.** 1987. Comparisons of feline panleukopenia virus, canine parvovirus, raccoon parvovirus, and mink enteritis virus and their pathogenicity for mink and ferrets. Am J Vet Res **48:**1429-35.

169. **Pilotte, J., D. Larocque, and S. Richard.** 2001. Nuclear translocation controlled by alternatively spliced isoforms inactivates the QUAKING apoptotic inducer. Genes Dev **15:**845-58.

170. **Pombo, A., J. Ferreira, E. Bridge, and M. Carmo-Fonseca.** 1994. Adenovirus replication and transcription sites are spatially separated in the nucleus of infected cells. EMBO J **13:**5075-85.

171. **Poole, B. D., Y. V. Karetnyi, and S. J. Naides.** 2004. Parvovirus B19-induced apoptosis of hepatocytes. J Virol **78:**7775-83.

172. **Poole, B. D., J. Zhou, A. Grote, A. Schiffenbauer, and S. J. Naides.** 2006. Apoptosis of liver-derived cells induced by parvovirus B19 nonstructural protein. J Virol **80:**4114-21.

173. **Pratelli, A., D. Buonavoglia, M. Tempesta, F. Guarda, L. Carmichael, and C. Buonavoglia.** 1999. Fatal canine parvovirus type-1 infection in pups from Italy. J.Vet.Diagn.Invest. **11:**365-367.

174. **Qiu, J., F. Cheng, L. R. Burger, and D. Pintel.** 2006. The transcription profile of Aleutian Mink Disease Virus (AMDV) in CRFK cells is generated by alternative processing of pre-mRNAs produced from a single promoter. J.Virol. **80:**654-662.

175. **Qiu, J., F. Cheng, F. B. Johnson, and D. Pintel.** 2007. The transcription profile of the bocavirus bovine parvovirus is unlike those of previously characterized parvoviruses. J Virol **81:**12080-5.

176. **Qiu, J., A. Handa, M. Kirby, and K. E. Brown.** 2000. The interaction of heparin sulfate and adeno-associated virus 2. Virology. **269:**137-147.

177. **Qiu, J., and D. J. Pintel.** 2002. The adeno-associated virus type 2 Rep protein regulates RNA processing via interaction with the transcription template. Mol Cell Biol **22:**3639-52.

178. **Raab, U., K. Beckenlehner, T. Lowin, H. H. Niller, S. Doyle, and S. Modrow.** 2002. NS1 protein of parvovirus B19 interacts directly with DNA sequences of the p6 promoter and with the cellular transcription factors Sp1/Sp3. Virology **293:**86-93.

179. **Raj, K., P. Ogston, and P. Beard.** 2001. Virus-mediated killing of cells that lack p53 activity. Nature **412:**914-7.

180. **Ran, Z., B. Rayet, J. Rommelaere, and S. Faisst.** 1999. Parvovirus H-1-induced cell death: influence of intracellular NAD consumption on the regulation of necrosis and apoptosis. Virus Res **65:**161-74.

181. **Rayet, B., J. A. Lopez-Guerrero, J. Rommelaere, and C. Dinsart.** 1998. Induction of programmed cell death by parvovirus H-1 in U937 cells: connection with the tumor necrosis factor alpha signalling pathway. J Virol **72:**8893-903.

182. **Riolobos, L., N. Valle, E. Hernando, B. Maroto, M. Kann, and J. M. Almendral.** 2010. Viral oncolysis that targets Raf-1 signaling control of nuclear transport. J Virol **84:**2090-9.

183. **Robertson, A. T., E. R. Stout, and R. C. Bates.** 1984. Aphidicolin inhibition of the production of replicative-form DNA during bovine parvovirus infection. J Virol **49:**652-7.

184. **Roperch, J. P., F. Lethrone, S. Prieur, L. Piouffre, D. Israeli, M. Tuynder, M. Nemani, P. Pasturaud, M. C. Gendron, J. Dausset, M. Oren, R. B. Amson, and A. Telerman.** 1999. SIAH-1 promotes apoptosis and tumor suppression through a network involving the regulation of protein folding, unfolding, and trafficking: identification of common effectors with p53 and p21(Waf1). Proc Natl Acad Sci U S A **96:**8070-3.

185. **Roux, P. P., and J. Blenis.** 2004. ERK and p38 MAPK-activated protein kinases: a family of protein kinases with diverse biological functions. Microbiol Mol Biol Rev **68:**320-44.

186. **Roy, S., and D. W. Nicholson.** 2000. Cross-talk in cell death signaling. J Exp Med **192:**F21-5.

187. **Saudan, P., J. Vlach, and P. Beard.** 2000. Inhibition of S-phase progression by adeno-associated virus Rep78 protein is mediated by hypophosphorylated pRb. EMBO J **19:**4351-61.

188. **Schildgen, O., A. Muller, T. Allander, I. M. Mackay, S. Volz, B. Kupfer, and A. Simon.** 2008. Human bocavirus: passenger or pathogen in acute respiratory tract infections? Clin.Microbiol.Rev. **21:**291-304, table.

189. **Schmidt, M., S. Afione, and R. M. Kotin.** 2000. Adeno-associated virus type 2 Rep78 induces apoptosis through caspase activation independently of p53. J Virol **74:**9441-50.

190. **Schwartz, D., B. Green, L. E. Carmichael, and C. R. Parrish.** 2002. The canine minute virus (minute virus of canines) is a distinct parvovirus that is most similar to bovine parvovirus. Virology. **302:**219-223.

191. **Schwartz, R. A., C. T. Carson, C. Schuberth, and M. D. Weitzman.** 2009. Adeno-associated virus replication induces a DNA damage response coordinated by DNA-dependent protein kinase. J Virol **83:**6269-78.

192. **Schwarz, T. F., A. Nerlich, and M. Roggendorf.** 1990. Parvovirus B19 infection in pregnancy. Behring Inst Mitt**:**69-73.

193. **Shimomura, S., S. Wong, K. E. Brown, N. Komatsu, S. Kajigaya, and N. S. Young.** 1993. Early and late gene expression in UT-7 cells infected with B19 parvovirus. Virology **194:**149-56.

194. **Sieff, C., D. Bicknell, G. Caine, J. Robinson, G. Lam, and M. F. Greaves.** 1982. Changes in cell surface antigen expression during hemopoietic differentiation. Blood. **60:**703-713.

195. **Sol, N., J. Le Junter, I. Vassias, J. M. Freyssinier, A. Thomas, A. F. Prigent, B. B. Rudkin, S. Fichelson, and F. Morinet.** 1999. Possible interactions between the NS-1 protein and tumor necrosis factor alpha pathways in erythroid cell apoptosis induced by human parvovirus B19. J Virol **73:**8762-70.

196. **Sol, N., F. Morinet, M. Alizon, and U. Hazan.** 1993. Trans-activation of the long terminal repeat of human immunodeficiency virus type 1 by the parvovirus B19 NS1 gene product. J Gen Virol **74 (Pt 9):**2011-4.

197. **Srivastava, A.** 2005. Hematopoietic stem cell transduction by recombinant adeno-associated virus vectors: problems and solutions. Hum Gene Ther **16:**792-8.

198. **Srivastava, A.** 2002. Obstacles to human hematopoietic stem cell transduction by recombinant adeno-associated virus 2 vectors. J Cell Biochem Suppl **38:**39-45.

199. **Srivastava, A., and L. Lu.** 1988. Replication of B19 parvovirus in highly enriched hematopoietic progenitor cells from normal human bone marrow. J.Virol. **62:**3059-3063.

200. **St Amand, J., and C. R. Astell.** 1993. Identification and characterization of a family of 11-kDa proteins encoded by the human parvovirus B19. Virology **192:**121-31.

201. **Strauss, L., C. Bergmann, M. J. Szczepanski, S. Lang, J. M. Kirkwood, and T. L. Whiteside.** 2008. Expression of ICOS on human melanoma-infiltrating CD4+CD25highFoxp3+ T regulatory cells: implications and impact on tumor-mediated immune suppression. J.Immunol. **180:**2967-2980.

202. **Sui, X., K. Tsuji, S. Tajima, R. Tanaka, K. Muraoka, Y. Ebihara, K. Ikebuchi, K. Yasukawa, T. Taga, T. Kishimoto, and T. Nakahata.** 1996. Erythropoietin-independent

erythrocyte production: signals through gp130 and c-kit dramatically promote erythropoiesis from human CD34+ cells. J.Exp.Med. **183:**837-845.

203. **Summerton, J.** 1999. Morpholino antisense oligomers: the case for an RNase H-independent structural type. Biochim.Biophys.Acta. **1489:**141-158.

204. **Sun, Y., A. Y. Chen, F. Cheng, W. Guan, F. B. Johnson, and J. Qiu.** 2009. Molecular characterization of infectious clones of the minute virus of canines reveals unique features of bocaviruses. J Virol **83:**3956-67.

205. **Suzuki, N., N. Suwabe, O. Ohneda, N. Obara, S. Imagawa, X. Pan, H. Motohashi, and M. Yamamoto.** 2003. Identification and characterization of 2 types of erythroid progenitors that express GATA-1 at distinct levels. Blood. **102:**3575-3583.

206. **Takahashi, T., K. Ozawa, K. Takahashi, S. Asano, and F. Takaku.** 1990. Susceptibility of human erythropoietic cells to B19 parvovirus in vitro increases with differentiation. Blood. **75:**603-610.

207. **Takizawa, T.** 2003. [Influenza virus infection and apoptosis]. Nippon Rinsho **61:**2001-5.

208. **Tattersall, P.** 2006. The evolution of parvovirus taxonomy, p. 5-14. *In* J. Kerr, S. F. Cotmore, M. E. Bloom, R. M. Linden, and C. R. Parrish (ed.), Parvoviruses. Hodder Arond, London.

209. **Tauer, T. J., M. H. Schneiderman, J. K. Vishwanatha, and S. L. Rhode.** 1996. DNA double-strand break repair functions defend against parvovirus infection. J.Virol. **70:**6446-6449.

210. **Tennant, R. W., K. R. Layman, and R. E. Hand.** 1969. Effect of Cell Physiological State on Infection by Rat Virus. J Virol **4:**872-878.

211. **Timpe, J. M., K. C. Verrill, B. N. Black, H. F. Ding, and J. P. Trempe.** 2007. Adeno-associated virus induces apoptosis during coinfection with adenovirus. Virology **358:**391-401.

212. **Tollefson, A. E., K. Toth, K. Doronin, M. Kuppuswamy, O. A. Doronina, D. L. Lichtenstein, T. W. Hermiston, C. A. Smith, and W. S. Wold.** 2001. Inhibition of TRAIL-induced apoptosis and forced internalization of TRAIL receptor 1 by adenovirus proteins. J.Virol. **75:**8875-8887.

213. **Trobridge, G., R. K. Hirata, and D. W. Russell.** 2005. Gene targeting by adeno-associated virus vectors is cell-cycle dependent. Hum Gene Ther **16:**522-6.

214. **Vainchenker, W., J. F. Deschamps, J. M. Bastin, J. Guichard, M. Titeux, J. Breton-Gorius, and A. J. McMichael.** 1982. Two monoclonal antiplatelet antibodies as markers of human megakaryocyte maturation: immunofluorescent staining and platelet peroxidase detection in megakaryocyte colonies and in in vivo cells from normal and leukemic patients. Blood **59:**514-21.

215. **van Leengoed, L. A., J. Vos, E. Gruys, P. Rondhuis, and A. Brand.** 1983. Porcine Parvovirus infection: review and diagnosis in a sow herd with reproductive failure. Vet Q **5:**131-41.

216. **Vermeulen, K., Z. N. Berneman, and D. R. Van Bockstaele.** 2003. Cell cycle and apoptosis. Cell Prolif **36:**165-75.

217. **Wang, J., H. J. Chun, W. Wong, D. M. Spencer, and M. J. Lenardo.** 2001. Caspase-10 is an initiator caspase in death receptor signaling. Proc Natl Acad Sci U S A **98:**13884-8.

218. **Weigel-Kelley, K. A., M. C. Yoder, and A. Srivastava.** 2003. Alpha5beta1 integrin as a cellular coreceptor for human parvovirus B19: requirement of functional activation of beta1 integrin for viral entry. Blood **102:**3927-33.

219. **Weigel-Kelley, K. A., M. C. Yoder, and A. Srivastava.** 2001. Recombinant human parvovirus B19 vectors: erythrocyte P antigen is necessary but not sufficient for successful transduction of human hematopoietic cells. J Virol **75:**4110-6.

220. **Winocour, E., M. F. Callaham, and E. Huberman.** 1988. Perturbation of the cell cycle by adeno-associated virus. Virology **167:**393-9.

221. **Wolter, S., R. Richards, and R. W. Armentrout.** 1980. Cell cycle-dependent replication of the DNA of minute virus of mice, a parvovirus. Biochim Biophys Acta **607:**420-31.

222. **Wong, S., N. Zhi, C. Filippone, K. Keyvanfar, S. Kajigaya, K. E. Brown, and N. S. Young.** 2008. Ex vivo-generated CD36+ erythroid progenitors are highly permissive to human parvovirus B19 replication. J Virol **82:**2470-6.

223. **Wu, H., U. Klingmuller, P. Besmer, and H. F. Lodish.** 1995. Interaction of the erythropoietin and stem-cell-factor receptors. Nature. **377:**242-246.

224. **Wu, H., X. Liu, R. Jaenisch, and H. F. Lodish.** 1995. Generation of committed erythroid BFU-E and CFU-E progenitors does not require erythropoietin or the erythropoietin receptor. Cell. **83:**59-67.

225. **Yaegashi, N., T. Niinuma, H. Chisaka, S. Uehara, S. Moffatt, K. Tada, M. Iwabuchi, Y. Matsunaga, M. Nakayama, C. Yutani, Y. Osamura, E. Hirayama, K. Okamura, K. Sugamura, and A. Yajima.** 1999. Parvovirus B19 infection induces apoptosis of erythroid cells in vitro and in vivo. J Infect **39:**68-76.

226. **Yoto, Y., J. Qiu, and D. J. Pintel.** 2006. Identification and characterization of two internal cleavage and polyadenylation sites of parvovirus B19 RNA. J Virol **80:**1604-9.

227. **Young, N. S., and K. E. Brown.** 2004. Parvovirus B19. N Engl J Med **350:**586-97.

228. **Zhao, R. Y., and R. T. Elder.** 2005. Viral infections and cell cycle G2/M regulation. Cell Res **15:**143-9.

229. **Zhi, N., I. P. Mills, J. Lu, S. Wong, C. Filippone, and K. E. Brown.** 2006. Molecular and functional analyses of a human parvovirus B19 infectious clone demonstrates essential roles for NS1, VP1, and the 11-kilodalton protein in virus replication and infectivity. J Virol **80:**5941-50.

230. **Zhi, N., Z. Zadori, K. E. Brown, and P. Tijssen.** 2004. Construction and sequencing of an infectious clone of the human parvovirus B19. Virology **318:**142-52.

231. **Zinkel, S., A. Gross, and E. Yang.** 2006. BCL2 family in DNA damage and cell cycle control. Cell Death Differ **13:**1351-9.

232. **Zoli, W., P. Ulivi, A. Tesei, F. Fabbri, M. Rosetti, R. Maltoni, D. C. Giunchi, L. Ricotti, G. Brigliadori, I. Vannini, and D. Amadori.** 2005. Addition of 5-fluorouracil to doxorubicin-paclitaxel sequence increases caspase-dependent apoptosis in breast cancer cell lines. Breast Cancer Res. **7:**R681-R689.